

Dissertation

Towards optimizing combination therapy
in ALK-positive neuroblastoma

Ines Gräßer

Division of Theoretical Systems Biology
German Cancer Research Center (DKFZ)

Heidelberg, Germany
September, 2020

Dissertation

submitted to the
Combined Faculty of Natural Sciences and Mathematics
of the Ruperto Carola University Heidelberg, Germany
for the degree of
Doctor of Natural Sciences

Presented by

Ines Gräßer

born in: Völklingen

Oral examination: 16.11.2020

Towards optimizing combination therapy
in ALK-positive neuroblastoma

Referees: Prof. Dr. Thomas Höfer
PD Dr. Frank Westermann

Table of Contents

Abstract	v
Zusammenfassung	vii
List of Figures	ix
List of Tables	xii
Abbreviations	xiii
1 Introduction	1
1.1 Clinical aspects of neuroblastoma	1
1.2 Genetic predisposition and familial neuroblastoma	3
1.3 Genomic alterations in neuroblastoma	4
1.3.1 Ploidy	4
1.3.2 Chromosomal gain and loss	4
1.3.3 <i>MYCN</i> amplification	5
1.3.4 Genomic alterations promoting telomere lengthening	5
1.3.5 Somatic mutations	6
1.4 Anaplastic lymphoma kinase	6
1.4.1 The ALK receptor	6
1.4.2 ALK expression	7
1.4.3 ALK function in normal development	8
1.4.4 <i>ALK</i> alterations in human cancers	9
1.4.5 <i>ALK</i> alterations in neuroblastoma	11
1.4.6 ALK activation and signaling	12
1.4.7 ALK in neuroblastoma tumorigenesis	15
1.4.8 ALK as a therapeutic target	16
1.4.8.1 Monotherapy	16
1.4.8.2 Combination therapy	17
1.5 Clinical treatment of neuroblastoma	18
1.6 Aim of this study	20

2	Material and Methods	21
2.1	Materials	21
2.2	Methods	27
2.2.1	General cell culture methods	27
2.2.1.1	Culturing of neuroblastoma cell lines	27
2.2.1.2	Cryo-preservation of neuroblastoma cell lines	27
2.2.1.3	Thawing of neuroblastoma cell lines	27
2.2.1.4	Spheroid tissue culture	27
2.2.2	Chemotherapeutic and kinase inhibitor treatment	28
2.2.3	Cell viability and cell confluence assay	28
2.2.4	Colony formation assay using Giemsa staining	29
2.2.5	Microscopy	29
2.2.5.1	Live-cell microscopy	29
2.2.5.2	Spheroid imaging	29
2.2.6	Flow Cytometry	30
2.2.6.1	Cell cycle	30
2.2.6.2	EdU incorporation	30
2.2.6.3	Caspase	30
2.2.7	Gene knock-down with siRNA	31
2.2.8	Quantitative RT-PCR	31
2.2.9	RNA-Sequencing	32
2.2.10	Protein quantification by SDS-PAGE and western blotting	32
3	Results	34
3.1	ALK in neuroblastoma patients	34
3.2	ALK in neuroblastoma cell lines	36
3.2.1	<i>ALK</i> status and expression in neuroblastoma cell lines	36
3.2.2	Model cell lines to study therapeutic ALK inhibition <i>in vitro</i>	37
3.3	Therapeutic targeting of ALK with the third generation ALK inhibitor lorlatinib	42
3.3.1	Comparison of the two ALK inhibitors lorlatinib and NVP-TAE684	43
3.3.2	Lorlatinib sensitivity depends on ALK protein levels and activation status	45
3.3.3	Lorlatinib causes dephosphorylation of ALK targets	49
3.3.4	The highly LOR-sensitive cell line NB-1 gains resistance after continuous treatment with lorlatinib	50

3.4	ALK-addicted cells benefit from combination treatment of lorlatinib with chemotherapeutics	53
3.4.1	Chemotherapeutics cause phase-specific cell cycle arrest	53
3.4.2	Combination treatment is effective only in ALK-addicted cell lines	55
3.5	Validation of combination therapy in NB-1 spheroids	59
3.5.1	Establishment of neuroblastoma spheroid tissue culture	59
3.5.2	NB-1 cells are equally sensitive to lorlatinib in 2D and 3D tissue culture	65
3.5.3	NB-1 spheroids respond well to treatment with cisplatin but are more resistant to vincristine	68
3.5.4	Combination treatment is more effective than chemotherapy alone	71
3.6	Whole transcriptome analysis to gain insights into the response to lorlatinib	75
3.6.1	A published ALK gene signature cannot fully explain the difference in sensitivity	76
3.6.2	Effect of lorlatinib on the transcriptome of a responder and a non-responder cell line	78
3.6.2.1	Optimization and experimental design of the RNAseq experiment	78
3.6.2.2	The transcriptome discriminates primarily between cell lines	81
3.6.2.3	Lorlatinib affects the transcriptome of the responder cell line NB-1 but not of the non-responder KELLY	82
3.6.2.4	Lorlatinib causes cell cycle arrest but not cell death of NB-1 cells	83
3.6.2.5	An alternative ALK gene signature determined by lorlatinib treatment	88
3.6.3	Examination of a possible target gene for ALK combination therapy	91
4	Discussion	96
4.1	ALK in neuroblastoma patients	96
4.2	ALK in neuroblastoma cell lines	97
4.3	Therapeutic targeting of ALK	98
4.4	ALK addicted cells benefit from combination treatment of lorlatinib with chemotherapeutics	100
4.5	Validation of combination therapy in NB-1 spheroids	102

4.6	Whole transcriptome analysis to gain insights into the response to lorlatinib	104
4.6.1	KELLY cells may be resistant to lorlatinib through activation of bypass signaling pathways	104
4.6.2	Lorlatinib causes cell cycle arrest rather than cell death	106
4.6.3	Response to the ALK inhibitor lorlatinib cannot be predicted by the transcriptome	107
4.7	Conclusion and perspective	107
	References	109
	Appendix	125
	Acknowledgements	128

Abstract

Neuroblastoma (NB) is the most common extracranial solid tumor in infants, arising from the developing sympathetic nervous system. A subgroup of approximately 6-8% of NB patients harbors an alteration in the anaplastic lymphoma kinase (*ALK*) gene, making this receptor tyrosine kinase an important therapeutic target. Small-molecule inhibitors targeting ALK are already in clinical use as monotherapies, but an optimal integration into the standard care has yet to be established. This study aims at characterizing the inhibitory properties of the third generation ALK inhibitor lorlatinib (LOR) on proliferation of tumor cells and its potential in a combinatorial therapy approach.

In this study, treatment with LOR was investigated in a selection of *ALK* amplified, F1174L and R1275Q mutated, as well as wild-type NB cell lines. We found that the sensitivity to LOR correlated with expression levels of activated ALK protein. ALK addicted NB-1 cells, which expressed the highest ALK protein levels, were the most sensitive amongst all tested cell lines and were further used as model system to study ALK inhibition *in vitro*. In these cells, LOR treatment reduced cell viability and proliferation by inhibiting the Ras-MAPK and PI3K-AKT signaling pathways, leading to a predominant G₁ cell cycle arrest. Cell death was induced only at concentrations above a clinically achievable level. Despite a high initial sensitivity to LOR, cells could overcome this arrest and gain resistance after long-term treatment. Thus, LOR may not be appropriate for sustained monotherapy. Therefore, we tested whether the treatment of NB-1 cells could benefit from combination therapy with the two first-line chemotherapeutics cisplatin (CDDP) and vincristine (VCR), both in a classical two-dimensional *in vitro* setting and also in multicellular tumor spheroids. Indeed, combination therapy could significantly reduce cell viability in NB-1 cells. In contrast, NB cell lines that harbor an *ALK* alteration but express lower amounts of active ALK protein were less sensitive or even resistant to LOR and could not benefit from combination therapies. Furthermore, basal expression of ALK signature genes did not reflect the sensitivity of the different cell lines to LOR. Therefore, RNAseq data that are frequently acquired for NB patients may not be adequate to predict therapy response.

Taken together, this study shows that not only the genomic *ALK* status is relevant for therapeutic success, suggesting that protein levels should be examined before the treatment with ALK inhibitors. Furthermore, this study indicates that a novel combinatorial approach of LOR with CDDP or VCR is feasible for ALK addicted NBs.

Zusammenfassung

Das Neuroblastom (NB) ist der häufigste extrakranielle solide Tumor im jungen Kindesalter und entsteht aus dem sich entwickelnden sympathischen Nervensystem. 6-8% aller Neuroblastompatienten tragen eine Veränderung im Gen der anaplastischen Lymphomkinase (*ALK*), weshalb dieser Rezeptor von großer Bedeutung für eine zielgerichtet Therapie ist. Obwohl ALK Inhibitoren bereits als Einzeltherapie in der klinischen Behandlung von Neuroblastompatienten verwendet werden, ist eine optimale Einbindung als Standardtherapeutikum in die Ersttherapie noch nicht etabliert. Das Ziel dieser Arbeit ist die Charakterisierung der inhibierenden Eigenschaften von Lorlatinib (LOR), ein ALK Inhibitor der dritten Generation, auf das Tumorwachstum und sein Potenzial in einem kombinationstherapeutischen Behandlungsansatz.

In dieser Arbeit wurde die Behandlung mit LOR an einer Auswahl von *ALK* amplifizierten, F1174L und R1275Q mutierten, sowie Wildtyp NB Zelllinien untersucht. Die Sensitivität gegenüber LOR korrelierte mit dem Expressionslevel von aktivem ALK Protein. Die ALK abhängige Zelllinie NB-1, die das höchste Proteinlevel aufwies, zeigte die größte Sensitivität und wurden daher als Modellsystem zur Untersuchung der ALK Inhibition *in vitro* verwendet. In diesen Zellen reduzierte eine Behandlung mit LOR die Zellviabilität und Proliferation durch Hemmung des Ras-MAPK und PI3K-AKT Signalwegs. Dies führte zu einem Zellzyklusarrest, vorwiegend in der G₁ Phase des Zellzyklus. Ausschließlich Konzentrationen oberhalb klinisch relevanter Dosen induzierten Zelltod. Obwohl die Zellen zunächst sehr sensitiv auf LOR reagierten, wurde der Zellzyklusarrest schnell überwunden und eine Resistenz nach Langzeitbehandlung entwickelt. Dies lässt darauf schließen, dass eine kontinuierlich Einzeltherapie mit LOR nicht effektive ist. Daher haben wir getestet, ob NB-1 Zellen von einer Kombinationstherapie mit den herkömmlichen Chemotherapeutika Cisplatin (CDDP) und Vincristin (VCR) profitieren können. Dies traf sowohl auf die klassische zweidimensionale *in vitro* Zellkultur als auch auf mehrzellige Tumorspheroide zu. Im Gegensatz dazu waren NB Zelllinien mit einer Veränderung des *ALK* Gens aber einer geringen Expression des aktiven Proteins, weniger sensitiv gegenüber LOR oder sogar resistent. Außerdem profitierten sie

nicht von der Kombinationstherapie. Zusätzlich konnte die basale Expression von ALK Signaturgenen die Sensitivität der verschiedenen Zelllinien nicht widerspiegeln. Dies lässt vermuten, dass die häufig generierten Genexpressionsdaten mittels RNA Sequenzierung nicht zur Vorhersage des Therapieerfolgs genutzt werden können.

Insgesamt zeigt diese Arbeit, dass nicht nur der genomische *ALK* Status für den Behandlungserfolg relevant ist. Dies deutet darauf hin, dass das Proteinlevel vor einer Behandlung mit ALK Inhibitoren untersucht werden sollte. Des Weiteren bietet diese Arbeit die Grundlage für einen neuen Therapieansatz mit der Kombination aus LOR mit den Chemotherapeutika CDDP oder VCR in Neuroblastompatienten mit ALK abhängigen Tumoren.

List of Figures

1	Full-length ALK receptor	7
2	<i>ALK</i> alterations in human cancers	10
3	<i>ALK</i> mutations in neuroblastoma	12
4	ALK signaling	14
5	Standard of care treatment of high-risk neuroblastomas	19
6	<i>ALK</i> mutations occur more often in NB patients with a relapse disease compared to patients with a primary disease	35
7	<i>ALK</i> expression depends on the <i>ALK</i> status and does not vary between primary and relapse disease	35
8	<i>ALK</i> is co-amplified with <i>MYCN</i> in NB-1 cells	36
9	Distribution of <i>ALK</i> alterations and expression level in NB cell lines .	37
10	<i>ALK</i> expression of the cell line panel	38
11	Model cell lines do not form ALK specific clusters based on hierarchical clustering	39
12	PCA does not result in ALK specific clusters	39
13	ALK mRNA and protein expression in the model cell lines	41
14	Morphology and growth behavior varies between model cell lines . . .	42
15	NB cell lines respond differently to NVP-TAE684 and lorlatinib . . .	44
16	Response to lorlatinib varies between model cell lines	45
17	Area under the curve at lorlatinib treatment.	47
18	EC50 and AUC values are positively correlated.	48
19	Lorlatinib response depends on <i>ALK</i> expression.	48
20	Lorlatinib causes dephosphorylation of ALK targets in LOR-sensitive cell lines	49
21	Long-term treatment with lorlatinib does not change morphology of NB-1 cells	51
22	Lorlatinib reduces cell confluence less in NB-1-R cells compared to NB-1 cells	52
23	Lorlatinib reduces cell viability less in NB-1-R cells compared to NB-1 cells	53

24	Chemotherapeutics cause phase-specific cell cycle arrest	54
25	ALK sensitive and intermediate sensitive cell lines respond differently to combination treatment with lorlatinib and cisplatin	56
26	ALK sensitive and intermediate sensitive cell lines respond differently to combination treatment with lorlatinib and vincristine.	57
27	ALK-addicted cells benefit from combination treatment	58
28	Two techniques to culture multicellular spheroids.	59
29	Normal growth of 500-cell spheroids and the effect of chemotherapy on their 3D structure.	61
30	Normal growth of 5000-cell spheroids and the effect of chemotherapy on their 3D structure.	62
31	Growth behavior of NB-1 spheroids	63
32	Exemplary NBL-S spheroid with a necrotic core	64
33	NB-1 cells are equally sensitive to lorlatinib in monolayer and spheroid tissue culture	66
34	NB-1 cells show similar growth behavior at lorlatinib treatment in monolayer and spheroid tissue culture	67
35	NB-1 cells have similar growth behavior at cisplatin treatment in monolayer and spheroid tissue culture	69
36	NB-1 cells are more sensitive to vincristine in monolayer tissue culture than spheroid culture	70
37	Combination treatment with lorlatinib and cisplatin is similar effec- tive in monolayer and spheroid culture	72
38	Combination treatment with lorlatinib and vincristine is more effec- tive in monolayer culture than in spheroid culture	73
39	Combination treatment with lorlatinib and cisplatin is more effective than the combination with lorlatinib and vincristine	74
40	Cell lines do not form clusters of sensitivity based on ALK signature genes	76
41	The ALK gene signature does not discriminate patients according to their <i>ALK</i> status	77
42	Optimization of concentration and time points for RNA sequencing of lorlatinib treated cell lines	79
43	Lorlatinib reduces phosphorylation of ALK	80
44	Experimental design of the RNAseq experiment	80
45	Hierarchical clustering of RNAseq samples	81
46	Principle component analysis of RNAseq samples	82
47	Only NB-1 cells have differentially expressed genes at lorlatinib treat- ment	83

48	Lorlatinib inhibits cell cycle and ALK downstream pathways in NB-1 cells	84
49	Lorlatinib inhibits cell cycle of NB-1 cells	85
50	Lorlatinib does not cause cell death mediated by caspase 3 and caspase 7	86
51	Lorlatinib causes cell cycle arrest	87
52	Lorlatinib causes early and late transcript responses in NB-1 cells	89
53	Cell lines do not form clusters of sensitivity based on the 100 most variable genes	90
54	The 100 most variable genes from lorlatinib treatment do not discriminate patients according to their <i>ALK</i> status	90
55	Components of the PI3K-AKT signaling pathway are differentially expressed in responder and non-responder cells	91
56	<i>MET</i> and <i>HGF</i> expression in model cell lines.	92
57	NB cell lines do not respond to the selective MET inhibitor tepotinib	93
58	MET knock-down does not effect cell viability and confluence	95
59	NB cell lines respond differently to varying treatment schedules of doxorubicine	125
60	Normal growth of 5000-cell NB spheroids and the effect of chemotherapy on the 3D structure	126
61	Genes involved in replication initiation are downregulated in LOR treated NB-1 cells	127

List of Tables

1	International Neuroblastoma Risk Group Staging System	2
2	Research equipment	21
3	Material	22
4	Molecular biology reagents	22
5	Chemicals and reagents	23
6	Kits for molecular biology	23
7	Antibodies for protein detection	24
8	Oligonucleotides and QuantiTect Primer Assays for qRT-PCR	24
9	siRNA for transient gene knock-down	24
10	Neuroblastoma cell lines	25
11	Media and supplements for cell culture	26
12	Cytostatics	26
13	Model cell lines to study ALK inhibition <i>in vitro</i>	38
14	EC50 concentrations of NVP-TAE684 and lorlatinib	44
15	EC50 concentration, area under the curve (AUC) and sensitivity of the model cell lines to lorlatinib	46
16	EC50 concentrations of cisplatin for LOR-sensitive cell lines at mono- and combination treatment.	56
17	EC50 concentrations of vincristine for LOR-sensitive cell lines at mono- and combination treatment.	57
18	EC50 concentrations of tepotinib in mono- and combination therapy with lorlatinib in <i>ALK</i> altered cell lines.	94

Abbreviations

2D	two-dimensional
3D	three-dimensional
aa	amino acid
ALCL	anaplastic large-cell non-Hodgkin's lymphoma
ALK	anaplastic lymphoma kinase
ALT	alternative lengthening of telomeres
ATC	anaplastic thyroid cancer
ATP	adenosine triphosphate
ATRX	α -thalassemia/mental retardation syndrom X-linked
AUC	Area under the curve
bp	basepair
BSA	bovine serum albumin
CCHS	congenital central hypoventilation syndrome
CDDP	cisplatin
cDNA	complementary DNA
CGH	comparative genome hybridization
CNS	central nervous system
COG	children's oncology group
CTB	CellTiter Blue
DAPI	4,6-diamidino-2-phenylindole
DLBCL	diffuse large B cell lymphoma
DMF	Dimethylformamid
DMSO	dimethylsulfoxid
DNA	desoxyribonucleic acid
DNase	desoxyribonuclease
DOX	doxorubicin
EC50	half maximal effective concentration
ECD	extracellular domain
ECL	enhanced chemiluminescence
EDTA	ethylendiamintetraacetic acid, Na-salt
EdU	5-ethynyl-2'-deoxyuridine
EML4	echinoderm microtubule-associated protein-like 4
ESCC	oesophageal squamous cell carcinoma

EtOH	ethanol
FACS	fluorescence activated cell sorting
FBS	fetal bovine serum
FISH	fluorescence in situ hybridization
g	gram
gDNA	genomic DNA
GO	gene ontology
h	hour(s)
HEPES	4-(2-hydroxyethyl)-1-piperazineethanesulfonic acid
HR	high-risk
HRP	horseradish peroxidase
HSCR	Hirschsprung disease
ICD	intracellular domain
IDRF	image defined risk factors
IMT	inflammatory myofibroblastic tumor
INRGSS	international neuroblastoma risk group staging system
INSS	international neuroblastoma staging system
kbp	kilo basepair
kDa	kilo dalton
LDLa	low-density lipoprotein class A
LOH	loss of heterozygosity
LOR	lorlatinib
LTK	leukocyte tyrosine kinase
LR	low-risk
m	milli
M	molar
MAM	meprin/A5/protein tyrosine phosphatase Mu
min	minute(s)
MK	midkine
MNA	MYCN-non amplified
mRNA	messenger RNA
n	nano
NB	neuroblastoma
NCPC	neuro crest progenitor cells
NPM	nucleophosmin
NSCLC	non-small cell lung cancer
PAGE	polyacrylamide gel electrophoreses
PBS	phosphate-buffered saline
PC1	principle component 1
PC2	principle component 2
PCA	principle component analysis

PCR	polymerase chain reaction
PDO	patient derived organoid
PDX	patient derived xenograft
PFA	paraformaldehyde
PI3K	phosphoinositol-3 kinase
PLC γ	phospholipase C γ
PNS	peripheral nervous system
PTN	pleiotrophin
RCC	renal cell carcinoma
RMC	renal medulla carcinoma
RNA	ribonucleic acid
RNAseq	RNA sequencing
rpm	rotation per minute
RT	room temperature
RTK	receptor tyrosine kinase
RT-qPCR	quantitative real-time PCR
SDS	sodiumdodecylsulfat
sec	second(d)
SIOPEN	international society of pediatric oncology european neuroblastoma
siRNA	short interfering RNA
SOC	serous ovarian carcinoma
STAT	signal transducer and activator of transcription
t	translocation
TAE	NVP-TAE684
TBS	Tris buffered saline
TEP	tepotinib
TERT	telomerase reverse transcriptase
TK	tyrosine kinase
TKI	thyrosine kinase inhibitor
Tris	tris-(hydroxymethyl)-aminomethan
ULA	ultra-low attachment
WB	western blotting
WES	whole exome sequencing
WGS	whole genome sequencing
wt	wild-type
VCR	vincristine

1 Introduction

1.1 Clinical aspects of neuroblastoma

Neuroblastoma (NB) is the most common extracranial solid tumor in early childhood accounting for 8-10% of pediatric malignancies, with a yearly incidence rate of one case per 100.000 children under the age of 15 (Brodeur 2003, Maris et al. 2007). The median age of diagnosis is 17 months, at which 37% of NB patients are diagnosed as infants and 90% are diagnosed before the age of five (London et al. 2005). Neuroblastomas originate from neural crest derived cells and can develop anywhere in the sympathetic nervous system. However, 65% of primary tumors occur within the abdomen, especially in the adrenal medulla, sympathetic ganglia and paraganglia. Other common sites include neck, chest and pelvis (Maris et al. 2007, Maris 2010, Johnsen et al. 2009).

NB is an extremely heterogeneous disease with a broad clinical outcome varying from spontaneous regression without any therapy to highly aggressive metastatic disease despite multimodal anti-cancer treatment (Brodeur 2003, Maris et al. 2007, Evans, D'Angio, and Randolph 1971). Indeed, NB shows the highest rate of spontaneous regression amongst all cancer entities, which is 10-100 fold greater than in other human cancers (Pritchard and Hickman 1994). In contrast to the spontaneous regression, which occurs mainly in infants and occasionally in older patients, the long-term survival of high-risk patients is less than 40% (D'Angio, Evans, and Koop 1971, Hero et al. 2008, Fiorillo et al. 1982, Eklof et al. 1983, De Bernardi et al. 2003, Matthay et al. 1999, Berthold et al. 1997). In general, infants younger than 18 months of age have a good prognosis for survival, while older patients have an unfavorable outcome. In adult or adolescent patients, the course of the disease is often lethal (Franks et al. 1997, London et al. 2005, Schmidt et al. 2005). Thus, the age at diagnosis plays an important role in clinical outcome of NB patients.

The comparability of clinical trials and biological studies, caused by the clinical and biological diversity of the disease, is still a major challenge. Therefore, the International Neuroblastoma Staging System (INSS) was established to determine

a consistent staging strategy with the following 6 stages: 1, 2A, 2B, 3, 4 and 4S. In general, stage 1 are small localized tumors that were completely resected. Stage 2 are small localized tumors with or without lymph node involvement that could not be resected completely. Large tumors crossing the midline of the patients that could not be resected completely are classified as stage 3. Metastatic tumors are grouped as stage 4, in which patients younger than one year are subclassified as 4S (Brodeur et al. 1988, Brodeur et al. 1993).

INSS is based on clinical radiographic imaging and surgical evaluation of the tumor, making the classification extremely dependent on the surgeon. Therefore, a new international staging system for pre-treatment risk stratification was developed, the International Neuroblastoma Risk Group Staging System (INRGSS) (Monclair et al. 2009, Cohn et al. 2009). Staging is based on clinical criteria and image-defined risk factors (IDRFs) and should predict successful and safe surgery. The INGRSS consists of the following 4 stages: L1, L2, M and MS (Table 1). In general, these stages discriminate between locoregional tumors without involvement of local structures (L1) and locally invasive tumors (L2) from metastatic tumors (M) that can also show INSS 4S pattern of disease (MS).

Table 1: International Neuroblastoma Risk Group Staging System (INRGSS). Adapted from Monclair et al. 2009.

Stage	Description
L1	Localized tumor not involving vital structures as defined by the list of image-defined risk factors and confined to one body compartment
L2	Locoregional tumor with presence of one or more image-defined risk factors
M	Distant metastatic disease (except stage MS)
MS	Metastatic disease in children younger than 18 months with metastases confined to skin, liver, and/or bone marrow

Based on age at diagnosis, INGR stage, histology, tumor differentiation, MYCN status, 11q LOH, and ploidy, four risk categories can be distinguished: very low-risk, low-risk, intermediate-risk and high-risk (Cohn et al. 2009). Low-risk patients have an event-free survival of 90% with observation or small therapeutic interventions, whereas intermediate-risk patients have 78% event free survival rates and receive surgery and chemotherapy (Monclair et al. 2009). Low- and intermediate-risk NBs occur mainly in children younger than 18 months of age, are hyperdiploid and have gains of whole chromosomes. Patients harboring a *MYCN* amplification and/or those older than 18 months with stage M disease are considered high-risk with a long-term survival of <40%. An additional characteristic of this NB subtype are

segmental chromosomal aberrations rather than whole chromosomal changes (Maris et al. 2007). The treatment of these patients involves chemotherapy, surgery, radiotherapy, biologics (e.g. cis-retinoid acid) and immunotherapy (Louis and Shohet 2015).

Despite the very aggressive multimodal treatment of high-risk NBs, patients often relapse and eventually die from the disease. Thus, many research groups are currently investigating novel treatment strategies to improve clinical outcome of these patients.

1.2 Genetic predisposition and familial neuroblastoma

Although NB usually occurs as sporadic tumors, a small fraction of 1-1.5% of cases are familial (Shojaei-Brosseau et al. 2004). Pedigrees of these patients suggest an autosomal mode of inheritance with incomplete penetrance (Tonini et al. 2003).

The major cause of familial NB are constitutively activating mutations of the anaplastic lymphoma kinase (*ALK*) gene (Mosse et al. 2008, Janoueix-Lerosey et al. 2008). *ALK* is a receptor tyrosine kinase (RTK) which acts as oncogenic driver of many different malignancies such as anaplastic large-cell non-Hodgkin's lymphoma (ALCL) or non-small cell lung cancer (NSCLC) (Morris et al. 1994, Soda et al. 2007). Due to the location on chromosome 2p23 and the close proximity to *MYCN*, *ALK* is occasionally co-amplified with *MYCN* and thereby activated (Janoueix-Lerosey et al. 2008). The same activating point mutations found in familial NB as well as amplification occurs also in approximately 10% of sporadic cases (see Section 1.4).

A subset of familial NB patients is associated with two additional disorders of neural-crest derived tissues, central hypoventilation syndrome (CCHS) and Hirschsprung disease (HSCR). Many patients with these diseases have a germline mutation of the paired-like homeobox 2B (*PHOX2B*), a gene encoding for a transcription factor involved in neuronal development (Amiel et al. 2003, Mosse et al. 2004, Trochet et al. 2004). Furthermore, *PHOX2B* mutations occur also in sporadic NB and are hereby often associated with CCHS and/or HSCR (Limpt et al. 2004).

1.3 Genomic alterations in neuroblastoma

1.3.1 Ploidy

Cytogenic analysis of NB tumors revealed four levels of ploidy found in neuroblastomas, near-diploid, near-triploid, near-tetraploid and near-pentaploid (Kaneko et al. 1987). Near-diploid and near-tetraploid karyotypes, which are often associated with *MYCN* amplification and 1p-deletion, are mainly observed in high-risk patients. These patients often do not respond to chemotherapy and have a poor clinical outcome. Near-triploid and near-pentaploid tumors, showing three or five almost complete haploid chromosomes, are found in patients with a favorable clinical outcome (Look et al. 1984, Cohn et al. 1990a, Gansler et al. 1986, Oppedal et al. 1989). This link of DNA content to the stage of disease and clinical outcome was shown in infants and patients of age 12-24 months, whereas the karyotype is not a prognostic factor in patients older than two years of age (Look et al. 1991).

1.3.2 Chromosomal gain and loss

Besides classical flow cytometry and cytogenetic analysis, comparative genome hybridization (CGH) has been used for genome-wide screening of chromosomal gains and losses in neuroblastoma (Brinkschmidt et al. 1997, Plantaz et al. 2001, Lastowska et al. 1997, Vandesompele et al. 2001). This includes full or partial gains or losses of chromosomes 1, 2, 6, 7, 8, 12, 13, 17, 18 and 22 or 3, 4, 9, 11, 14 and X, respectively (Vandesompele et al. 2001). Among these, 1p deletion and 17q gain are the most recurring aberrations in NB.

1p deletion Deletion of the short arm of chromosome 1p was first described by Brodeur, Sekhon, and Goldstein in 1977 (Brodeur, Sekhon, and Goldstein 1977). 1p deletion correlates with *MYCN* amplification and tumor ploidy. While 1p deletion has a negative prognostic impact on di- or tetraploid tumors, there is no effect on survival in triploid tumors (Fong et al. 1989, Kaneko et al. 1999).

17q gain Full or partial gain of chromosome 17 is observed in approximately 50% of NB tumors. 17q gain is strongly associated with 1p deletion and *MYCN* amplification and observed in advanced tumors and patients older than one year of age.

While gain of the whole chromosome is predominantly associated with low-stage tumors, partial gain is observed in high-stage NB (Vandesompele et al. 2001). Thus, 17q gain is of prognostic importance for NB patients.

1.3.3 *MYCN* amplification

MYCN is one of the most prominent proto-oncogenes in NB, with alterations being either copy number increase or amplification on chromosome 2p24 (Schwab et al. 1983). Amplification values can range from 5-fold to more than 500-fold and copy numbers are consistent within one tumor and during different times of tumor growth (Brodeur et al. 1987). Approximately 20% of primary tumors and 50% of high-risk cases harbor a *MYCN* amplification. This correlates highly with an advanced stage of the disease and an unfavorable clinical outcome due to treatment failure (Brodeur et al. 1984, Seeger et al. 1985).

1.3.4 Genomic alterations promoting telomere lengthening

Telomeres are non-coding repetitive DNA sequences at the end of each chromosome preventing chromosomal instability (Moyzis et al. 1988). In combination with the protein complex shelterin, telomeres protect chromosomes from end-to-end fusion, recombination and degradation and allow discrimination from double-strand breaks (Rice et al. 2017, Steensel, Smogorzewska, and Lange 1998). With each replication event, telomere length is shortened ("end-replication problem"), ultimately leading to cellular senescence and thus to a limited lifespan of somatic cells (Hayflick 1965, Olovnikov 1971). Mechanisms to maintain the telomere length can lead to immortalization of cells and is a prominent survival mechanism observed in cancer cells. Telomere maintenance is promoted by increased activation of telomerase, an enzyme adding telomere repeat sequences to the end of telomeres, or by alternative lengthening of telomeres (ALT). Increased telomerase activity is associated with the rearrangement of the telomerase reverse transcriptase (*TERT*) gene and found in 23% of high-risk patients (Peifer et al. 2015, Valentijn et al. 2015). ALT is associated with inactivating mutations of the RNA-helicase *ATRX* gene (α -thalassemia/mental retardation syndrom X-linked) and occurs in 11% of high-risk NBs (Cheung et al. 2012, Molenaar et al. 2012, Pugh et al. 2013, Peifer et al. 2015). *TERT* rearrangement, *ATRX* deletions and *MYCN* amplification occur mutually exclusive and form three subgroups of high-stage NB with unfavorable clinical outcome (Peifer et al. 2015).

1.3.5 Somatic mutations

Similar to other pediatric malignancies, the rate of exonic mutations in NB is very low compared to adult carcinomas. In the first whole genome sequencing (WGS) study of 87 untreated primary NB tumors of all risk stages, a frequency of twelve somatic mutations per tumor was detected (Molenaar et al. 2012). Besides mutations in genes involved in neuronal growth cone stabilization (*ODZ3*, *PTPRD* and *CSMD1*), mutations were also identified in *ATRX*, *TIAM1* (T-cell lymphoma invasion and metastasis 1) and regulators of the Rac/Rho pathway, indicating defects in neuritogenesis. Furthermore, focal deletions of the chromatin remodeling genes *ARID1A* and *ARID1B* were identified (Sausen et al. 2013). In a study of 240 high-risk NBs, *PTPN11* (2.9%) and *NRAS* (0.83%) had a significant somatic mutation frequency besides *ALK* and *ATRX* (Pugh et al. 2013). Comparative analysis of primary and relapse tumors revealed an increased number of mutations in the relapse samples and many of these mutations were assigned to genes of the Ras-MAPK pathway (e.g. *NRAS*, *HRAS*, *KRAS*, *BRAF*, *FGFR1* or *NF1*) (Eleveld et al. 2015, Schramm et al. 2015, Padovan-Merhar et al. 2016). These studies show the importance of clonal evolution and the accumulation of additional genetic alterations in NB, which may have a prognostic impact in the relapse setting.

1.4 Anaplastic lymphoma kinase

ALK is a receptor tyrosine kinase which is closely related to the leukocyte tyrosine kinase (LTK) and ROS receptors, constituting the insulin receptor subfamily of RTKs (Iwahara et al. 1997, Morris et al. 1997). The *ALK* gene was first described as the fusion partner of nucleophosmin (*NPM*) as the result of a t(2;5)(p23;q35) translocation event. Thereby, the NPM-ALK fusion protein contains the N-terminal part of NPM and the C-terminal part of ALK causing a constitutive activation of ALK (Shiota et al. 1994, Morris et al. 1994). In neuroblastoma, expression of oncogenic *ALK* was first described by Lamant et al. in 2000 (Lamant et al. 2000).

1.4.1 The ALK receptor

Human *ALK* is a 26 exon containing gene located on chromosome 2p23.2-p23.1 in close proximity to the *MYCN* oncogene. It encodes for a 177 kDa polypeptide of 1620 amino acids (aa), which is further post-translationally modified by

N-glycosylation into a mature 200-220 kDa large protein (Morris et al. 1997, Pulford et al. 1997). Full-length ALK can be proteolytically cleaved at the extracellular domain, which results in a truncated 140 kDa protein and an 80 kDa protein, which is released into the extracellular space (Moog-Lutz et al. 2005). The mammalian full-length ALK protein consists of an extracellular ligand-binding domain (ECD, aa 1-1038), a transmembrane domain (TM, aa 1039-1059) and an intracellular tyrosine kinase domain (ICD, aa 1060-1620) (Iwahara et al. 1997, Morris et al. 1997). The ECD contains one glycin-rich region (GR) and two MAM (meprin/A5/protein tyrosine phosphatase Mu) domains flanking one LDLa (low-density lipoprotein class A) domain, Figure 1. The ECD functions are ligand binding, interactions with coreceptors and secreted regulatory proteins, as well as dimerization. The ECD of ALK with its two MAM domains enclosing a LDLa domain is unique amongst all members of the RTK (Huang 2018). The TK domain in the ICD contains an amino-terminal lobe (N lobe), composed of a five-stranded antiparallel β -sheet and a single α -helix (α C), and a predominant α -helical carboxy-terminal lobe (C lobe) containing the activation loop (A-loop). N and C lobes are connected by the hinge region, altogether forming a cleft containing the ATP binding pocket. The A-loop contains a Y'XXX'YY autophosphorylation motif, at which the tyrosine at position Y1278 is the first residue to be phosphorylated upon activation (Bossi et al. 2010, Lee et al. 2010). The TK function is to catalyze the transfer of a gamma-phosphate group from adenosine triphosphate (ATP) to a tyrosine residue on a substrate protein.

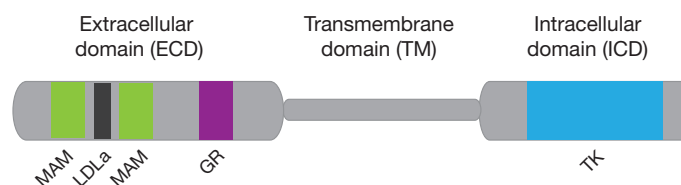


Figure 1: Full-length ALK receptor. ECD - extracellular domain, ICD - intracellular domain, TM - transmembrane domain, green - MAM (meprin/A5/protein tyrosine phosphatase Mu) domain, black - LDLa (low-density lipoprotein class A) domain, purple - GR (glycin-rich) domain, blue - TK (tyrosine kinase) domain. Redrawn from Schulte et al. 2013b.

1.4.2 ALK expression

In a first study on normal tissues and rhabdomyosarcoma, human *ALK* mRNA expression was observed mainly in the central and peripheral nervous system (CNS and PNS) (Morris et al. 1994). Subsequent studies in mice showed *ALK* mRNA expression in the developing brain and spinal cord and in situ hybridization revealed expression in the thalamus, hypothalamus, midbrain, olfactory bulb and cranial

ganglia. High levels of *ALK* mRNA at embryogenesis, starting from day eleven, decrease during gestation and remain at very low neonatal levels (Iwahara et al. 1997, Morris et al. 1997). Consistent with the mRNA decrease, ALK protein also declines postnatal and stays at low levels in adult animals (Iwahara et al. 1997, Vernersson et al. 2006). A similar protein expression pattern was also observed for human ALK, which is expressed at low levels in the adult CNS, mainly located in scattered neural cells, pericytes and endothelial cells (Pulford et al. 1997, Falini et al. 1999). Additional studies from Vernersson et al. showed ALK expression in eye, nasal epithelium, olfactory nerve, tongue, skin, tissue surrounding the esophagus, stomach and midgut, testis and ovary (Vernersson et al. 2006). A study from Reiff et al. showed that ALK can autoregulate its expression via *HAND2*, a phenomenon which was previously reported in glioblastoma (Reiff et al. 2011, Powers et al. 2002).

1.4.3 ALK function in normal development

The normal function of the ALK receptor is still not entirely clear, although the expression patterns of mRNA and protein depicts the importance of ALK in neuronal development. To better understand the function of ALK, several model organisms have been studied. In *Caenorhabditis elegans*, ALK (*ceALK*) was found to inhibit or destabilize presynaptic neural differentiation (Liao et al. 2004). *Drosophila lenaogaster* ALK (*dALK*) is essential for survival and plays a major role in visceral mesoderm development, where loss in *dALK* leads to failure in gut development. Furthermore, *dALK* mediates neuronal circuit assembly in the fly visual system (Loren et al. 2001, Loren et al. 2003, Bazigou et al. 2007). A study in zebrafish by Yao et al. showed that ectopic ALK overexpression promotes cell proliferation and aberrant neurogenesis, while inhibition of endogenous ALK compromises neuronal differentiation and neuron survival in the CNS (Yao et al. 2013). Thus, ALK plays a major role in neural progenitor proliferation, differentiation and survival during embryogenic neurogenesis. In adult mice, ALK plays a crucial role in hippocampal neurogenesis and ALK knockout causes behavioral defects in an antidepressant manner, although the mice are viable and do not show any apparent developmental or anatomical deficits (Bilsland et al. 2008). Furthermore, ALK affects learning and spatial memory as well as the ethanol-related behavior of adult mice (Weiss et al. 2012, Lasek et al. 2011). To study the effect of ALK on the vertebrate sympathetic nervous system development, chick embryos were used as model system. Here, Reiff et al. demonstrated an increased proliferation of immature sympathetic neurons upon ALK activation. Together with its ligand midkine, ALK may control sympathetic neurogenesis (Reiff et al. 2011).

1.4.4 *ALK* alterations in human cancers

Since the discovery of the NPM-*ALK* fusion protein in ALCL in 1994, oncogenically activated *ALK* has been reported in many other tumor entities including haematopoietic malignancies and solid tumors, Figure 2 (Hallberg and Palmer 2013, Lin, Riely, and Shaw 2017). Several mechanisms of *ALK* activation have been reported in human malignancies, including gene fusion, point mutation, overexpression and amplification. These alterations cause an increased *ALK* signaling and show high oncogenic potential.

Gene fusion proteins originate from translocation events and were reported in anaplastic large-cell non-Hodgkin's lymphoma (ALCL), inflammatory myofibroblastic tumor (IMT), diffuse large B cell lymphoma (DLBCL), non-small cell lung cancer (NSCLC), renal medulla carcinoma (RMC), renal cell carcinoma (RCC), breast cancer, colon carcinoma, serous ovarian carcinoma (SOC) and oesophageal squamous cell carcinoma (ESCC). More than 20 fusion genes have been reported to date and within one tumor entity, *ALK* can have several different fusion partners. In general, regulatory regions of the partner gene drive initiation of transcription of the *ALK* fusion protein and the partner protein determines subcellular localization (nucleus and/or cytoplasm) and induces dimerization followed by transautophosphorylation and activation of the *ALK* kinase domain. Interestingly, the prognostic factor of *ALK* fusion varies between cancer entities. While *ALK* translocation in ALCL and IMT correlate with a better prognosis, *ALK* fusions in DLBCL and NSCLC are associated with an unfavorable outcome.

Overexpression and amplification of the *ALK* gene was detected in many different tumor samples and cancer cell lines, including melanoma, NSCLC, neuroblastoma, glioblastoma, rhabdomyosarcoma, ovarian and breast cancer, astrocytoma, ewing's sarcoma and retinoblastoma. In neuroblastoma, both overexpression and amplification of the wild-type *ALK* receptor are associated with unfavorable clinical outcome (Passoni et al. 2009, De Brouwer et al. 2010, Schulte et al. 2011, Duijkers et al. 2012)

Point mutations cause a constitutive *ALK* activation and signaling and were found in neuroblastoma, NSCLC, IMT and anaplastic thyroid cancer (ATC). Secondary mutations acquired during the treatment with small-molecule inhibitors are associated with NSCLC, IMT and ATC, while primary tumor-associated mutations occur mainly in NB but also in NSCLC and ATC.

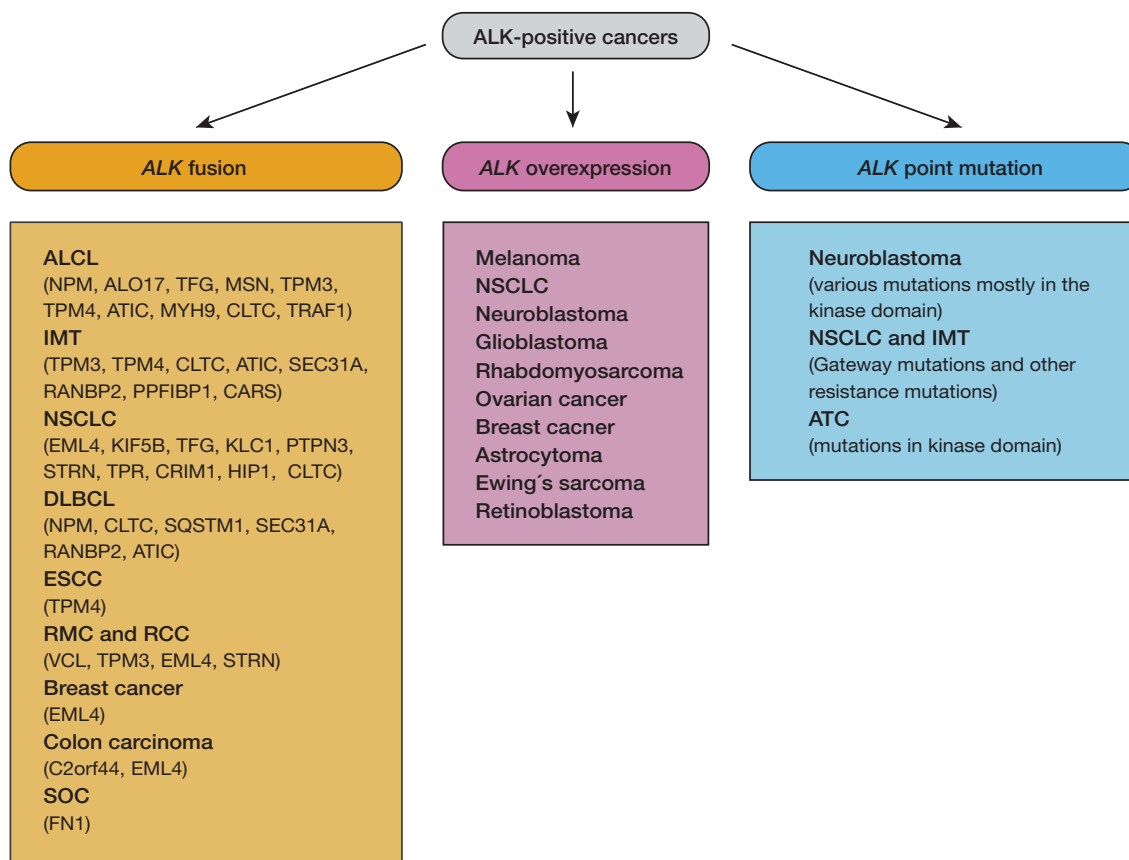


Figure 2: *ALK* alterations in human cancers. Schematic summary of *ALK*-positive cancers. orange - *ALK* fusion proteins, in which the kinase domain of *ALK* is fused to the amino-terminal portion of various proteins (indicated in the brackets) were reported in anaplastic large-cell non-Hodgkin's lymphoma (ALCL), inflammatory myofibroblastic tumor (IMT), diffuse large B cell lymphoma (DLBCL), non-small cell lung cancer (NSCLC), renal medulla carcinoma (RMC), renal cell carcinoma (RCC), breast cancer, colon, carcinoma, serous ovarian carcinoma (SOC) and oesophageal squamous cell carcinoma (ESCC). pink - *ALK* overexpression was detected in melanoma, NSCLC, neuroblastoma, glioblastoma, rhabdomyosarcoma, ovarian cancer, breast cancer, astrocytoma, ewing's sarcoma and retinoblastoma. blue - *ALK* primary and secondary point mutations were found in Neuroblastoma, NSCLC, IMT and anaplastic thyroid cancer (ATC). ALO17 - *ALK* lymphoma oligomerization partner on chromosome 17; CARS - cystein-tRNA synthetase; CLTL - clathrin heavy chain; CRIM1 - cysteine rich transmembrane BMP regulator 1; EML4 echinoderm microtubule-associated protein-like 4; FN1 - fibronectin 1, HIP1 - huntingtin interacting protein 1; KIF5B - kinesin family member 5B; KLC1, kinesin light chain 1; MSN - moesin, MYH9 - myosin heavy chain 9; NPM nucleophosmin; PPFIBP2 - PTPRF-interacting protein-binding protein 1; PTPN3 - protein tyrosine phosphatase non-receptor type 3; RANBP2 - RAN-binding protein 2; SQTM1 - sequestosome 1; STRN - stratin; TFG - TRK-fused gene; TPM - tropomyosin; TRAF1 - TNF receptor associated factor 1; VCL - vinculin. Redrawn from Hallberg and Palmer 2013.

1.4.5 *ALK* alterations in neuroblastoma

ALK is the most recurrently altered gene in neuroblastoma. To date, point mutation, gain/amplification and overexpression have been identified in NB patients and are associated with particularly poor outcome (Janoueix-Lerosey et al. 2008), whereas no case of an *ALK* fusion protein was reported yet. Aberrant copy number status of *ALK* is obtained either by unbalanced gain of large genomic regions at 2p including the *ALK* locus or high-level amplification of *ALK*. Approximately 25% of neuroblastomas harbor a significant copy number increase which is associated with high-risk disease and a poor clinical outcome (Mosse et al. 2008, Janoueix-Lerosey et al. 2008). Similar to other *ALK*-positive cancer entities, genomic rearrangements have also been reported in NB leading to a lack of parts of the ECD. This includes deletion of exons $\Delta 2-3$, $\Delta 4-11$ and $\Delta 1-5$ (Okubo et al. 2012, Cazes et al. 2013, Fransson et al. 2015).

Point mutations, the main alteration of *ALK* in NB, are present in both familial and sporadic cases and were observed in tumor samples and NB cell lines, in an almost mutually exclusive fashion with *ALK* amplification (Caren et al. 2008, Chen et al. 2008, George et al. 2008, Janoueix-Lerosey et al. 2008, Mosse et al. 2008, Martinsson et al. 2011, De Brouwer et al. 2010, Janoueix-Lerosey et al. 2018). A large number of mutations distributed within the ICD have been identified in NB to date, but the majority of *ALK* mutations are located in the kinase domain, with three major hotspots at positions R1275 (43%, R to L/Q), F1174 (30%, F to L/V/S/I/C) and F1245 (12%, F to C/I/L/V) accounting for 85% of all mutations (Bresler et al. 2014). In general, mutations occur in the juxtamembrane region (R1060H, K1062M, T1087I, D1091N, A1099T), P-loop (G1128A), N-lobe (T1151M, I1183T, R1192P), C-lobe (L1240F, R1231Q, I1250T, T1343I, D1349H), α C/A-loop (M1166R, I1170N, I1170S, I1171N, R1275Q, Y1278S), Phe-core (F1174I, F1174L, F1174S, L1240V, F1245C, F1245V), A-loop (G1286R), active site (L1196M, A1200V, D1270G) and other regions (A1234T, A1464STOP) (Janoueix-Lerosey et al. 2018). Chand et al. determined three different classes of *ALK* mutations: (1) gain-of-function ligand-independent, (2) ligand-dependent, and (3) kinase-dead, Figure 3 (Chand et al. 2013). Of these mutations R1275Q, R1192P, T1087I, I1250T, T1152I and G1128A occur as germline mutations (Janoueix-Lerosey et al. 2008, Chen et al. 2008, Mosse et al. 2008, Bourdeaut et al. 2012).

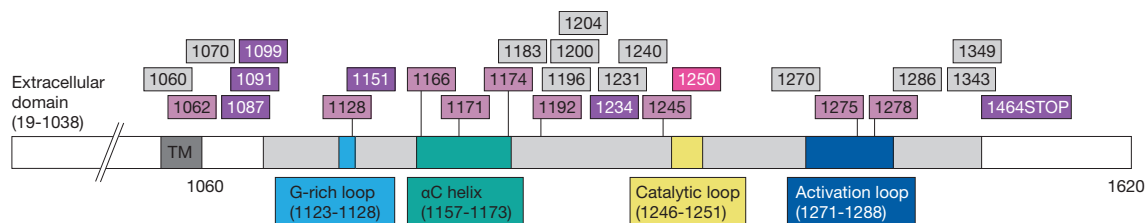


Figure 3: *ALK* mutations in neuroblastoma. Schematic diagram of the full-length *ALK* protein structure and boundaries representing certain domains such as the extracellular domain (1-1038), the transmembrane domain (1039-1059; dark grey) and the tyrosine kinase domain (1116-1392; light grey) including the G-rich loop (1123-1128; light blue), the α C helix (1157-1173; green), the catalytic loop (1246-1251; yellow) and the activation loop (1271-1288; dark blue). Numbers above the schematic diagram indicate verified ligand-independent mutations (pale lilac), ligand-dependent mutations (dark lilac), kinase-dead mutations (pink) and unclassified mutations (grey) in neuroblastomas. Numbers indicate amino acids in the *ALK* 1620 aa long polypeptide. Redrawn and modified from Hallberg and Palmer 2013 and Lin, Riely, and Shaw 2017.

A study on 709 NB tumors revealed a similar frequency of *ALK* mutations in favorable (INSS 1,2 and 4S, 5.7%) and unfavorable (INSS 3 and 4, 7.5%) neuroblastomas (De Brouwer et al. 2010). Furthermore, there was no difference in survival when comparing *ALK* wild-type and mutation or amplification. However, comparison of wild-type and R1275Q with F1174L mutations showed a significant difference in survival. This may be explained by the fact that the frequency of co-occurrence of the F1174L mutation with *MYCN* amplification is much higher compared to R1275Q. Interestingly, the common F1174L mutation has not been detected in the germline of *ALK* patients, which could be explained by a very low survival rate and embryonic lethality when *ALK* F1174L and *MYCN* amplification co-occur.

1.4.6 *ALK* activation and signaling

The wild-type *ALK* receptor is activated by ligand-induced dimerization and subsequent autophosphorylation of the kinase domain. In invertebrates, Jeb and HEN-1 were identified as ligands of d*ALK* and ce*ALK*, respectively (Englund et al. 2003, Lee et al. 2003, Ishihara et al. 2002). In vertebrates, the heparin-binding growth factors midkine (MK) and pleiotrophin (PTN) were initially described as ligands activating mammalian *ALK* (Stoica et al. 2001, Stoica et al. 2002). It was shown that PTN indirectly causes *ALK* phosphorylation by stimulation of the receptor protein tyrosine phosphatase beta/zeta complex (RPTP β/ζ), which also dephosphorylates *ALK* in the absence of PTN (Perez-Pinera et al. 2007). However, the role of PTN as *ALK* ligand remains controversial, as several groups could not confirm a PTN induced ligand-dependent *ALK* activation (Moog-Lutz et al. 2005, Miyake et al. 2002,

Mathivet2007). Recently, Murray et al. described heparin as a specific, high-affinity ALK ligand that binds to a N-terminal region in the ECD causing dimerization and activation by phosphorylation (Murray et al. 2015). Human secreted proteins FAM150A and FAM150B were shown to be ligands for both ALK and LTK, binding to the glycine-rich region of the ECD. While FAM150B is a dual activator of ALK and LTK, FAM150A has a higher specificity for LTK. Furthermore, both proteins can bind constitutively active ALK in NB causing a 'superactivation' (Guan et al. 2015, Reshetnyak et al. 2015).

While the downstream signaling of ALK fusion proteins such as NPM-ALK or EML4-ALK has been well characterized, signaling of full-length ALK has not been studied as extensively, due to the lack of well described ligands. To overcome this limitation, strategies such as generation of chimeras between ALK and various receptor domains, usage of ALK agonist antibodies inducing dimerization or usage of ALK agonist and antagonist antibodies as well as small-molecule inhibitors in NB cell lines, were used (Janoueix-Lerosey et al. 2018). In general, the main pathways triggered by ALK are JAK-Stat3, PI3K-AKT, Ras-MAPK and PLC γ , which are engaged in proliferation, differentiation and survival, Figure 4. However, the signaling pathways activated highly depend on the ALK isoform (full-length or truncated, wild-type or mutated and the fusion partner in ALK fusion proteins) and the sub-cellular localization (Umapathy et al. 2014, Wiesner et al. 2015, Chiarle et al. 2008, Gouzi et al. 2005).

Concerning the full-length receptor and neuroblastoma, major pathways involved in ALK signaling are the Ras-MAPK pathway and PI3K-AKT pathway. These pathways are inactivated upon ALK knock-down or inhibition with small-molecule inhibitors, which was revealed by the dephosphorylation of ERK1/2 and AKT (Stolica et al. 2002, Mathivet, Mazot, and Vigny 2007, Janoueix-Lerosey et al. 2008, George et al. 2008, Bresler et al. 2011, Duijkers et al. 2011, Schonherr et al. 2011, Heukamp et al. 2012, Sattu et al. 2013, Moore et al. 2014, Umapathy et al. 2014, Guan et al. 2016). Additionally, the signal transducer and activator of transcription 3 (STAT3) was identified as ALK downstream target. However, STAT3 phosphorylation and dephosphorylation is delayed compared to ERK1/2 and AKT, suggesting that STAT3 is an indirect target of ALK (Schonherr et al. 2011, Sattu et al. 2013). Several studies demonstrated the transcriptional activation of *MYCN* by ALK (Reiff et al. 2011, Berry et al. 2012, Schonherr et al. 2011, Sattu et al. 2013, Umapathy et al. 2014). Umapathy et al. showed that this activation is mediated by the PI3K signaling cascade including AKT, MEKK3 and MEK5 resulting in the phosphorylation of ERK5 (Umapathy et al. 2014). Phosphoproteomics on ALK altered NB cell lines revealed ALK-dependent cell cycle progression and survival promoted by

the Ras-JNK pathway, in which inhibition of either ALK or JNK causes cell cycle arrest or apoptosis (Chen et al. 2016).

ALK signaling

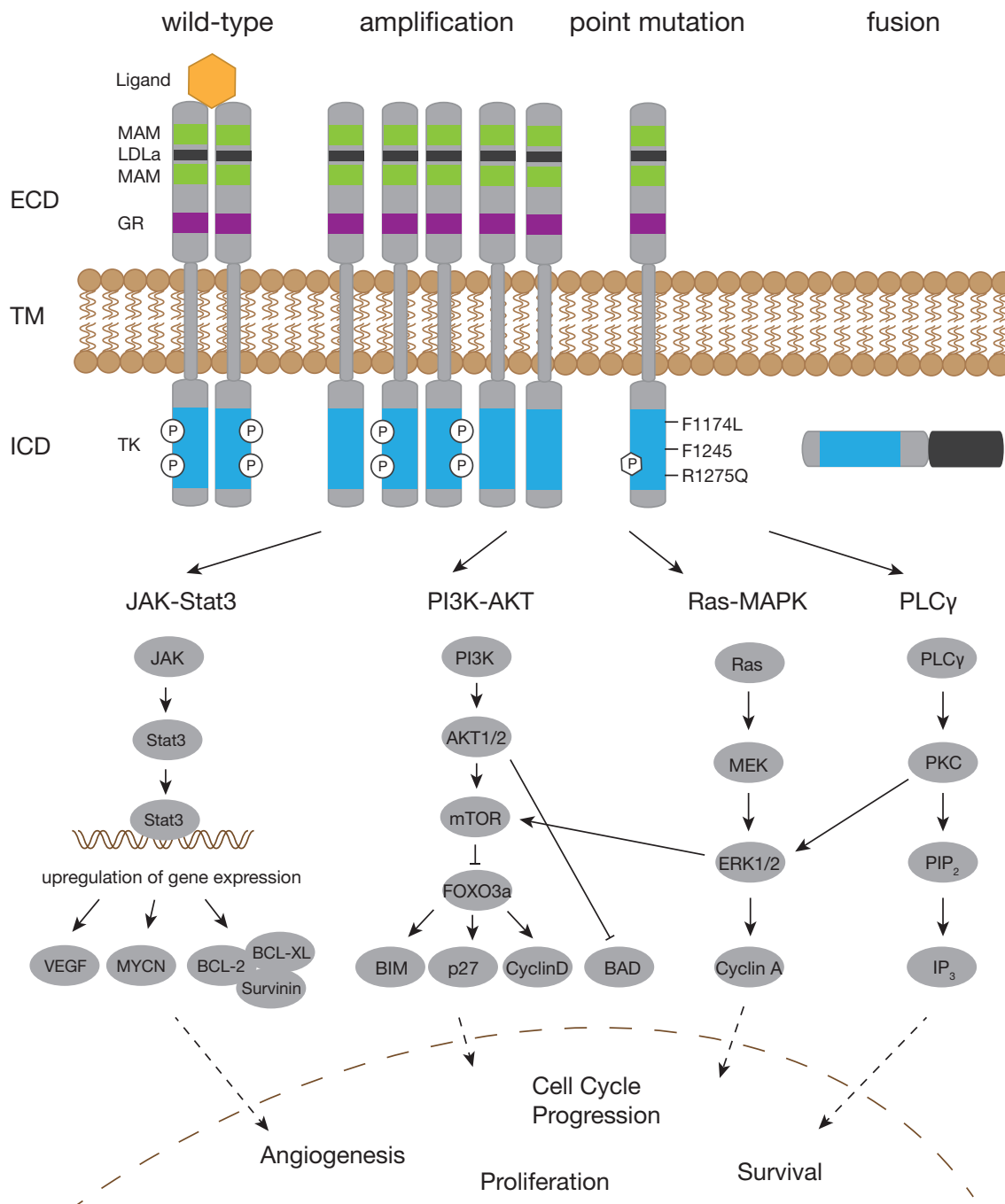


Figure 4: ALK signaling. ECD - extracellular ligand-binding domain, ICD - intracellular tyrosine kinase domain, TM - transmembrane domain, green - MAM (meprin/A5/protein tyrosine phosphatase Mu) domain, black - LDLa (low-density lipoprotein class A) domain, purple - GR (glycin-rich) domain, blue - TK (tyrosine kinase) domain, orange - ligand. P - Phosphate residue. Redrawn from Schulte et al. 2013b.

1.4.7 ALK in neuroblastoma tumorigenesis

Several *in-vitro* and *in-vivo* studies were performed to better understand the role of ALK in NB tumorigenesis. Therefore, the effect of ALK signaling was investigated in murine neural crest progenitor cells (NCPC) MONC-1 and JoMa-1 (Schulte et al. 2013a, Montavon et al. 2014), as well as chick sympathetic neuroblasts (Reiff et al. 2011, Kramer et al. 2016). In NCPCs, ALK expression maintained proliferation and survival, being sufficient to immortalize NCPCs without oncogene MYC. Orthotopic transplantation of these ALK-positive cells into nude mice caused undifferentiated tumor formation but no NB formation, although subcutaneous transplantation of ALK-F1174L-JoMa1 cells led to development of NB-like tumors. In chick sympathetic neuroblasts constitutive activation of the ALK F1174L mutant causes a short term increase in proliferation which subsequently turns into cell cycle arrest, neuron differentiation and long-term survival of postmitotic sympathetic neurons. This suggests that ALK signaling in neuroblasts rather than neural crest progenitors contributes to NB tumorigenesis. A meta-analysis on 254 human neuroblastomas by De Brouwer et al. revealed a higher transforming capacity of the *ALK* F1174L mutation compared to the R1275Q mutation, as well as a positive cooperative effect between *ALK* F1174L and *MYCN* amplification leading to a particularly poor outcome (De Brouwer et al. 2010). To further study this combined ALK and *MYCN* effect in NB tumor formation, several zebrafish and mouse models have been established (Berry et al. 2012, Zhu et al. 2012, Heukamp et al. 2012, Cazes et al. 2014). Hereby, a special focus lies on the F1174L mutation, which has a higher oncogenic potential. In zebrafish, only the combined activation of ALK and *MYCN* led to the formation of tumors comparable to human neuroblastomas, but not ALK alone (Zhu et al. 2012). In mouse models, similar observations were made, where *ALK* expressed under the *Th* or the endogenous promotor was not sufficient to induce tumor formation by itself but only in the presence of *MYCN* amplification (Berry et al. 2012, Cazes et al. 2014). However, under the strong β -actin promotor, ALK alone was able to induce NB tumors (Heukamp et al. 2012). Together, activated ALK and *MYCN* overexpression cooperate to elicit NB tumor development from sympathoadrenal progenitors with a decreased latency of tumor onset compared to tumor initiation by *MYCN* alone.

1.4.8 ALK as a therapeutic target

Oncogenic ALK expression in the form of activating fusion proteins and mutated or overexpressed/amplified proteins has been identified in many different cancer entities. Due to the limited expression of the wild-type receptor in very few adult tissues, ALK serves as an exceeding therapeutic target with few expected toxic side effects. Since the discovery of ALK-positive tumors, several small-molecule tyrosine kinase inhibitors (TKIs) targeting ALK have been developed by academia and pharmaceutical companies (Wan et al. 2006, Christensen et al. 2007, Galkin et al. 2007, Li and Morris 2008, McDermott et al. 2008). These targeted drugs were initially developed and assessed for the treatment of ALK-positive NSCLC patients and only later introduced to the clinical treatment of neuroblastoma (Kwak et al. 2010, Mosse et al. 2013). ALK TKIs are grouped into first (NVP-TAE684, crizotinib), second (ceritinib, alectinib, brigatinib, entrectinib) and third (lorlatinib) generation inhibitors. In general, they are ATP competitive substances binding to the ATP binding pocket in the kinase domain of ALK (Hallberg and Palmer 2016, Umapathy et al. 2019). However, due to their different structures, interactions with kinase residues and subsequent inhibition varies between the drugs. Additionally, most of these inhibitors are not specific for ALK but can also inhibit other RTKs such as c-MET or ROS1 (Christensen et al. 2007, Yasuda et al. 2012).

1.4.8.1 Monotherapy

NVP-TAE684 and crizotinib belong to the first generation of ALK inhibitors and initial studies demonstrated their antiproliferative potential in NSCLC, ALCL and NB cell lines (Galkin et al. 2007, McDermott et al. 2008, Schonherr et al. 2011). While NVP-TAE684 was exclusively used for preclinical testing due to its high toxicity, crizotinib entered the clinic as the first FDA approved ALK inhibitor for the treatment of ALK-positive NSCLC in 2011 (Kwak et al. 2010). In these patients, a good initial response, which was even superior to standard first-line chemotherapy, was reported and similar efficacies were shown in other cancer entities including pediatric patients with ALCL and IMT (Shaw et al. 2013, Mosse et al. 2013, Solomon et al. 2014, Gambacorti Passerini et al. 2014, Mosse et al. 2017). Despite the good initial response, crizotinib treated patients were found to develop a resistance by acquiring secondary mutations in the kinase domain of ALK itself, by activation of bypass signaling pathways (such as EGFR, IGFR, MET, KIT) or by ALK copy number gain (Choi et al. 2010, Camidge and Doebele 2012, Gainor et al. 2016, Dagogo-Jack, Shaw, and Riely 2017). The secondary acquired resistance mutations found in ALK-fusion proteins include positions F1174, F1245 and the gatekeeper

mutation L1196M amongst others, which are common mutations of the full-length ALK receptor in neuroblastoma (Friboulet et al. 2014, Kodityal et al. 2016). A first clinical trial including NB patients demonstrated that ALK inhibitors could be beneficial also for ALK-positive neuroblastomas (Mosse et al. 2013). Due to the crizotinib resistance, a number of second generation ALK inhibitors were developed. While ceritinib, derived from NVP-TAE684, was tested in NB patients in Phase I clinical trials (NCT-01742286, NCT02780128) and alectinib was applied to one extensively treated, refractory, metastatic ALK-F1145C NB patient (Heath et al. 2018), brigatinib and entrectinib are only studied in preclinical models. While ceritinib, alectinib and brigatinib/entrectinib were approved by the FDA in 2014, 2016 and 2017, respectively for the treatment of ALK-positive NSCLC, ceritinib showed high toxicity in NB patients and thus cannot be used for the treatment of ALK-positive neuroblastomas. In general, second generation inhibitors show superior efficacy to crizotinib and can overcome secondary mutations acquired during crizotinib treatment in ALK-fusion proteins (Friboulet et al. 2014, Ignatius Ou et al. 2014, Katayama et al. 2014, Shaw et al. 2014, Tucker et al. 2017, Guan et al. 2018). However, there are several ALK mutations, including G1202R, I1171N/T/S and G1123S, causing a resistance towards these drugs (Toyokawa et al. 2015, Katayama et al. 2014). Thus, third generation ALK inhibitors have been developed, with lorlatinib being FDA approved since 2018 for the treatment of NSCLC patients and already tested in clinical trials in NB (Phase I/II-NANT: New Approaches to Neuroblastoma Therapy). This dual ALK/ROS1 inhibitor is the most potent one when comparing all ALK inhibitors and can overcome almost all resistance mutations (Shaw et al. 2017). Interestingly, an ALK-positive lung cancer patient, with a crizotinib-resistance mutation, acquired a L1198F lorlatinib resistance mutation which resensitized the patient to crizotinib treatment (Shaw et al. 2016). In neuroblastoma, lorlatinib shows strong activity towards almost all mutant variants in *in-vitro* and *in-vivo* assays (Infarinato et al. 2016, Guan et al. 2016).

1.4.8.2 Combination therapy

Despite the reduction of cell proliferation and survival in *in-vitro* and *in-vivo* studies, monotherapies with ALK inhibitors were not effective in ALK-positive NB patients so far. This suggests the emerging need to develop combinatorial approaches including ALK bypass signaling pathways. Several preclinical studies on combinatorial treatments have been performed in ALK-positive NB cell lines and xenografts to address this issue, resulting in synergistic as well as antagonistic effects. Wood et al. showed a synergistic effect of ceritinib with the dual CDK4/6 inhibitor ribociclib, leading to enhanced growth inhibition, cell cycle arrest and caspase independent cell

death (Wood et al. 2017). Similar synergisms of proliferation and tumor growth inhibition was shown in the combined treatment of crizotinib with the ERK5 inhibitor XMD8-92 (Umapathy et al. 2014). Furthermore, combined inhibition of ALK and MDM2 was synergistic in TP53 wild-type NB cell lines and xenografts. However, tumors started growing at discontinuation of the treatment (Wang et al. 2017). In contrast, the inhibition of the Ras-MAPK pathway with the MEK inhibitor trametinib led to an increased AKT activity, advising against a combined treatment (Umapathy et al. 2017). Diverse effects were observed by dual inhibition with crizotinib and the PI3K/AKT/mTOR inhibitor Torin 2 in a MYCN-dependent manner. While the combination reduced proliferation and tumor growth in *ALK* mutated, *MYCN* amplified cells, increased PI3K activity was observed in a wild-type *MYCN* background suggesting an ALK/mTOR/PI3K triple inhibition (Berry et al. 2012, Moore et al. 2014). Indeed, a Phase I clinical trial (NTR-5584) comprising of the ALK inhibitor crizotinib and the dual mTOR/PI3K inhibitor temsirolimus was initiated. Besides the combination of ALK inhibitors with other targeted drugs, Krytska et al. performed a preclinical study in which crizotinib was applied together with the two standard of care chemotherapeutics topotecan and cyclophosphamide (Krytska et al. 2016). In comparison to the single agent treatment, combination therapy achieved synergistic cytotoxicity and higher caspase-dependent apoptosis in NB cell lines and enhanced tumor response and mouse event-free survival. Together, these studies demonstrated that combinatorial treatments could be beneficial for ALK-positive NB patients. However, possible combinations have to be examined carefully in order to avoid antagonistic effect.

1.5 Clinical treatment of neuroblastoma

Based on age, INGR stage, MYCN status and other characteristics, NB patients are grouped into low-risk, intermediate-risk and high-risk, leading to varying therapeutic strategies. These strategies are based on clinical trials conducted on the different risk groups by the American Children's Oncology Group (COG) and the International Society of Pediatric Oncology European Neuroblastoma (SIOPEN). The clinical outcome of low-risk and intermediate-risk patients is excellent, thus these patients receive a highly reduced therapy compared to high-risk patients. In the case of a low-risk disease, surgery alone is sufficient to cure patients suffering from NB, including cases in which the tumor could not be resected completely (Strother et al. 2012, De Bernardi et al. 2008). Furthermore, a subset of these patients show spontaneous regression and are thus being observed only without any treatment (Nuchtern et al. 2012, Hero et al. 2008). Young intermediate-risk patients

with unresectable tumors or disseminated NB without *MYCN* amplification receive a reduced chemotherapy with respect to duration and dosage (Baker et al. 2010, Rubie et al. 2011, De Bernardi et al. 2009, Kohler et al. 2013). Older patients with unresectable tumors and unfavorable histology receive a more intense chemotherapy including radiotherapy. The overall survival of high-risk NB patients is still very low, despite a very extensive multimodal treatment including three blocks: induction, consolidation and post-consolidation therapy, Figure 5. The induction phase starts with five to six cycles of induction chemotherapy which can include several different chemotherapeutic agents (cisplatin, cyclophosphamide, doxorubicin, etoposide, topotecan and vincristine) and surgery. During consolidation, patients are treated with a high-dose myeloablative chemotherapy with several different regimens (cisplatin/etoposide/melphalan, busulfan/melphalan and thiotepa/cyclophosphamide plus cisplatin/etoposide/melphalan). This treatment is followed by autologous hematopoietic stem-cell rescue and irradiation (Matthay et al. 1999). As half of the patients relapse after achieving a clinical remission, a post-consolidation therapy is necessary to treat residual disease. This phase includes the application of cytokines and isotretinoin together with immunotherapy.

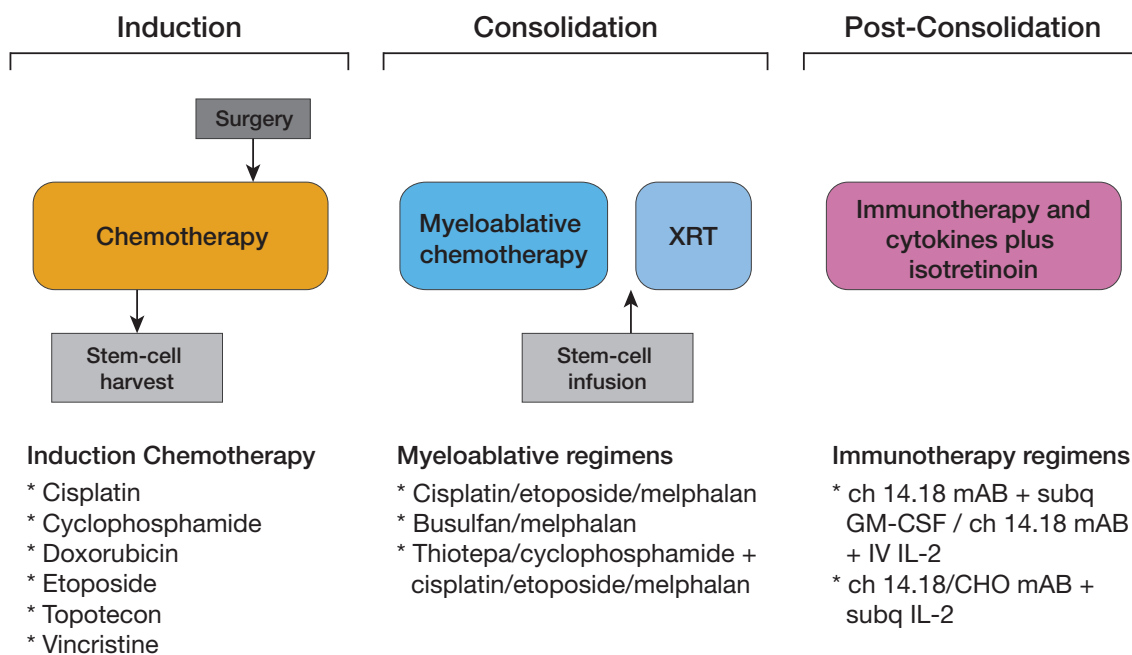


Figure 5: Standard of care treatment of high-risk neuroblastomas. Treatment of high-risk patients consists of induction (chemotherapy and primary tumor resection), consolidation (high-dose chemotherapy with autologous stem cell rescue and external beam radiotherapy [XRT]) and post-consolidation (anti-ganglioside 2 immunotherapy with cytokines and cis-retinoic acid). ch - chimeric, CHO - chinese hamster ovary, GM-CSF - granulocyte macrophage colony-stimulating factor, IL-2 - interleukin-2, IV - intravenous, mAB - monoclonal antibody. Redrawn from Pinto et al. 2015.

1.6 Aim of this study

Neuroblastoma is a very heterogeneous disease that has rare recurrent somatic mutations. This makes it extremely difficult to address therapies with targeted drugs in addition to the standard first-line chemotherapy that NB patients receive. The receptor tyrosine kinase ALK is one of the few druggable targets in NB. In the past years, many different small molecule inhibitors targeting ALK have been intensively studied and some inhibitors are currently used in the clinical treatment of NB patients. However, the introduction of ALK inhibitors in the standard care still remains a major challenge as no optimal treatment regimen for these targeted drugs was determined yet. Furthermore, therapy response of patients treated with an ALK inhibitor is highly variable, as some patients respond very well to the treatment, while others are not affected by the treatment or even gain a resistance mutation during the therapy. Thus, this study is aiming at investigating combination therapies with classical first line chemotherapeutics as well as other targeted drugs. This project is addressing the following questions:

- Is the combination of ALK inhibitors with classical first-line chemotherapeutics beneficial for treatment outcome?

For this purpose, NB cell lines with different *ALK* alterations are treated with combinations of an ALK inhibitor and chemotherapeutics used in the standard care of NB patients. This analysis is aiming at determining for which patients harboring an *ALK* alteration, combination therapies can be beneficial.

- Can the basal gene expression predict the response to treatment with ALK inhibitors?

Some patients receiving treatment with an ALK inhibitor do not respond to the treatment. In order to investigate whether one can predict the therapy outcome, whole transcriptome analysis is performed on cell line as well as patient data.

2 Material and Methods

2.1 Materials

Table 2: Research equipment

Research Equipment	
2200 TapeStation	Agilent Technologies
Cell culture hood Hera	Heraeus
Centrifuges	Eppendorf and Heraeus
DI 15000 Incubator STXG-TIZWX-SET	Tokai Hit
EMCCD camera, Andor iXON3 885	Andor Technologies
EPSON Perfection 2450 Photo Scanner	Epson
Freezing container, Mr. Frosty	Nalgene
iBlot2 Dry Blotting System	Invitrogen
Light Cyclor 480 II	Roche
LUNA automated cell counter	Logos Biosystems
Microscope Nikon Ti-E	Nikon
MACSQuant VYB Analyzer	Miltenyi
NanoDrop ND-1000 Spectrophotometer	Thermo Scientific
Plan Fluor 10X Ph1 DLL objective	Nikon
Plan Apo λ 20X Ph2 DM objective	Nikon
Qubit 2.0 Fluorometer	Invitrogen
SDS-gel electrophoresis chamber	BioRad
Shaking Platform	Heidolf Polymax 2040
Steri-cult CO ₂ incubator	Thermo Scientific
Tecan Sparks	Tecan
Thermo water baths	GFL, Hans Bayer, Julabo
Transfer chamber	BioRad
Vortex Genie	NeoLab

Centrifuge and microcentrifuge tubes, cryo tubes, Cuvettes Semi-Micro and tissue culture flasks, plates and dishes were purchased from Eppendorf, Falcon, TPP, Sarstedt, NalgeneNunc and Greiner Bio-One.

Table 3: Material

Material	
5ml polystyrene round-bottom tubes, cell-strainer cap	Falcon
Agilent High Sensitivity D5000 Screen Tapes	Agilent Technologies
Cell imaging plates, black, 24-well	Eppendorf
iBlot 2 Transfer Stacks, NC, regular size	Thermo Scientific
LUNA cell counter slides	Logos Biosystems
MicroAmp Optical Adhesive Film	Thermo Scientific
Nitrocellulose Membrane, 0.45mm	GE Healthcare
NuPAGE 3-8% Tris-Acetate Midi Protein Gels	Thermo Scientific
NuPAGE 4-12% Bis-Tris Midi Protein Gels	Thermo Scientific
PVDF membrane, 0.45mm	Millipore
PrimeSurface 96U plate	Sbio
qPCR 96-well TW-MT-plate	Biozym
qPCR optical adhesive film	Applied Biosystems
Qubit Assay Tubes	Invitrogen
Super Nalgene Versi-Dry lab soakers	Th Geyer
Whatman 3MM Paper	Whatman Dassel

Table 4: Molecular biology reagents

Molecular biology reagent	
10mM dNTPs	Thermo Scientific
4x NuPAGE Sample Buffer	Thermo Scientific
20x PBS	Santa Cruz
Amersham ECL Prime Western Blotting Detection Reagent	GE Healthcare
BM Chemiluminescence Blotting Substrate	Roche
Bovine Serum Albumin	Sigma
CellTiter Blue Cell Viability Assay	Promega
Clarity Western ECL Substrate	BioRad
EDTA	Carl Roth
EDTA-free Mini Complete Protease Inhibitor Cocktail	Roche
Lipofectamine RNAiMAX	Thermo Scientific
NuPAGE MOPS SDS Running Buffer	Thermo Scientific
NuPAGE Tris Acetate SDS Running Buffer	Thermo Scientific
Oligo(dt) ₂₀ Primer	Thermo Scientific
PhosStop Phosphatase Inhibitor Cocktail	Roche
Ponceau S	Sigma
PowerUp SYBR Green Master Mix	Thermo Scientific
Protein Assay Dye Reagent Concentrate	BioRad
QIAzol Lysis Reagent	Qiagen
RNaseOUT Recombinant Ribonuclease Inhibitor	Thermo Scientific
SuperScript IV Reverse Transcriptase	Thermo Scientific

Table 5: Chemicals and reagents

Chemicals and reagents	
DAPI	Sigma
DMF	Serva
DMSO	AppliChem
Ethanol	Sigma
Formaldehyde 4%	Biolegend
FxCycle Violet Stain	Life Technologies
Giemsa's Azure Eosin Methylene Blue solution	Merck
Glutaraldehyde	Sigma
Isopropanol	Greiner Bio One
Methanol	Greiner Bio One
Nuclease free water	Ambion
Triton X-100	Sigma
Trypan Blue	AppliChem
Tween-20	Merck

Table 6: Kits for molecular biology

Kits for molecular biology	Supplier	Cat.no
CellEvent Caspase-3/7 Green Flow Cytometry Assay Kit	Invitrogen	C10427
Click-it EdU Alexa Fluor 488 Flow Cytometry Assay Kit	Thermo Scientific	C-10420
High-Sensitivity D5000 Reagents	Agilent Technologies	5067-5593
High-Sensitivity RNA ScreenTapes	Agilent Technologies	5067-5592
High-Sensitivity RNA ScreenTape Ladder	Agilent Technologies	5067-5579
High-Sensitivity RNA ScreenTape Sample Buffer	Agilent Technologies	5067-5580
miRNeasy Mini Kit	Qiagen	217004
NEBNext MultiplexOligos for Illumina (Dual Index Primer Set1)	BioLabs	E7600
NEBNext Ultra II Directional RNA Library Prep Kit for Illumina	BioLabs	E7760
Qubit dsDNA HS Assay Kit	Invitrogen	Q32854
Qubit RNA BR Assay Kit	Invitrogen	Q10210
RNase-free DNase Set	Qiagen	79254
RNaseOUT Recombinant Ribonuclease Inhibitor	Thermo Scientific	10777019
SuperScript IV Reverse Transcriptase	Thermo Scientific	18090-200

Table 7: Antibodies for protein detection

Specificity	Host	Supplier	Dilution	Type
β -Actin-HRP	mouse	Sigma	1:5000	primary
AKT	rabbit	Cell Signaling	1:1000	primary
phospho-AKT (Ser473)	rabbit	Cell Signaling	1:1000	primary
ALK	rabbit	Cell Signaling	1:1000	primary
phospho-ALK (Tyr1604)	rabbit	Cell Signaling	1:500	primary
MET	rabbit	Cell Signaling	1:800	primary
p44/42	rabbit	Cell Signaling	1:1000	primary
phospho-p44/42 (Tyr202/204)	rabbit	Cell Signaling	1:1000	primary
Vinculin-HRP	mouse	Santa Cruz	1:2500	primary
Anti Mouse-HRP	goat	Santa Cruz	1:5000	secondary
Anti Rabbit-HRP	goat	Santa Cruz	1:5000	secondary

PageRuler prestained protein ladder (cat.no 26616) or Spectra Multicolor High Range protein ladder (cat.no 26625) purchased from Thermo scientific were used as marker for molecular weight.

Table 8: Oligonucleotides and QuantiTect Primer Assays for qRT-PCR

Gene	Assay ID or Sequence 5'-3'	Cat. No	Supplier
ALK	Hs_ALK_1_SG	QT00028847	Qiagen
CCNE2	Hs_CCNE2_1_SG	QT00063511	Qiagen
CCNG2	Hs_CCNG2_1_SG	QT00998193	Qiagen
KLF7	Hs_KLF7_1_SG	QT00079065	Qiagen
PDCD4	Hs_PDCD4_1_SG	QT00030548	Qiagen
PIK3C2A	Hs_PIK3C2A_1_SG	QT00034013	Qiagen
PTPRE	Hs_PTPRE_1_SG	QT00021567	Qiagen
HPRT1 (for)	TGACACTGGCAAACAATGCA		Sigma
HPRT1 (rev)	GGTCCTTTTCACCAGCAAGCT		Sigma
SDHA (for)	TGGGAACAAGAGGGCATCTG		Sigma
SDHA (rev)	CCACCACTGCATCAAATTCATG)		Sigma

Table 9: siRNA for transient gene knock-down

Target gene	siRNA ID	Sense sequence 5'-3'
MET	s8700	GCACUAGCAAAGUCCGAGAtt
MET	s8701	CACCUUAUCCUGACGUAAAAtt
MET	s8702	GCUACUUAUGUGAACGUAAAtt
PLK1	s448	CCAUUAACGAGCUGCUUAAAtt
Negative control No 1	4390843	not provided
Negative control No 2	4390846	not provided

All siRNAs were Silencer Select siRNAs purchased from Ambion.

Table 10: Neuroblastoma cell lines

Cell line	<i>ALK</i> status	Reference
CHLA-15	R1275Q	Keshelava et al. 1998
CHLA-20	R1275Q	Keshelava et al. 1998
CHLA-90	F1245V	Keshelava et al. 1998
CHP-126	wild-type	Schlesinger et al. 1976
CHP-134	wild-type	Schlesinger et al. 1976
CLB-BAR	amplified	Bouzas-Rodriguez et al. 2010
CLB-GA	R1275Q	Combaret et al. 1995
COG-N-291	wild-type	Farooqi et al. 2014
GI-M-EN	wild-type	Donti et al. 1988
HD-N-33	wild-type	Schwab, unpublished
IMR-32	wild-type	Tumilowicz et al. 1970
IMR-5/75	wild-type	Tumilowicz et al. 1970
KELLY	F1174L	Schwab et al. 1983
KP-N-SI9S	wild-type	Sugimoto et al. 1991
KP-N-YN	wild-type	Sugimoto et al. 1991
LAN-1	F1174L	Seeger et al. 1977
LAN-2	wild-type	Seeger et al. 1977
LAN-5	R1275Q	Seeger et al. 1982
LAN-6	D1091N	Wada et al. 1993
LS	wild-type	Rudolph et al. 1991
MHH-NB-11	wild-type	Pietsch et al. 1988
NB-1	amplified	Miyake S. 1973
NB69	R1275L	Mena et al. 1989
NB-7	wild-type	Westermann, unpublished
NBL-S	wild-type	Cohn et al. 1990b
NGP	wild-type	Brodeur, Sekhon, and Goldstein 1977
NMB	wild-type	Brodeur, Sekhon, and Goldstein 1977
SH-EP	F1174L	Ross, Spengler, and Biedler 1983
SH-SY5Y	F1174L	Biedler et al. 1978
SIMA	wild-type	Marini et al. 1999
SJ-NB-1	wild-type	Van Roy et al. 2006
SJ-NB-12	wild-type	Van Roy et al. 2006
SK-N-AS	wild-type	El-Badry et al. 1989
SK-N-BE(2C)	wild-type	Biedler and Spengler 1976
SK-N-DZ	wild-type	Sugimoto et al. 1984
SK-N-FI	wild-type	Sugimoto et al. 1984
SK-N-SH	F1174L	Biedler, Helson, and Spengler 1973
SMS-KCN	F1174L	Reynolds et al. 1986
SMS-KCNR	F1174L	Reynolds et al. 1986
TET21N	F1174L	Lutz et al. 1996
TR14	R1275Q	Cowell and Rupniak 1983

Table 11: Media and supplements for cell culture

Media and Supplements for cell culture	
OptiMEM (1X)	Gibco Life Technologies
RPMI-1640 (1mM L-Glutamine, 25mM HEPES)	Gibco Life Technologies
RPMI-1640 (1mM L-Glutamine, Phenol-red free)	Gibco Life Technologies
Fetal bovine serum (FBS)	Gibco Life Technologies
Hygromycin B	Sigma
G418	Sigma

Table 12: Cytostatics

Cytostatics	
Cisplatin	Sigma
Doxorubicin	Tocris
Lorlatinib	Tocris
NVP-TAE684	Selleckchem
Tepotinib	Selleckchem
Vincristine	Selleckchem

Software

Adobe Illustrator and Photoshop CS5

ChemiCapt 5000

Fiji 1.0

FlowJo 10.5.3

GraphPad Prism 6.0

ImageJ 1.52q

NIS Elements 5.02.01

R 3.6.0

R Studio 1.0.153

TapeStation Analysis Software 3.1

2.2 Methods

2.2.1 General cell culture methods

2.2.1.1 Culturing of neuroblastoma cell lines

All NB cell lines were cultivated in RPMI-1640 supplemented with 10% FBS at 37°C in a cell culture incubator with 5% CO₂ and 80% humidity. Cell culture medium was substituted with pre-heated medium every 2-4 days and cells were split once or twice per week at ratios 1:3 to 1:15 when cells reached sub-confluence. Therefore, cells were gently detached by incubation in versene (10mM EDTA in 1xPBS, pH 7.0) for 1-5min at 37°C or with normal cell culture medium, depending on the cell line. Cell morphology was observed with a light microscope (Zeiss Axiovert microscope).

2.2.1.2 Cryo-preservation of neuroblastoma cell lines

For cryo-preservation, adherent cells were detached either with normal growth medium or by versenization, centrifuged (800rpm, 5min, room temperature) and re-suspended in ice-cold cryo-preservation medium (RPMI-1640 supplemented with 40% FBS and 10% sterile-filtered DMSO). Cryogenic vials containing 1 ml of the cell suspension were transferred into cryocontainers (Mr. Frosty, Nalgene) and gently cooled down at -80°C overnight before long-term storage in liquid nitrogen.

2.2.1.3 Thawing of neuroblastoma cell lines

For re-cultivation, cryo-preserved cells were thawed at 37°C for approximately 1min and re-suspended in normal growth medium. Cells were allowed to attach overnight before substitution of medium to remove excess DMSO.

2.2.1.4 Spheroid tissue culture

NB spheroids were either cultivated in round-bottom 96-well plates (PrimeSurface 96-U plates, Sbio) or in agarose-coated flat bottom 96-well plates (TPP). For this, flat bottom 96-well plates were coated with 50 μ l of 1% agarose in ddH₂O and left to dry for 2h prior to seeding. Cell suspension with adjusted cell numbers was seeded onto spheroid 96-well plates and incubated for 24h to allow spheroid formation. During this time, plates must not be moved within the cell culture incubator. To

study the effect of chemotherapeutics or kinase inhibitors, drug solution was applied on top of the seeding medium.

2.2.2 Chemotherapeutic and kinase inhibitor treatment

In this study, the following chemotherapeutics and kinase inhibitors were used: doxorubicin (DOX, Tocris), vincristine (VCR, Selleckchem), cisplatin (CDDP, Sigma), lorlatinib (LOR, Tocris), NVP-TAE683 (TAE, Selleckchem) and tepotinib (TEP, Selleckchem). Stock solutions were prepared with the following solvents: H₂O (DOX), DMSO (VCR, LOR, TAE, TEP) and DMF (CDDP). If not otherwise indicated, EC₅₀ values were used as working concentrations. These values were determined with the CellTiter Blue (CTB) viability assay, section 2.2.3, for each cell line and drug individually.

2.2.3 Cell viability and cell confluence assay

CellTiter Blue (CTB) viability assay (Promage) was used to measure metabolic activity in order to determine the viability of the cells during and after drug treatment.

Cells were seeded into black (viability) and transparent (confluence, 2D culture) or round-bottom (spheroid assay) 96-well plates with the following densities: CLB-BAR (8000 c/well), CLB-GA (5000 c/well), IMR-32 (2000 c/well), KELLY (3000 c/well), KP-N-YN (7000 c/well), LAN-1 (1500 c/well), LAN-5 (8000c/well), NB-1 (5000 c/well), NBL-S (3000 c/well), NMB (3000 c/well), SH-EP (500c/well), SH-SY5Y (3000 c/well), SK-N-AS (3000 c/well), SK-N-BE(2C) (2000 c/well), SK-N-FI (8000 c/well) and SMS-KCNR (5000 c/well). Cell numbers were adjusted for each cell line in order to reach 70-80% confluence at the end of the treatment. Cells were incubated overnight to allow cells to attach or form spheroids before treatment with drug solution and appropriate solvent controls for indicated time points.

To determine cell viability, CTB Reagent (Promega) was applied at a ratio of 1:10 for 5h before detection of fluorescence with the Tecan Sparks (Tecan) using 540 nm excitation and 580 nm emission filters. Here, black 96-well plates were used for 2D culture directly. For 3D spheroid cultures, CTB containing medium was transferred from the spheroid plates into black 96-well plates directly before measuring. Control wells containing normal growth medium in the absence of cells were used to correct for background fluorescence. Fluorescence of solvent control wells were set to 100%

and cell viability of the different drug concentrations was calculated as percentage of controls.

Confluence of transparent 96-well plates were measured with the Tecan Sparks using a coverage of each well with 9 images. Confluence of spheroids was determined by measuring the area of the spheroid described in section 2.2.5.2.

2.2.4 Colony formation assay using Giemsa staining

Colony formation assays were performed to evaluate the colony formation capacity of NB cells at drug treatment.

Seeding and drug treatment was performed as described in section 2.2.3. Cells were fixed in 11% glutaraldehyde for 30min, washed 2x 5min in 1xPBS and stained with Giemsa solution (10% Giemsa Azure Eosin Methylen Blue solution in 1xPBS) overnight. After washing 2x 5min in 1xPBS and 1x 5min in ddH₂O, plates were allowed to dry overnight before imaging with an EPSON Perfection 2450 Photo scanner. Images were analyzed with ImageJ using the ColonyArea plugin.

2.2.5 Microscopy

2.2.5.1 Live-cell microscopy

Cells were grown on 24-well glass-bottom cell imaging plates (Eppendorf) in phenolred-free RPMI-1640 medium and imaged every 20min for the indicated time duration. Growth conditions (37°C, 5% CO₂ and 80% humidity) were controlled with a Tokai-Hit incubation system (Tokai Hit Stagetop Incubator STX). Images were acquired with an inverted widefield Nikon Ti-E microscope using an EMCCD camera (Andor iXON3 885) and a Plan Fluor 10X Ph1 DLL objective (Nikon). A light engine lamp (Lumencor) was used to acquire phase contrast images. Cells were tracked in FIJI software using the MTrackJ plugin for manual tracking.

2.2.5.2 Spheroid imaging

Spheroids were generated as described in section 2.2.1.4 and images were acquired for each well individually with the Nikon Ti-E microscope using an EMCCD camera and a Plan Fluor 10X Ph1 DLL objective (Nikon). Images were analyzed with Fiji software to determine the area of the spheroid. Spheroids grown in solvent

controls were set to 100% and confluence of drug treated spheroids was calculated as percentage area of controls.

2.2.6 Flow Cytometry

All flow cytometry samples were measured on the Miltenyi MACSQuant VYB Analyzer and data was analyzed using FlowJo software. For cell cycle analysis, cells with DNA content below that of the G1 fraction were considered dead and excluded for cell cycle analysis with the Dean-Jette-Fox algorithm.

2.2.6.1 Cell cycle

Adherent and non-adherent cells were harvested and centrifuged for 5min at 800rpm. Excess media was removed leaving 500 μ l to re-suspend the pellet. Cells were fixed in a citric acid buffer (0.1 M citric acid in 1xPBS with 0.5% Tween-20) and incubated at 4°C at least overnight but not longer than one week. Cells were washed in 1xPBS and stained with DAPI for 30min before measuring.

2.2.6.2 EdU incorporation

Cells were incubated with 10 μ M EdU 1.5h prior to harvest, fixed and stained with the Click-it Plus EdU Flow Cytometry Assay kit (Thermo Scientific) according to the manufacturer's instructions. After washing, the cells were stained with Violet Blue dye for cell cycle analysis.

2.2.6.3 Caspase

Adherent and non-adherent cells were harvested, centrifuged for 5min at 800rpm, re-suspended in 1 ml medium and stained with the CellEvent Caspase-3/7 Green Flow Cytometry Assay kit (Invitrogen), according to the manufacturer's instructions.

2.2.7 Gene knock-down with siRNA

To perform gene knock-down with short interfering RNAs (siRNA), cells were seeded into 96-well plates (KELLY: 3000 cells and SH-EP: 500 cells in 90 μ l media) and 10 cm dishes (KELLY: 5×10^5 cells and SH-EP: 1.5×10^5 cells in 9 ml media) 24h prior to treatment. Before siRNA knock-down, 10 μ l or 1 ml of a 10 nM LOR solution and corresponding DMSO controls were applied to 96-well plates or 10 cm dishes, respectively. For gene knock-down, siRNAs from a 50 μ M stock solution were diluted in serum-free OptiMEM medium at ratio 1:250. Lipofectamine RNAiMAX transfection reagent was diluted in serum-free OptiMEM at cell line specific ratios (KELLY: 1:50, SH-EP: 1:100). Both solutions were mixed at ratio 1:1 and incubator for 15min at room temperature. 10 μ l or 1 ml of siRNA-RNAiMAX solution was applied to the 96-well plates and 10 cm dishes, respectively. After five days of treatment, 96-well plates were used to determine cell viability and cell confluence with the CTB assay and Giemsa staining, respectively. Cells treated in 10 cm dishes were collected and protein levels of the target genes were determined by western blot.

2.2.8 Quantitative RT-PCR

After the indicated treatment, cells were collected, washed in ice-cold 1xPBS, lysed in QIAzol Lysis Reagent and stored at -80°C . RNA was purified using the miRNAeasy Mini Kit (Qiagen) with an additional DNase digestion step (RNA-free DNase Set, Qiagen) according to the manufacturer's protocol. Concentration of RNA was measured with the Qubit RNA BR Assay (Invitrogen). 500 ng of isolated RNA was reverse transcribed into cDNA using SuperScript IV Reverse Transcriptase (Invitrogen) following the manufacturer's instructions and stored at -20°C until further use. The DNA was quantified in a 96-well format (PCR 96-well TW-MT-plate, Biozym) using the LightCycler 480 II (Roche). To perform the quantitative RT-PCR, the PowerUp SYBR Green master mix (Invitrogen) was used together with QuantiTect primers (Qiagen). For this, 2 μ l of cDNA was mixed with 10 μ l SYBR Green master mix, 2 μ l QuantiTect primer and 6 μ l H_2O . The reaction was carried out with the following conditions: 2min at 45°C , 2min at 95°C and 40 cycles of 15sec at 95°C followed by 30sec at 60°C . A melting curve was assessed at 97°C . The relative gene expression of the target genes and internal reference genes were calculated using the crossing points (ΔCp) method (Morse et al. 2005, Livak and Schmittgen 2001). Results for the target genes were normalized by the two internal reference genes (*SDHA* and *HPRT1*) for comparison between different target genes.

2.2.9 RNA-Sequencing

3×10^6 cells were seeded onto 15 cm petri dishes and treated with $10 \mu\text{M}$ LOR and corresponding DMSO controls respectively for 8h and 24h. Cells were harvested, washed in cold 1xPBS and lysed in QIAzol Lysis Reagent (Qiagen). RNA was purified using the miRNAasy Mini Kit (Qiagen) with an additional DNase digestion step (RNA-free DNase Set, Qiagen) according to the manufacturer's protocol. RNA concentration was determined using the Qubit RNA BR (broad range) Assay Kit (Invitrogen) and quality was assessed with the NanoDrop Spectrophotometer (Thermo Scientific). $1 \mu\text{g}$ total RNA was purified from ribosomal RNA using the NEBNext rRNA Depletion Kit (BioLabs) according to the manufacturer's instructions. The quality of the rRNA-depleted RNA was assessed by running the sample on a TapeStation using the High Sensitivity RNA ScreenTape System (Agilent Technologies) and RNA Integrity Numbers (RIN) were determined. Libraries were prepared with the NEBNext Ultra II Directional RNA Library Prep Kit for Illumina (BioLabs). Based on the measured RINs, fragmentation was performed for 15min at 94°C . Barcodes were added for each individual sample using the NEBNext MultiplexOligos for Illumina Kit (Dual Index Primer Set 1, BioLabs) to multiplex eight samples per one sequencing lane. Seven cycles of enrichment PCR were performed before purification of cDNA with NEBNext Sample Purification beads (BioLabs). Quality of libraries was assessed using the Agilent High Sensitivity D5000 ScreenTape System (Agilent Technologies) on a 2200 TapeStation System (Agilent Technologies). Concentration of libraries was determined with the Qubit dsDNA HS Assay (Invitrogen). Sequencing was performed on an Illumina platform with HiSeq 4000 Paired-end 100bp sequencing type. Quality control and alignment of the raw reads was performed by Dr. Xi Wang and CPM-TMM normalization of read counts was performed by Dr. Umut Toprak.

2.2.10 Protein quantification by SDS-PAGE and western blotting

Protein lysates Cells were seeded onto 15 cm dishes and incubated in indicated drug solution and time points. Adherent and non-adherent cells were harvested, immediately placed on ice, washed in ice-cold 1xPBS and lysed in mPER buffer (mPER supplemented with EDTA-free Mini Complete Protease Inhibitor Cocktail, PhosStop Phosphatase Inhibitor Cocktail and $8 \mu\text{M}$ EDTA) at a concentration of 5×10^5 cells per $10 \mu\text{l}$ mPER buffer. Protein lysates were stored at -80°C at least for 24h before centrifugation for 5min at 13000rpm at 4°C .

SDS PAGE The sodium dodecyl sulfate-polyacrylamide gel electrophoresis (SDS-PAGE) was used to separate proteins. Therefore, protein lysates were mixed with 4x NuPage LDS-Sample buffer (NP007, Thermo Scientific), denatured for 10min at 70°C and loaded into any NuPage Midi Protein gel (Thermo Scientific). Protein lysates of 5x10⁵ cells were loaded when all samples belonged to the same cell line. If protein expression was compared between different cell lines, 50 µg total protein was loaded into the gel. Protein concentration was determined with the Bradford method using Protein Assay Dye Reagent Concentrate (BioRad). Gels were run at 100V.

Western blot Proteins were transferred to a nitrocellulose membrane using the iBlot2 Dry Blotting System (Thermo Scientific) and iBlot2 Transfer Stacks (Thermo Scientific). Proteins with large molecular weight, such as ALK, were transferred to a PVDF membrane in a fully submerged tank transfer system (BioRad) for 2.5h at 100V.

Immunodetection After transfer, the membrane was blocked in blocking buffer (BM Chemiluminescence Blotting Substrate, Roche) for 1h at room temperature, washed 3x 5min in TBS-T buffer (0.01% Tween in 1x TBS) and incubated in primary antibody diluted in TBS-T supplemented with 5% BSA at 4°C overnight. After washing 3x 5min in TBS-T, membranes were incubated in HRP-conjugated secondary antibody diluted in TBS-T for 2h and washed again 3x 5min in TBS-T. Proteins were detected using the Clarity and Clarity Max Western ECL Blotting Substrates (BioRad) or the ECL Plus Western Blotting Detection System (GE Healthcare) and a CCD camera (BioRad).

3 Results

The clinical outcome of neuroblastoma (NB) patients still remains a major challenge, with low long-term survival rates for high-risk patients despite highly aggressive multimodal chemo- and radiotherapy. Thus, a lot of effort was made to introduce novel approaches to the clinical therapy, such as the treatment with targeted drugs. One of the few druggable targets in NB is the anaplastic lymphoma kinase (ALK) and many inhibitors targeting this receptor tyrosine kinase have been both preclinically and clinically studied in the past years. However, to date there is no optimal treatment regimen for ALK inhibitors in the first-line therapy.

3.1 ALK in neuroblastoma patients

The current standard of care of NB patients includes the identification of their genomic *ALK* status. Patients with an *ALK* alteration such as point mutation will receive treatment with an ALK inhibitor. To date, more than 20 different *ALK* mutations were discovered, Figure 3, the majority of which occur at the three hotspots F1174, R1275 and F1245. In the present study, the two main mutations F1174L and R1275Q were used to study the transcriptome of NB patients and the response to ALK inhibitors in NB cell lines.

In this study, whole transcriptome analysis was performed on two patient cohorts, "primary enriched tumors" and "relapsed tumors". The primary enriched tumor cohort included data from 182 patients with mainly primary but also a few relapsed tumors. In this cohort, there were five amplified, nine R1275Q mutated, five F1174L mutated, eight otherwise mutated and 155 wild-type (wt) cases. The relapsed tumor cohort consisted of 81 patients with a relapse disease. This cohort included four amplified, three R1275Q mutated, seven F1174L mutated, seven otherwise mutated and 60 wild-type patients. Distribution of the different *ALK* alterations were calculated as percentage of total patients, Figure 6. Interestingly, the frequency of *ALK* alterations increased from 15% in the primary setting to 26% in the relapse cohort. This was due to an increasing fraction of patients with mutations. While alterations

occurred in a range of 3-5% in the primary enriched tumor cohort, the F1174L and other mutation subgroups each represented 9% of relapsed patients.

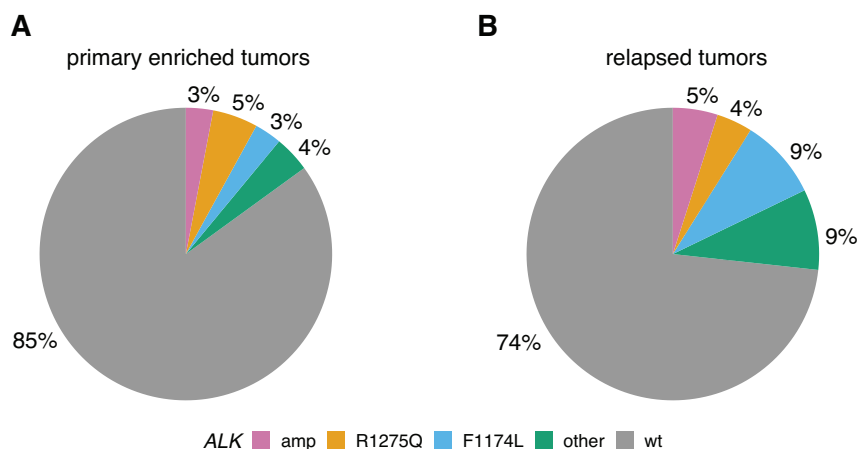


Figure 6: *ALK* mutations occur more often in NB patients with a relapse disease compared to patients with a primary disease. Percentage of patients with a specific *ALK* status in **A** the primary enriched tumor cohort and **B** the relapsed tumor cohort. Patients were grouped into amplified (amp, purple), R1275Q mutated (yellow), F1174L mutated (blue), otherwise mutated (other, green) and wild-type (wt, gray). n=1.

Next, *ALK* expression levels were compared between the five different subgroups. For this purpose, RNAseq data was normalized with the CPM-TMM method and log₂ transformed. Both cohorts had similar expression levels of *ALK*, of which amplified cases had the highest gene expression. Mutated cases had intermediate expression levels and wild-type expression ranged from intermediate to low, Figure 7.

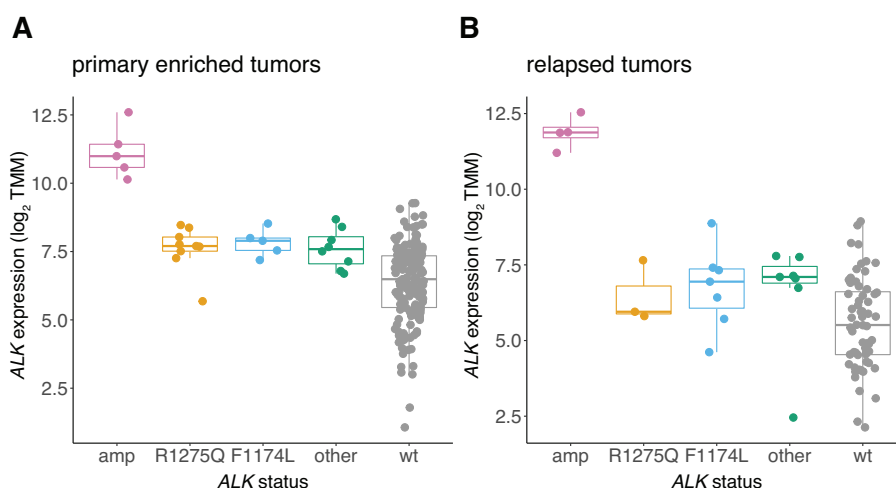


Figure 7: *ALK* expression depends on the *ALK* status and does not vary between primary and relapse disease. *ALK* expression in **A** the primary enriched tumor cohort and **B** the relapsed tumor cohort. Patients were grouped into amplified (amp, purple), R1275Q mutated (yellow), F1174L mutated (blue), otherwise mutated (other, green) and wild-type (wt, gray). n=1.

3.2 ALK in neuroblastoma cell lines

3.2.1 *ALK* status and expression in neuroblastoma cell lines

One aim of this study was to investigate combination treatments for ALK-positive neuroblastomas. Therefore, the genomic *ALK* status of a large panel of NB cell lines, which represented all major genetic lesions found in NB, was determined using whole genome sequencing (WGS), whole exome sequencing (WES) and RNA sequencing (RNAseq) data, Table 10. Results were provided by Dr. Umut Toprak. Fluorescence in situ hybridization (FISH) for *ALK* and *MYCN* genes performed by Dr. Larissa Savelyeva showed a co-amplification of *ALK* with *MYCN* in the NB-1 cell line, Figure 8.

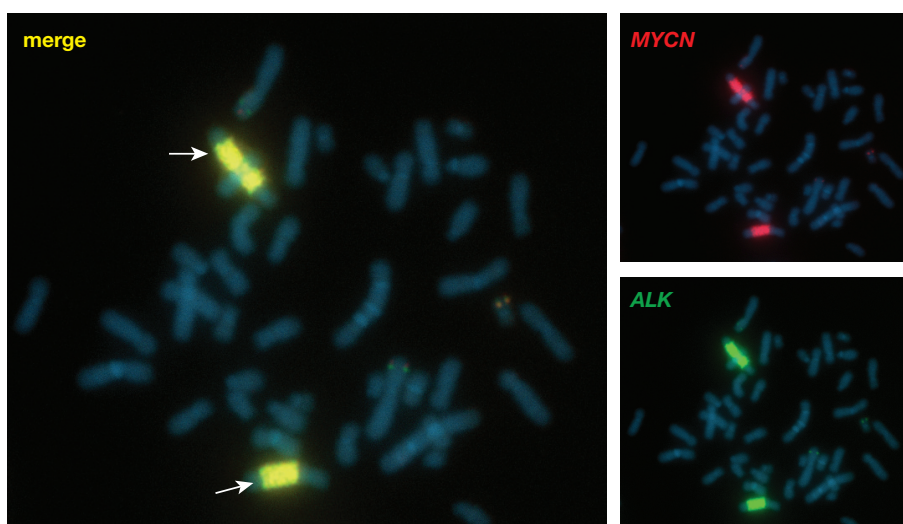


Figure 8: *ALK* is co-amplified with *MYCN* in NB-1 cells. Fluorescence in situ Hybridization (FISH) analysis of *ALK* and *MYCN* in NB-1 cells. Arrows indicate *ALK* and *MYCN* loci. Green: *ALK*, red: *MYCN*, blue: DAPI. Images provided by Dr. Larissa Savelyeva. n=1.

The cell line panel consisted of 39 cell lines with one amplified, five R1275Q mutated, seven F1174L, three otherwise mutated and 23 wild-type cell lines. The *ALK* amplified cell line CLB-BAR was not included in this panel, as there was no RNAseq data available at the time of this study. In general, *ALK* alterations in the cell line cohort occurred at a much higher frequency (42%) compared to both patient cohorts (15% and 26%), Figure 9A. This difference was due to a higher frequency of *ALK* mutations, with 13% R1275Q mutated, 18% F1174L mutated and 8% otherwise mutated cell lines.

Next, the *ALK* expression level of each cell line was determined. One replicate at normal growth conditions was sequenced to determine the gene expression. Read

counts were normalized with the CPM-TMM method and log₂ transformed. This dataset was generated in the laboratory of PD Dr. Frank Westermann and provided by Dr. Umut Toprak. In general, expression levels in the different *ALK* groups were similar to those of NB patients, Figure 9B. Amplified cells had the highest *ALK* expression, while mutated cells had intermediate levels and wild-type cell lines had intermediate to low expression levels.

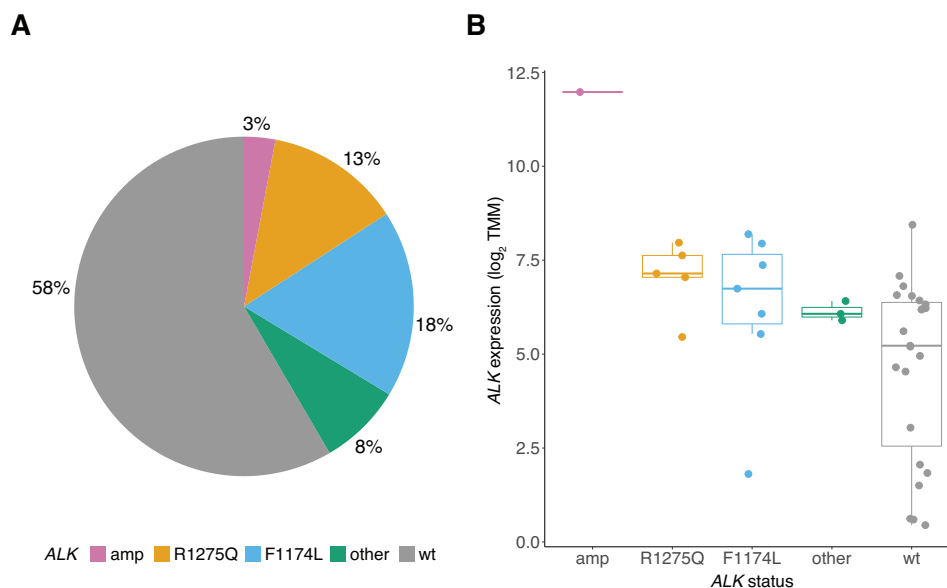


Figure 9: Distribution of *ALK* alterations and expression level in NB cell lines. **A** Percentage of cell lines with a specific *ALK* status. **B** *ALK* expression levels of the cell line panel. Cell lines were grouped into amplified (amp, purple), R1275Q mutated (yellow), F1174L mutated (blue), otherwise mutated (other, green) and wild-type (wt, gray). n=1.

3.2.2 Model cell lines to study therapeutic *ALK* inhibition *in vitro*

Based on the genetic *ALK* status and expression level, a panel of 15 NB cell lines harboring different *ALK* alterations such as amplification and point mutation as well as wild-type cell lines were chosen, Figure 10. Besides NB-1, a second *ALK* amplified cell line CLB-BAR, not shown in Figure 10, was included in the panel. Concerning *ALK* mutations, the focus was on the two main hotspot mutations, R1275Q and F1174L. Selected wild-type cell lines had intermediate, as well as low expression levels of *ALK*, representing the broad expression range found across the patient and cell line cohorts. In total, two *ALK* amplified (NB-1, CLB-BAR), two R1275Q mutated (LAN-5, CLB-GA), four F1174L mutated (SMS-KCNR, LAN-1, SH-SY5Y, KELLY) and seven wild-type (NBL-S, NMB, IMR-32, KP-N-YN, SK-N-AS, SK-N-BE(2C), SK-N-FI) cell lines were studied, Table 13.

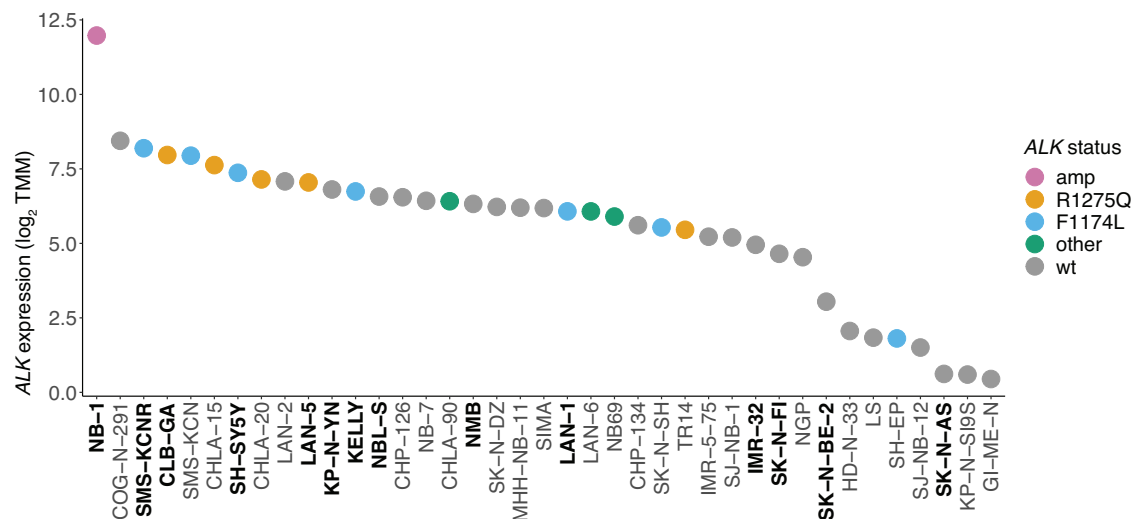


Figure 10: *ALK* expression of the cell line panel. *ALK* expression of the NB cell lines panel. Cells were grouped by their *ALK* status into amplified (amp, purple), R1275Q mutated (yellow), F1174L mutated (blue), otherwise mutated (other, green) and wild-type (wt, gray). Black: model cell lines selected for further analysis. n=1.

Table 13: Model cell lines to study *ALK* inhibition *in vitro*.

Amplified	R1275Q	F1174L	Wild-type
NB-1	LAN-5	SMS-KCNR	NBL-S
CLB-BAR	CLB-GA	LAN-1	NMB
		SH-SY5Y	IMR-32
		KELLY	KP-N-YN
			SK-N-AS
			SK-N-BE(2C)
			SK-N-FI

Next, hierarchical clustering of all cell lines, Figure 11, as well as a principle component analysis (PCA) on the 5000 most variable genes, Figure 12, were performed. Both analyses revealed two small cell line clusters, the mesenchymal cluster including HD-N-33, KP-N-SI9S, SH-EP, SK-N-AS and GI-ME-N, as well as a second cluster containing the NB-7, MHH-NB-11, TR14 and CHP-134 cell lines, which has not been described yet. The chosen model cell lines to study therapeutic inhibition of *ALK* did not form a specific cluster based on their gene expression. This indicates that the selection of cell lines represented a broad range of different gene expression profiles.

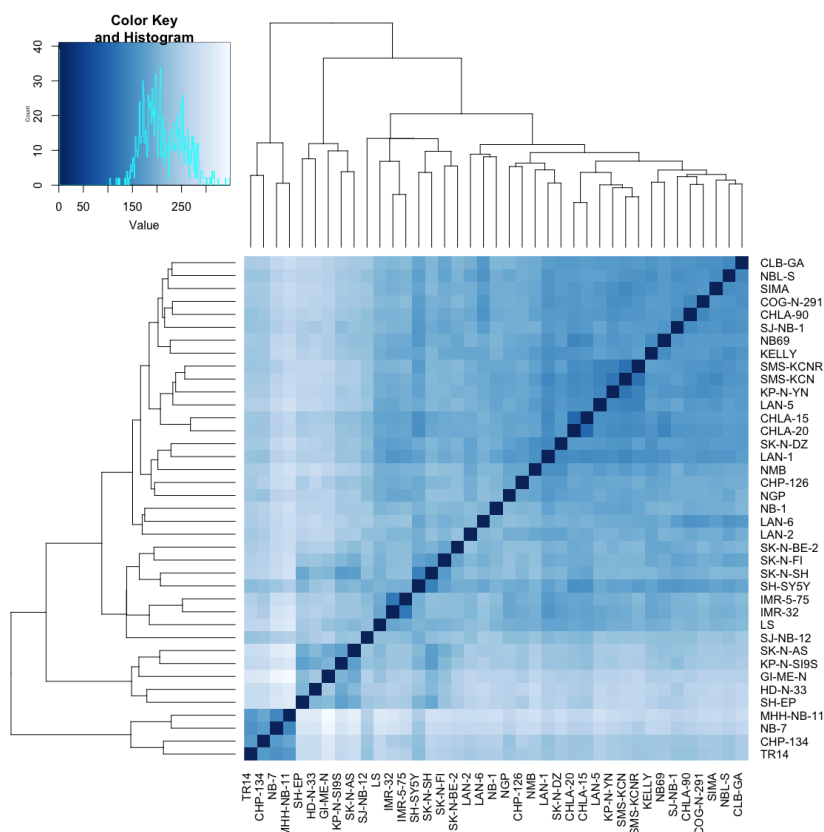


Figure 11: Model cell lines do not form ALK specific clusters based on hierarchical clustering. Hierarchical clustering of the whole NB cell line panel.

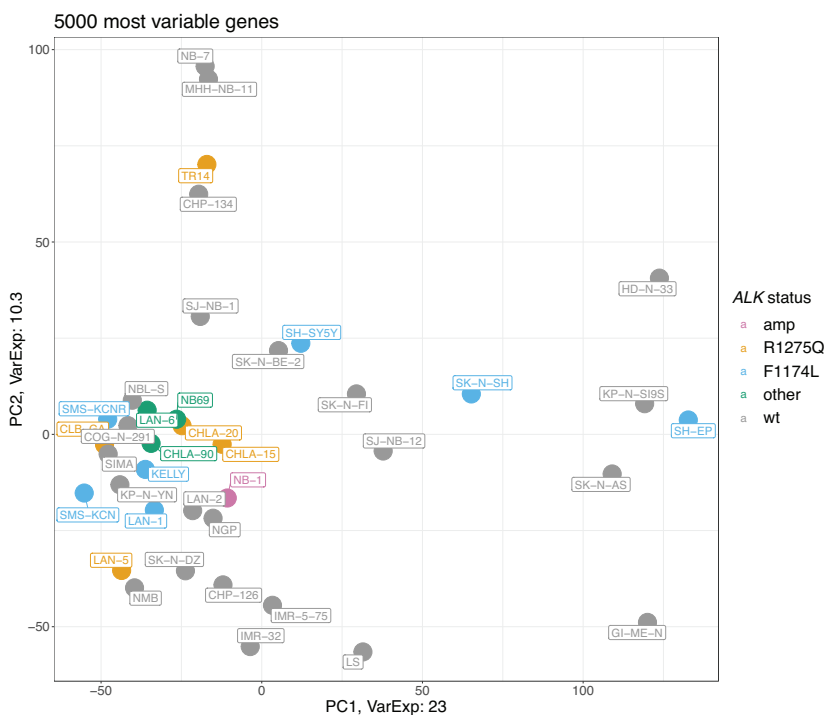


Figure 12: PCA does not result in ALK specific clusters. PCA on the 5000 most variable genes across the whole NB cell line panel.

The provided RNAseq data contained one replicate per cell line and did not include the cell line CLB-BAR. Thus, the relative *ALK* mRNA expression was validated by qRT-PCR. For this purpose, cells were cultured at normal growth conditions, harvested and lysed. RNA was isolated, reverse transcribed and mRNA levels were quantified. The relative *ALK* mRNA expression was calculated by normalization with expression levels of the two internal controls *SDHA* and *HPRT1*, Figure 13A. The highest expression level was detected in the *ALK* amplified cell line CLB-BAR. A much lower expression level was detected for the rest of the cell lines. Here, the F1174L mutated cell lines SMS-KCNR and SH-SY5Y had the second highest expression level followed by two wild-type cell lines NMB and SK-N-BE(2C) and the R1275Q mutated cell lines CLB-GA and LAN-5. KELLY and LAN-1 cells had a much lower *ALK* expression level than the other F1174L mutated cell lines. Low mRNA expression in NB-1 cells was due to the binding of primers to exons 2 and 3, which are deleted in NB-1 cells (Okubo et al. 2012). For the rest of the cell lines, *ALK* expression levels measured by qRT-PCR resembled those determined by RNAseq.

Next, ALK protein levels were determined for all cell lines. Cells were cultured at normal growth conditions, harvested and protein lysates analyzed by western blot, Figure 13B. Three different ALK bands were observed, the full length ALK at 220 kDa, the cleaved ALK at 140 kDa and a second form of truncated ALK at 180 kDa. First, membranes were exposed for 8sec, Figure 13B upper panel. A strong signal was detected for the ALK amplified cell line NB-1. All other cell lines had a much weaker or no detectable signal. Interestingly the second ALK amplified cell line CLB-BAR also had a much lower ALK protein level compared to NB-1. While NB-1 had high expression of full-length and cleaved ALK, CLB-BAR cell lines expressed an ALK protein of 180 kDa. This is due to the deletion of exons 4-11 in CLB-BAR cells which leads to the deletion of the extracellular domain of the ALK protein.

To better detect lower ALK levels, a longer exposure time of 2min 33sec was used, Figure 13B lower panel. In contrast to mRNA expression levels, the R1275Q mutated cell lines CLB-GA and LAN-5 had the highest ALK protein expression among all ALK mutated cell lines. Similar to mRNA expression, the F1174L cell lines SMS-KCNR and SH-SY5Y had higher ALK protein levels compared to KELLY and LAN-1 cells. The wild-type cell lines KP-N-YN, NMB and IMR-32 had similar expression levels compared to KELLY and LAN-1 cells, while SK-N-FI and SK-N-AS cells did not express total ALK protein. All cell lines express low levels of the 180 kDa and 140 kDa ALK.

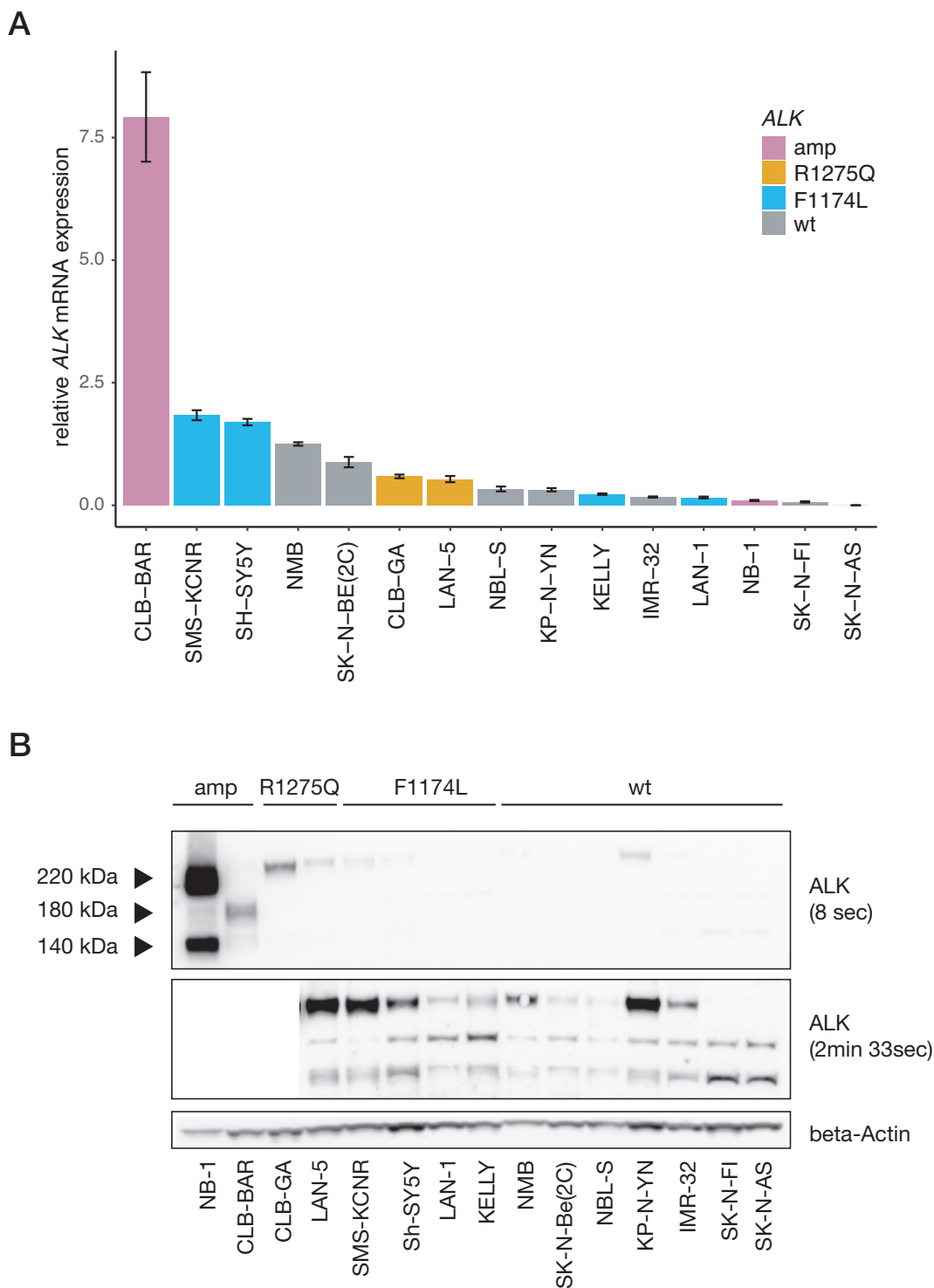


Figure 13: ALK mRNA and protein expression in the model cell lines. A *ALK* mRNA expression. Cells were cultured at normal growth conditions, harvested, isolated RNA reverse transcribed and *ALK* mRNA expression quantified with qRT-PCR. Mean \pm SD. n=3. **B** *ALK* protein expression. Cells were cultured at normal growth conditions, harvested and lysates were analyzed by western blot. Blots were exposed for 8sec (upper panel) and 2min 33sec (lower panel). n=2. One representative experiment is shown.

3.3 Therapeutic targeting of ALK with the third generation ALK inhibitor lorlatinib

ALK is one of the few frequently altered genes in neuroblastoma that can be used in a targeted therapy. Thus, several small molecule inhibitors targeting this receptor tyrosine kinase are currently in clinical trials or already used to treat NB

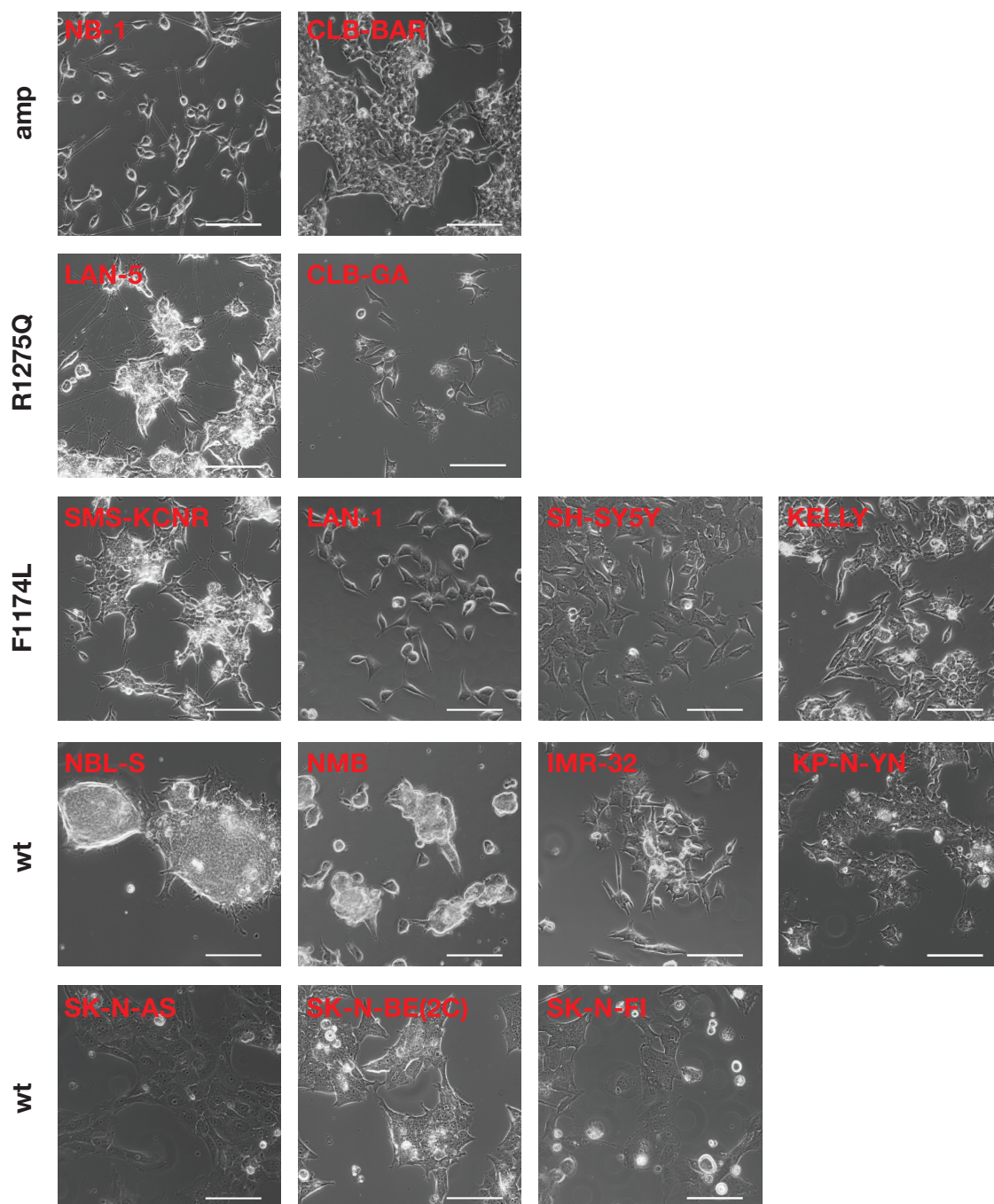


Figure 14: Morphology and growth behavior varies between model cell lines. Images represent the growth behavior of the model cell lines in a monolayer cell culture setting. Scale bar: 100 μm .

patients with an *ALK* aberration such as amplification or mutation. In this study the two *ALK* inhibitors NVP-TAE684 (TAE) and lorlatinib (LOR) were tested on the model cell lines. In order to investigate the response of a cell line to a certain chemotherapeutic or targeted drug, dose response curves are generated. The read-out to generate these curves can be confluence or cell viability among others. Cell viability can be measured with various assays, such as the CellTiter Blue (CTB) viability assay, and is not limited by the growth behavior of different cell lines. To determine the confluence, the percentage of area covered by cells is measured. This is an accurate readout for cell lines that grow in a single layer in culture. To determine whether this is a valid and comparable measurement for all of the selected cell lines, the morphology and growth behavior of the cells was assessed, Figure 14. Many of the cell lines grew in a single layer, where cells grew separated from one another (e.g. NB-1, LAN-1 or SH-SY5Y) or in a dense cell layer (e.g. CLB-BAR, KP-N-YN or SK-N-BE(2C)). A few of the cell lines (LAN-5, SMS-KCNR, NBL-S and NMB) however showed a three-dimensional (3D) growth behavior. These cells grew in multiple layers or formed tumor spheroids adhering to the surface of tissue culture plates. Due to the large difference in growth behavior, cell viability, measured with the CTB assay, was used in this study to determine the response of cell lines to chemotherapeutics and targeted drugs.

3.3.1 Comparison of the two *ALK* inhibitors lorlatinib and NVP-TAE684

In order to determine the sensitivity of NB cell lines to the two *ALK* inhibitors NVP-TAE684 (TAE) and lorlatinib (LOR), the CTB viability assay was performed on a subset of the model cell lines (LAN-5, CLB-GA, KELLY, SH-SY5Y, SK-N-BE(2C) and SK-N-FI). For this purpose, cells were incubated with different concentrations of the two inhibitors for five days and cell viability was determined with the CTB assay, Figure 15. In general, all cell lines showed a higher sensitivity to the first generation *ALK* inhibitor TAE compared to the third generation *ALK* inhibitor LOR. Here, a cell viability of less than 10% could be reached for all cell lines but KELLY and SK-N-FI. In contrast, LOR reduced cell viability in the *ALK* mutated cell lines LAN-5, CLB-GA and SH-SY5Y by approximately 50% only. *ALK* wild-type cells SK-N-FI and SK-N-BE(2C) as well as the F1174L mutated cell line KELLY did not reach the 50% level of inhibition. Considering this, EC50 concentrations were determined for both inhibitors using GraphPad Prism, Table 14. Hereby, EC50 values represent the drug concentration, at which 50% of the maximal effect is reached. This was calculated as 50% between baseline and maximum of the dose

response curve. Generally, EC50 values of TAE were smaller compared to those of LOR, with the exception of CLB-GA. Overall, a larger reduction in cell viability at TAE treatment was observed. The sensitivity of the two *ALK* wild-type cell lines SK-N-BE(2C) and SK-N-FI, which express very low levels of *ALK* protein, to TAE suggested that this inhibitor is not *ALK* specific. Therefore, all subsequent experiments in this study were performed with LOR.

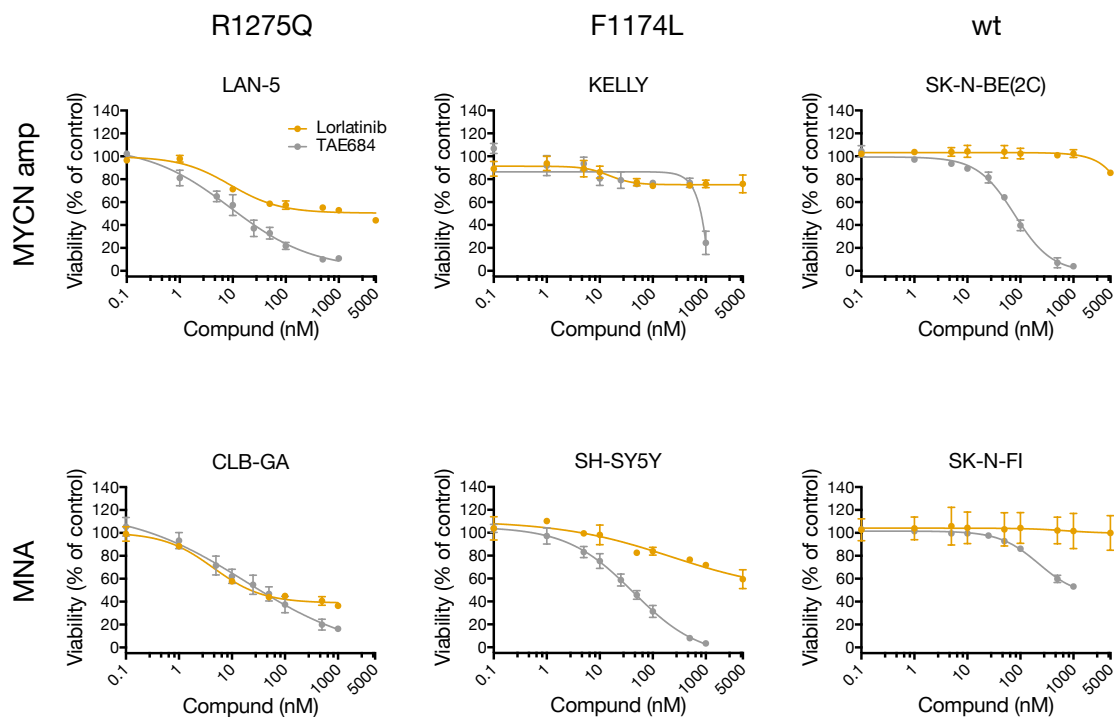


Figure 15: NB cell lines respond differently to NVP-TAE684 and lorlatinib. Six NB cell lines (LAN-5, CLB-GA, KELLY, SH-SY5Y, SK-N-BE(2C) and SK-N-FI) were treated with different concentrations of TAE and LOR and cell viability was measured after five days with the CTB viability assay. GraphPad Prism was used to generate dose response curves and to calculate EC50 concentrations. Gray - TAE, orange - LOR. MNA - *MYCN* non-amplified, MYCN amp - *MYCN* amplified. wt - wild-type. Mean \pm SD. $n=3$.

Table 14: EC50 concentrations of NVP-TAE684 and lorlatinib

Cell line	TAE (nM)	LOR (nM)
CLB-GA	18	4.5
LAN-5	9	10
SH-SY5Y	43	210
KELLY	794	> 5000
SK-N-BE(2C)	77	> 5000
SK-N-FI	221	> 5000

3.3.2 Lorlatinib sensitivity depends on ALK protein levels and activation status

Following the comparison between the two ALK inhibitors, LOR sensitivity was determined for the remaining cell lines of the selected 15 cell line panel, Figure 16, and EC50 values were calculated, Table 15.

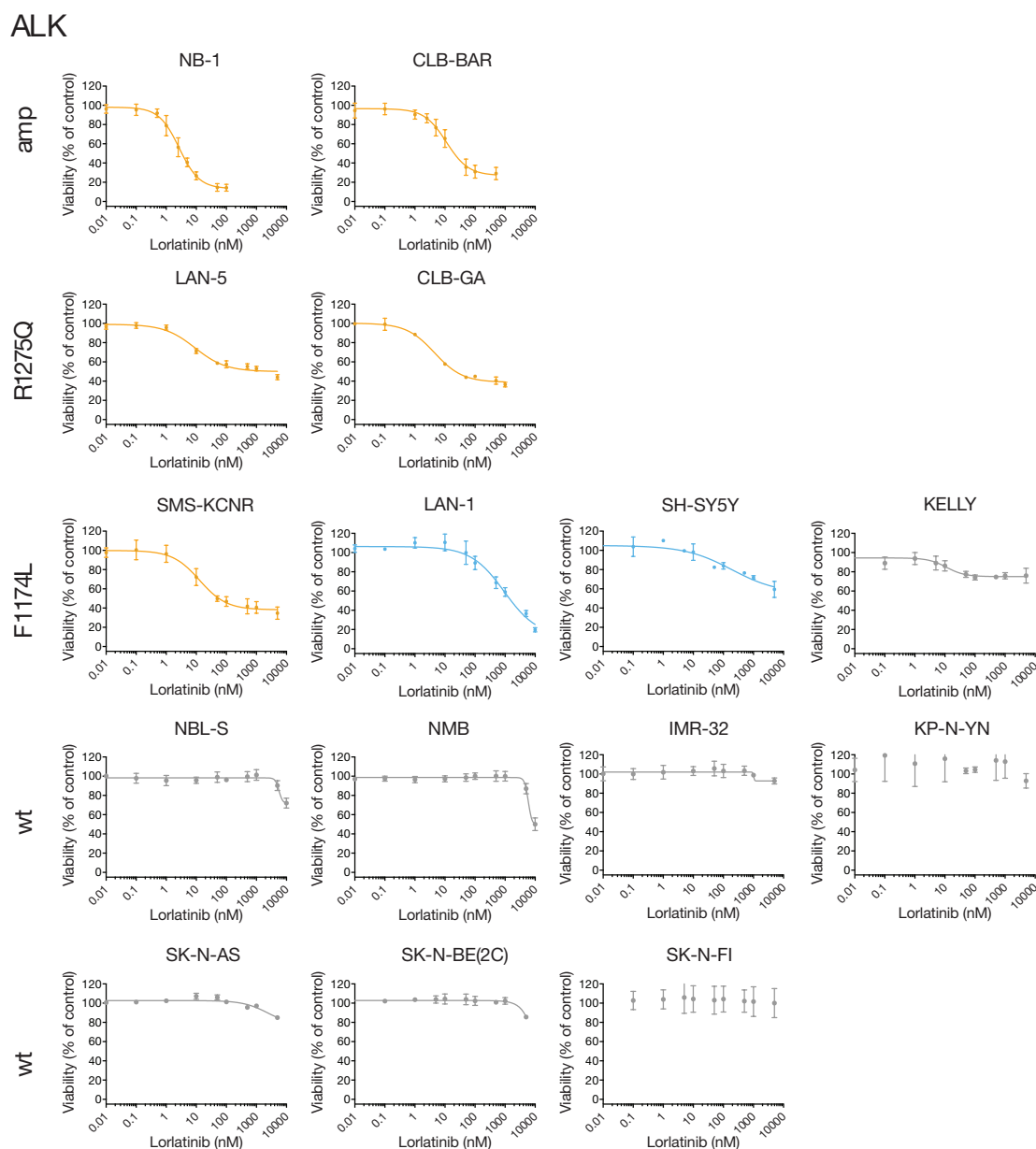


Figure 16: Response to lorlatinib varies between model cell lines. The 15 model cell lines were treated with different concentrations of LOR and cell viability was measured after five days with the CTB viability assay. GraphPad Prism was used to generate dose response curves and to calculate EC50 concentrations. Orange - sensitive, blue - intermediate sensitive, gray - resistant cell lines. wt - wild-type. Mean \pm SD. n=3.

Table 15: EC50 concentration, area under the curve (AUC) and sensitivity of the model cell lines to lorlatinib

Cell line	EC50 (nM)	AUC (%)	Sensitivity
NB-1	2.5	14.52	sensitive
CLB-GA	5	27.95	sensitive
LAN-5	10	51.88	sensitive
CLB-BAR	10	29.40	sensitive
SMS-KCNR	12.5	38.90	sensitive
SH-SY5Y	210	57.71	intermediate sensitive
LAN-1	936	35.06	intermediate sensitive
KELLY	> 5000	82.38	resistant
NBL-S	> 5000	90.67	resistant
NMB	> 5000	81.58	resistant
IMR-32	> 5000	95.74	resistant
KP-N-YN	> 5000	94.75	resistant
SK-N-AS	> 5000	84.52	resistant
SK-N-BE(2C)	> 5000	85.71	resistant
SK-N-FI	> 5000	96.32	resistant

Both *ALK* amplified cell lines NB-1 and CLB-BAR as well as the F1174L mutated cell line LAN-1 were affected most by LOR with a reduction in cell viability to 14%, 28% and 24%, respectively. However, LAN-1 response was observed at much higher concentrations (EC50: 936 nM) compared to NB-1 and CLB-BAR (EC50: 2.5 nM and 10 nM). For CLB-GA, LAN-5 and SMS-KCNR cells, a reduction in viability to approximately 50% was observed with EC50 values of 5 nM, 10 nM and 12.5 nM. For KELLY cells and all wild-type cell lines an effect was observed only at LOR concentrations $> 5 \mu M$.

In addition to EC50 values, the area under the curve (AUC) was calculated to also account for remaining viability at high LOR concentration, e.g. seen for LAN-5. For this purpose, dose response curves were generated with the 'drc' package in R by fitting a four-parameter log-logistic function, Figure 17. Then, the area under the fit was calculated and normalized by the total area, Table 15. The total area was calculated as the area of the rectangular enclosing the fit. This includes a concentration range of 10^{-2} to 10^4 nM and the maximal fitted viability for each cell line. EC50 and AUC values were positive correlated throughout the cell line panel, Figure 18. The cell lines LAN-1 and LAN-5 were exceptions with a small AUC (35.06%) and a high EC50 (936 nM) and a high AUC (51.88%) and a low EC50 (10 nM), respectively. According to EC50 and AUC values, cell lines were grouped into LOR sensitive (low EC50 and AUC: NB-1, CLB-BAR, LAN-5, CLB-GA and SMS-KCNR), intermediate sensitive (intermediate EC50 and low or intermediate AUC:

LAN-1 and SH-SY5Y) and resistant cell lines (high EC50 and AUC: KELLY, NBL-S, NMB, IMR-32, KP-N-YN, SK-N-AS, SK-N-BE(2C) and SK-N-FI), Table 15.

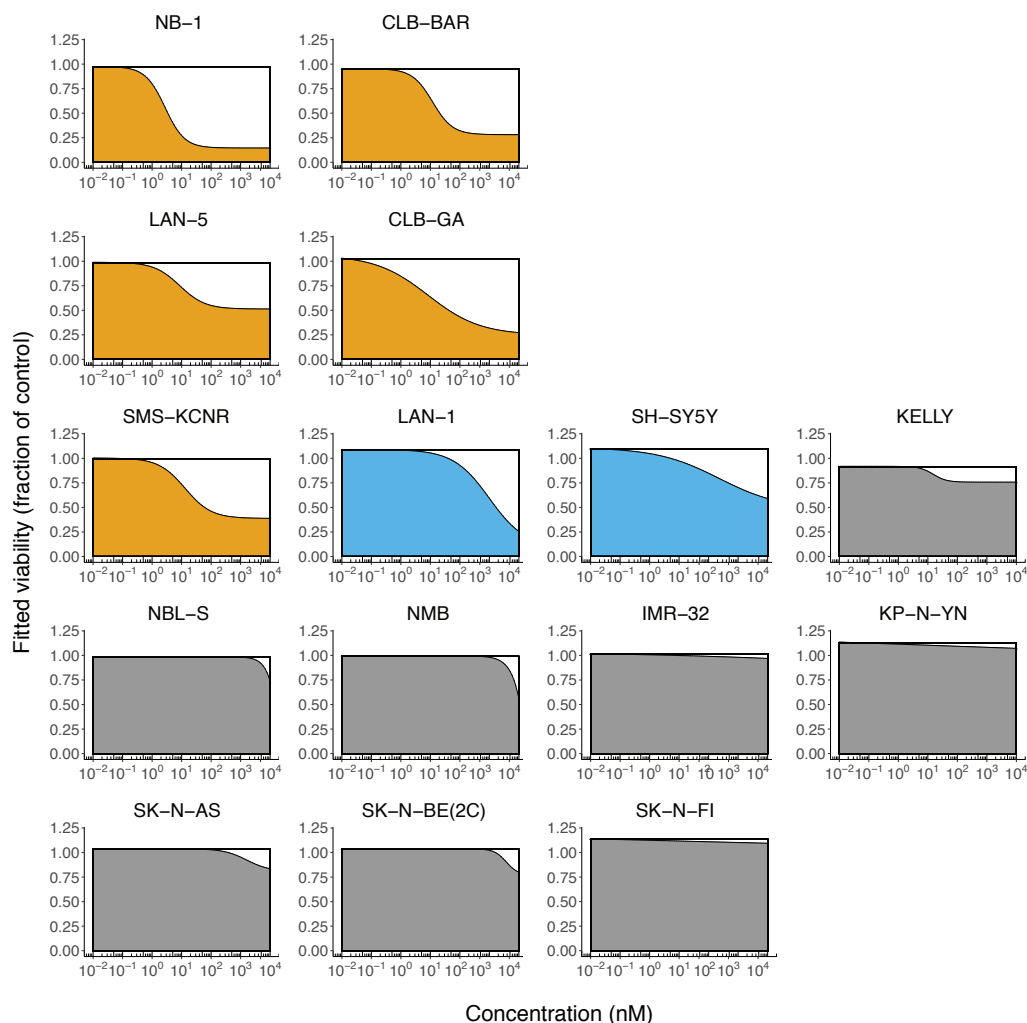


Figure 17: Area under the curve at lorlatinib treatment. Dose response from data shown in Figure 16 was fitted to a four-parameter log-logistic function and the area under the curve was calculated as percentage of the total area, represented by the rectangular. Orange - sensitive, blue - intermediate sensitive, gray - resistant cell lines.

Notably, EC50 values in the range of 10 nM could be activated in clinical application. Therefore, all cell lines in this range were assigned as sensitive. While *ALK* amplified and R1275Q mutated cell lines were sensitive and wild-type cells were resistant, F1174L mutated cell lines showed different levels of sensitivity to LOR. SMS-KCNR were sensitive, LAN-1 and SH-SY5Y were intermediate sensitive and KELLY cells were resistant to the treatment. Interestingly, LAN-1 and KELLY cells have a similar genetic background - same *ALK* mutation and expression level, *MYCN* amplification and a *TP53* mutation - but showed a different response to the treatment. LAN-1 was sensitive while KELLY was not effected by LOR even at high concentrations.

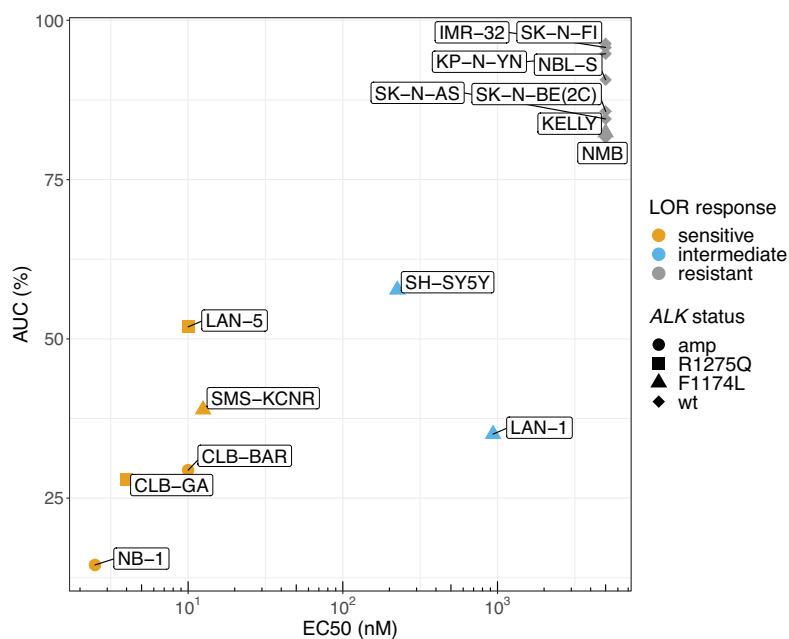


Figure 18: EC50 and AUC values are positively correlated. EC50 values and normalized AUC values were correlated for the tested cell line panel. A positive correlation was observed, with LAN-1 and LAN-5 being outliers. LAN-1 had high EC50 and little residual viability at high LOR concentrations, while LAN-5 behaved in the opposite way.

Additionally, EC50 values were correlated with RNAseq *ALK* expression levels, Figure 19. CLB-BAR cells were excluded from this analysis, as there were no RNAseq data available at the time of this study. In general, cell lines with high *ALK* expression levels had EC50 values in the low nanomolar range. However, this applied only for *ALK* amplified or mutant cell lines. Wild-type cell lines with intermediate high *ALK* mRNA and protein expression levels, such as KP-N-YN, NBL-S or IMR-32, had high EC50 values. Thus, a high *ALK* protein level and activation by amplification or mutation is necessary for a high LOR sensitivity.

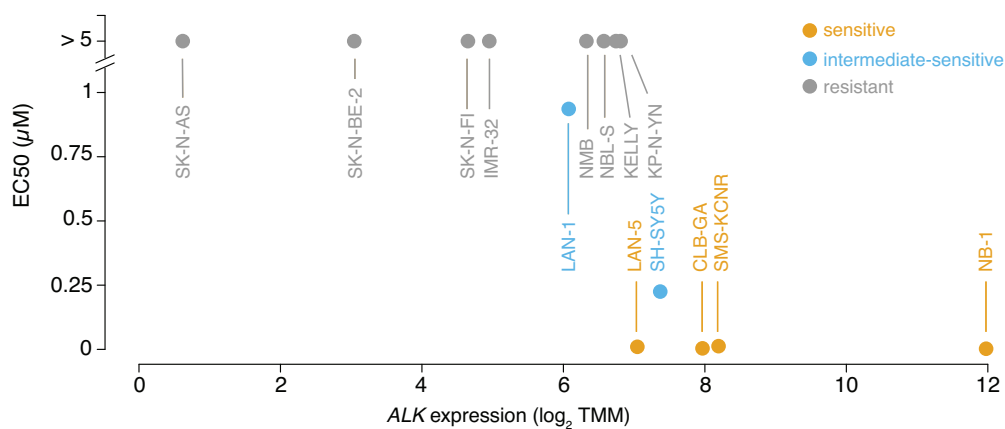


Figure 19: Lorlatinib response depends on *ALK* expression. EC50 concentrations were correlated with normalized *ALK* expression levels.

3.3.3 Lorlatinib causes dephosphorylation of ALK targets

The response of the model cell lines to the ALK inhibitor LOR was used to classify cells into sensitive, intermediate sensitive and resistant. Sensitive cell lines NB-1,

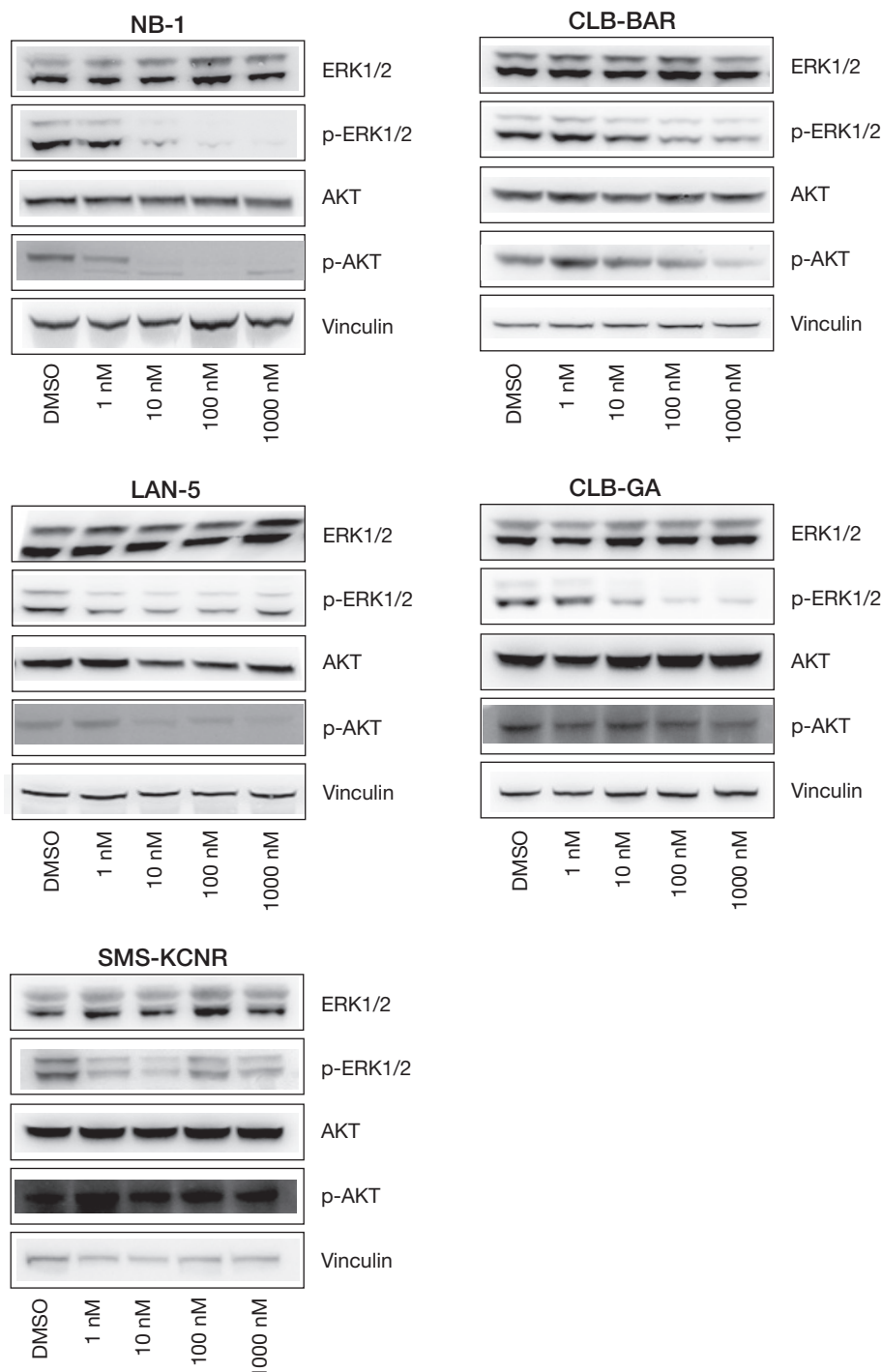


Figure 20: Lorlatinib causes dephosphorylation of ALK targets of LOR-sensitive cell lines. Protein expression of ERK1/2 and AKT in LOR treated cells. LOR-sensitive cell lines were treated with different concentrations of LOR and a corresponding DMSO control for 6h. Total and phosphorylated protein was measured by western blot. p-ERK1/2 Tyr202/Tyr204. p-AKT Ser473. n=2. A representative experiment is shown.

CLB-BAR, LAN-5, CLB-GA and SMS-KCNR were further used to investigate the effect of LOR on the ALK downstream targets ERK1/2 and AKT. For this purpose, cells were treated with different doses of LOR for 6h, harvested and protein levels measured by western blot. Expression levels of total ERK1/2 and AKT as well as the phosphorylated proteins at residues tyrosine 202/204 and serine 473, respectively, were determined, Figure 20. In general, LOR treatment caused a reduction in phosphorylation of both proteins with a stronger effect on ERK1/2. NB-1 cells had a small reduction in phosphorylation for 1 nM and a stronger reduction for 10 nM for both proteins. Proteins were almost completely dephosphorylated at a treatment with 100 nM and 1000 nM LOR.

CLB-BAR and CLB-GA cells had a similar decrease in phosphorylation of ERK1/2 to the NB-1 cell line. However, the overall effect was weaker in these two cell lines. No gradual dephosphorylation of ERK1/2 was seen in LAN-5 and SMS-KCNR cells. However, a slight decrease in phosphorylation of the treated samples compared to the control samples was observed. Concerning AKT, CLB-BAR, LAN-5 and CLB-GA cells had a slight decrease in phosphorylation compared to the control. In SMS-KCNR cells, LOR treatment did not effect the phosphorylation of AKT.

Taken together, LOR inhibited ALK signaling which resulted in a partial dephosphorylation of the ALK targets ERK1/2 and AKT. The effect of LOR on NB-1 cells was stronger compared to the rest of the cell lines, which was in accordance with the response in cell viability observed previously, section 3.3.2.

3.3.4 The highly LOR-sensitive cell line NB-1 gains resistance after continuous treatment with lorlatinib

The ALK "addicted" cell line NB-1 was highly susceptible to LOR, which can be seen by the large effect on cell viability and the dephosphorylation of ALK downstream targets upon LOR treatment. To see how these cells respond to a continuous treatment with LOR, cells were cultured in 1 nM, 2.5 nM or 5 nM LOR for four weeks. From now on, these cells will be named NB-1-R. For each concentration three independent NB-1-R cell lines were generated, NB-1-R #1,#2,#3. At the end of this long-term treatment, the overall morphology of NB-1-R cells was similar to DMSO treated NB-1 cells that were cultured in parallel, Figure 21. For both untreated and treated cell lines, cells grew mainly as single cells but formed cell contacts with others cells. However, the general vitality of NB-1-R cells was weaker compared to NB-1 cells, especially for the two higher concentrations 2.5 nM and 5 nM.

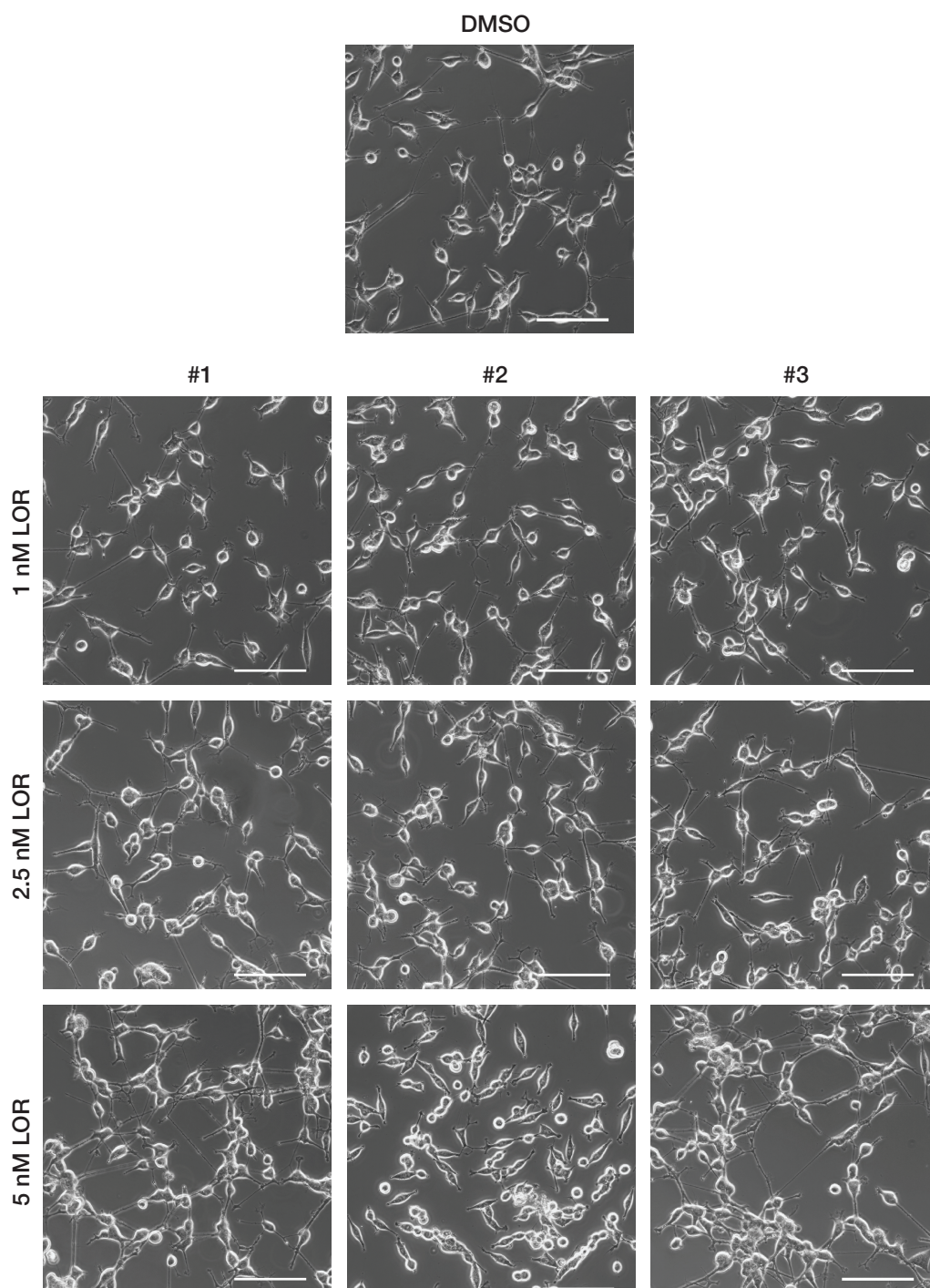


Figure 21: Long-term treatment with lorlatinib does not change morphology of NB-1 cells. NB-1 cells were treated with 1 nM, 2.5 nM or 5 nM LOR for four weeks and medium was changed every three days. Images were acquired after the long-term culture in LOR. Scale bar: 100 μm .

In order to investigate whether the long term treatment has an effect on the response to LOR, both NB-1 and NB-1-R cells were treated with 2.5 nM LOR, the EC₅₀ of LOR for NB-1 cells, for five days. Cell viability was measured with the CTB assay and cell confluence was determined with Giemsa staining. Viability and confluence were calculated as percentage of DMSO treated control samples, Figure

22,23. 2.5 nM and 5 nM treated NB-1-R cells had significantly higher cell viability and confluence after LOR treatment compared to normal NB-1 cells. This indicates that NB-1 cells gained resistance after long-term exposure to LOR, despite a good initial response.

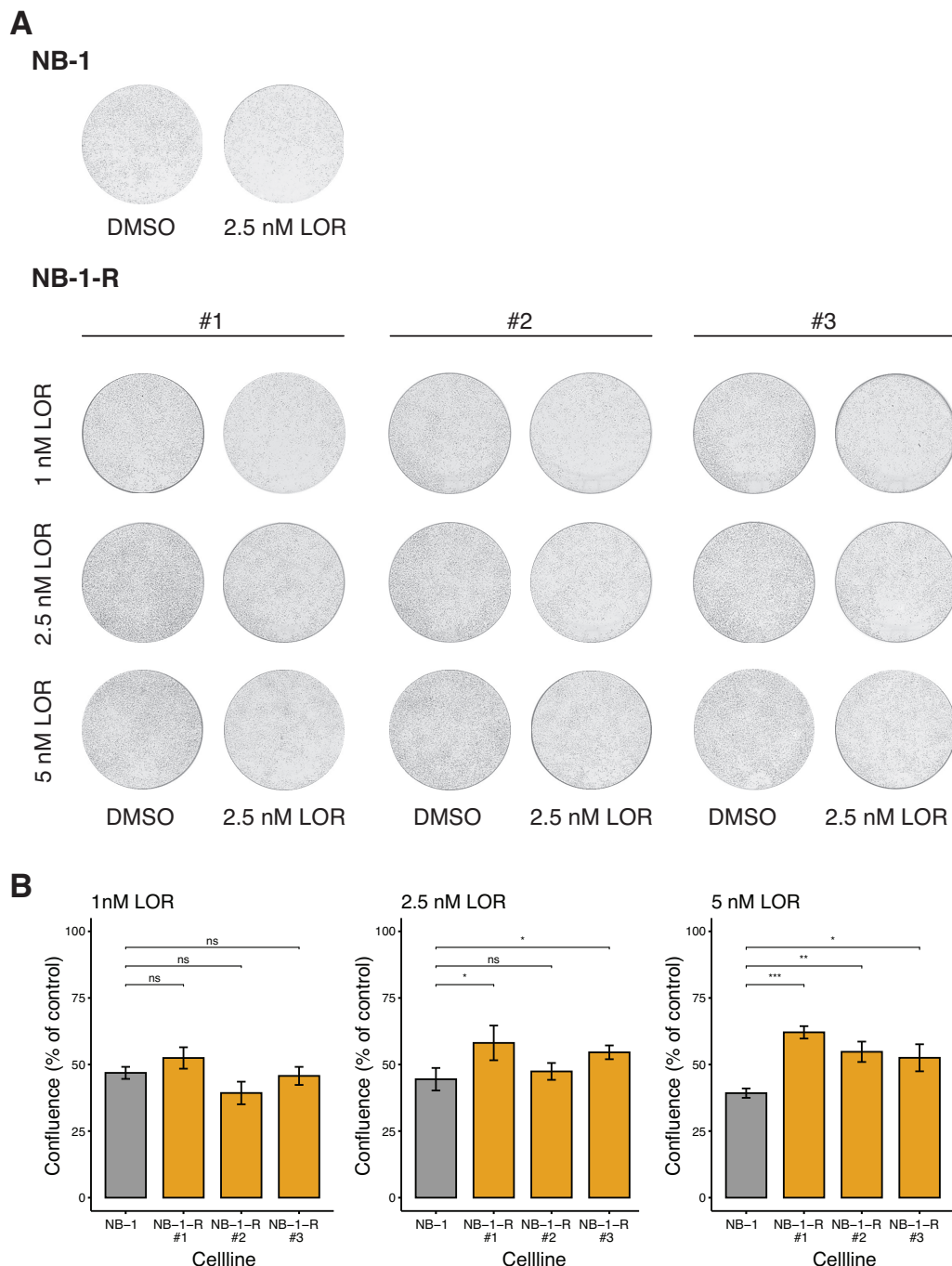


Figure 22: Lorlatinib reduces cell confluence less in NB-1-R cells compared to NB-1 cells. NB-1 and NB-1-R cells were treated with 2.5 nM LOR for five days and stained with Giemsa to determine cell confluence. **A** One representative Giemsa staining. **B** Normalized confluence. Gray - parental NB-1 cells, orange - LOR-resistant NB-1-R cells, that were treated with 1 nM, 2.5 nM or 5 nM LOR for four weeks, respectively. Mean \pm SD. n=3. Statistical analysis was performed with an unpaired t-test, ns: $p > 0.05$, *: $p < 0.05$, **: $p < 0.01$, ***: $p < 0.001$.

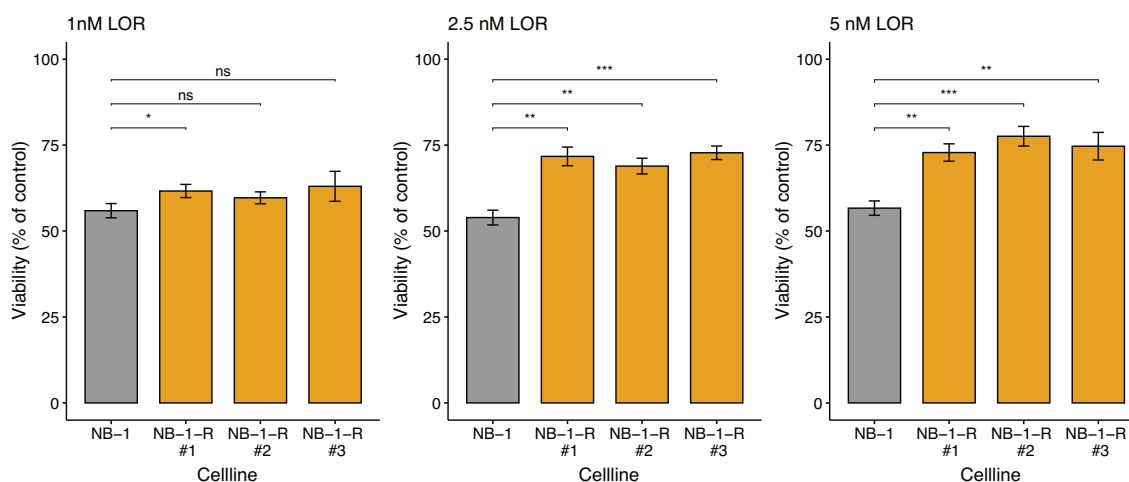


Figure 23: Lorlatinib reduces cell viability less in NB-1-R cells compared to NB-1 cells. NB-1 and NB-1-R cells were treated with 2.5 nM LOR for five days and cell viability was measured with the CTB assay. Gray - parental NB-1 cells, orange - LOR-resistant NB-1-R cells, that were treated with 1 nM, 2.5 nM or 5 nM LOR for four weeks, respectively. Mean \pm SD. $n=3$. Statistical analysis was performed with an unpaired t-test, ns: $p > 0.05$, *: $p < 0.05$, **: $p < 0.01$, ***: $p < 0.001$.

3.4 ALK-addicted cells benefit from combination treatment of lorlatinib with chemotherapeutics

3.4.1 Chemotherapeutics cause phase-specific cell cycle arrest

ALK inhibitors are currently in clinical use as monotherapies. However, to date it is unclear how to include these drugs in the first-line care of NB patients. Therefore, this study aimed at evaluating the combination of lorlatinib with vincristine (VCR) and cisplatin (CDDP), two chemotherapeutics used in the induction chemotherapy of NB treatment (Pinto et al. 2015). These two chemotherapeutics were chosen due to their different mode of action. CDDP is a DNA intercalating agent resulting in DNA damage and thus the inhibition of transcription and replication. In contrast, VCR is a spindle toxin which blocks mitosis by interfering with microtubule dynamics. Treatment of the NB cell line SH-EP TET21N with CDDP caused a predominant cell cycle arrest in G1 phase, while VCR treatment lead to a predominant G2 arrest, Figure 24. ALK inhibitors are currently in clinical use as monotherapies. However, to date it is unclear how to include these drugs in the first-line care of NB patients. Therefore, this study aimed at evaluating the combination of lorlatinib with vincristine (VCR) and cisplatin (CDDP), two chemotherapeutics used in the induction chemotherapy of NB treatment (Pinto et al. 2015). These two chemotherapeutics were chosen due to their different mode of action. CDDP is a DNA intercalating

agent resulting in DNA damage and thus the inhibition of transcription and replication. In contrast, VCR is a spindle toxin which blocks mitosis by interfering with microtubule dynamics. Treatment of the NB cell line SH-EP TET21N with CDDP caused a predominant cell cycle arrest in G1 phase, while VCR treatment lead to a predominant G2 arrest, Figure 24.

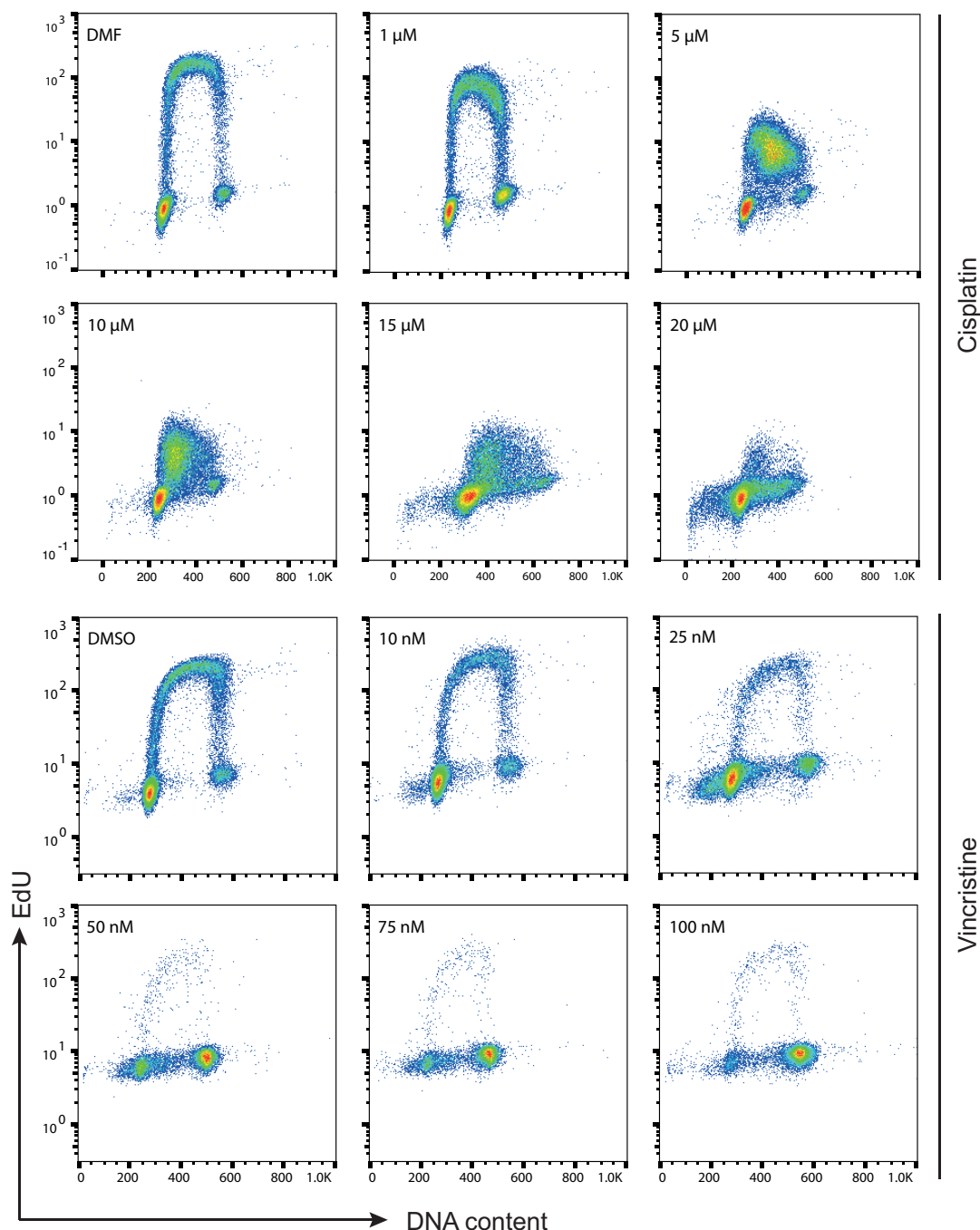


Figure 24: Chemotherapeutics cause phase-specific cell cycle arrest. SH-EP TET21N cells were treated with different concentrations of cisplatin (CDDP) and vincristine (VCR) for 24h and cell cycle progression was determined by flow cytometry. DNA content determined by DAPI vs. DNA synthesis (S-Phase) determined by EdU incorporation. n=3. A representative experiment is shown.

3.4.2 Combination treatment is effective only in ALK-addicted cell lines

Following the analysis of single agent treatment with LOR on cell lines with a different *ALK* status, the combination of LOR with the two chemotherapeutics CDDP and VCR was investigated. For this purpose, all cell lines with an *ALK* mutation or amplification as well as the two wild-type cell lines SK-N-FI and SK-N-BE(2C) were studied. Cells were treated with different concentrations of the chemotherapeutics as a single agent and in combination with the cell line specific EC50 concentration of LOR. Resistant cell lines were treated with 1 μM LOR. Cell viability was measured with the CTB viability assay after five days of treatment. Dose response curves were determined with GraphPad Prism, Figure 25,26, and used to calculate EC50 concentrations, Table 16,17. For both chemotherapeutics, a combinatorial effect was detected only for LOR sensitive and LOR intermediate sensitive cell lines. For KELLY cells and both wild-type cell lines, dose response curves for both mono- and combination treatment were highly similar. Concerning the remaining cell lines, a reduction in cell viability was seen for low chemotherapeutic concentrations. This reduction represented the effect of the specific EC50 concentrations of LOR on the different cell lines. EC50 concentrations of LOR in the *ALK* amplified cell lines NB-1 and CLB-BAR, as well as the two F1174L mutated cell lines SMS-KCNR and LAN-1 caused a larger reduction in viability than observed in the other *ALK* mutated cell lines. This resulted in a larger difference between the dose response curves of mono- and combination treatment. With increasing concentrations curves of the mono- and combination treatment overlapped, which indicated that the LOR effect was overtaken by the cytotoxic effect of the chemotherapeutics.

ALK

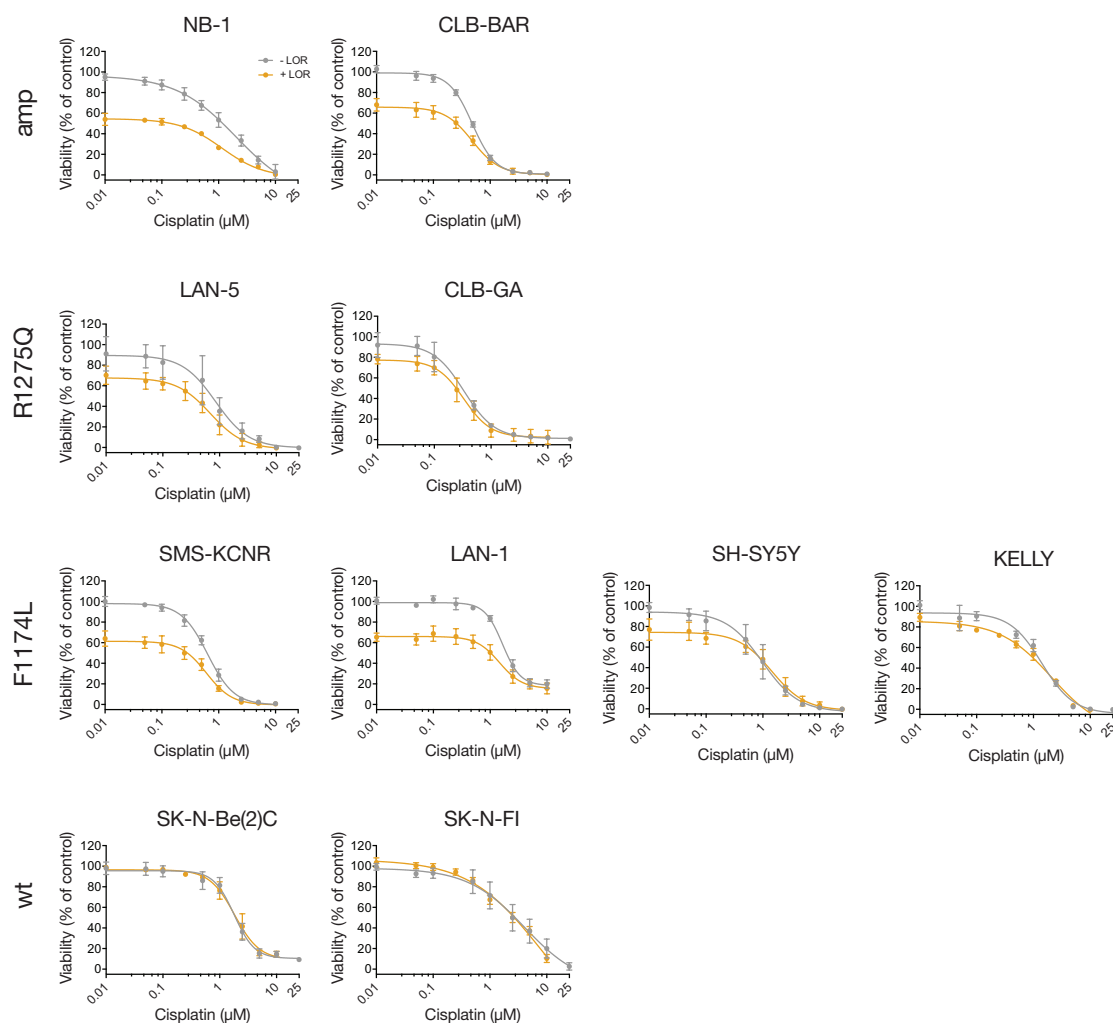


Figure 25: ALK sensitive and intermediate sensitive cell lines respond differently to combination treatment with lorlatinib and cisplatin. A selection of the 15 cell line panel was treated with different concentrations of CDDP alone or in combination with EC50 concentrations of LOR for five days and cell viability was determined with the CTB assay. GraphPad Prism was used to determine dose response curves and EC50 values. Gray - CDDP alone, orange - CDDP + EC50 LOR. Mean \pm SD. $n=3$.

Table 16: EC50 concentrations of cisplatin for LOR-sensitive cell lines at mono- and combination treatment.

Cell line	CDDP (μM)	CDDP + LOR (μM)
NB-1	2.05	1.18
CLB-BAR	0.48	0.48
LAN-5	0.85	0.68
CLB-GA	0.33	0.33
SMS-KCNR	0.64	0.61

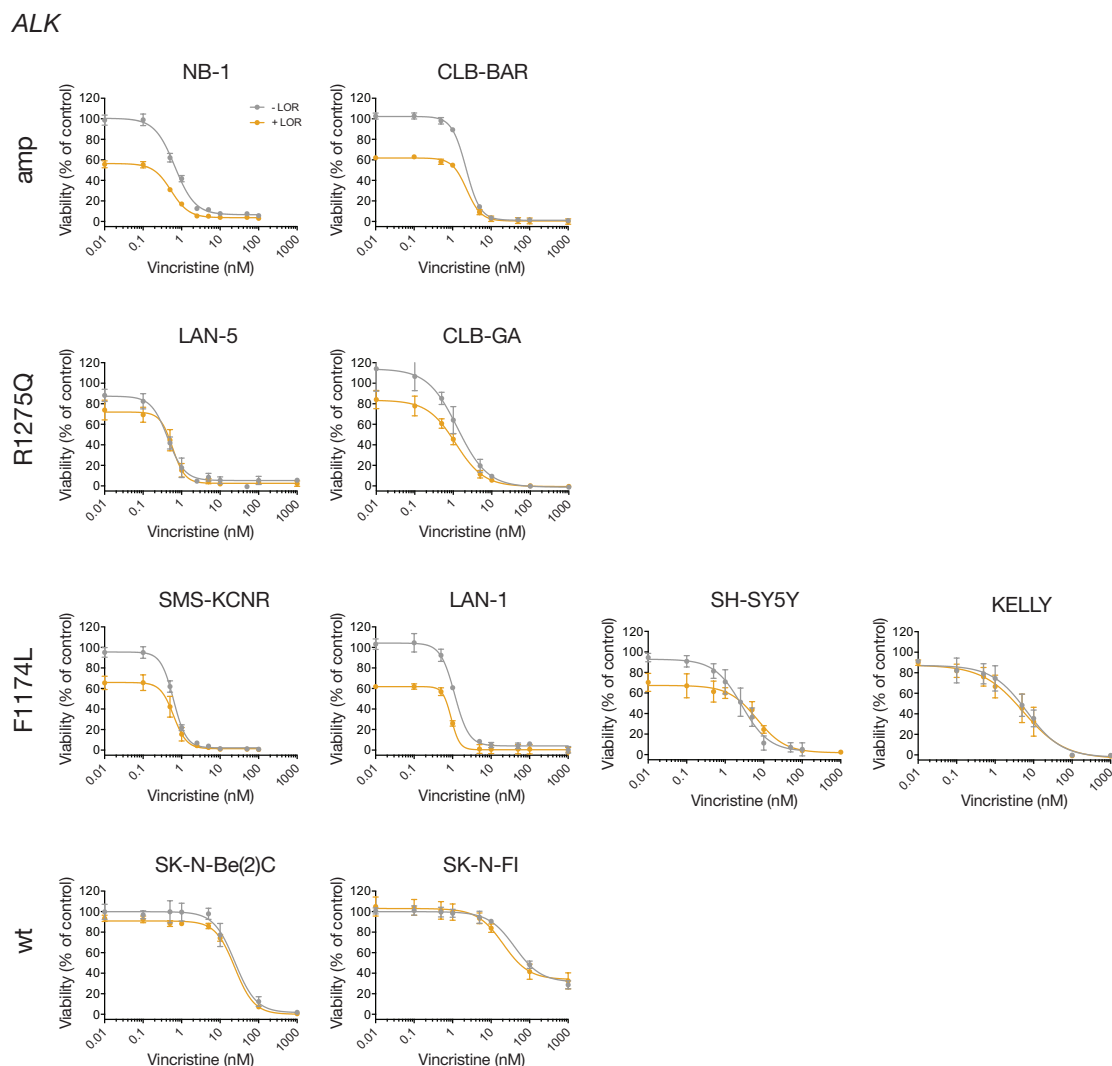


Figure 26: ALK sensitive and intermediate sensitive cell lines respond differently to combination treatment with vincristine. A selection of the 15 cell line panel was treated with different concentrations of VCR alone or in combination with EC50 concentrations of LOR for five days and cell viability was determined with the CTBassay. Graphpad Prism was used to determine dose response curves and EC50 values. Gray - VCR alone, orange - VCR + EC50 LOR. Mean \pm SD. n=3.

Table 17: EC50 concentrations of vincristine for LOR-sensitive cell lines at mono- and combination treatment.

Cell line	VCR (nM)	VCR + LOR (nM)
NB-1	0.67	0.53
CLB-BAR	2.23	2.32
LAN-5	0.44	0.58
CLB-GA	1.29	1.15
SMS-KCNR	0.62	0.62

Next, LOR-sensitive cell lines were treated with EC50 concentrations of the three drugs as monotherapy and combination treatments with LOR and VCR or CDDP, respectively, Figure 27. A significant combination effect for both VCR and CDDP was seen in the *ALK* amplified cell line NB-1. Here, the viability was reduced from approximately 50% to less than 25%. The cell lines LAN-5 and CLB-GA had a significant reduction in viability with the combination of LOR and VCR or CDDP, respectively. In both CLB-BAR and SMS-KCNR cells, the combination did not have any significant effect. Interestingly, the combination of LOR and CDDP seemed to be less effective than the monotherapy in LAN-5 cells. Altogether, the combination of chemotherapy with the targeted inhibitor LOR was effective especially in the *ALK*-addicted cell line NB-1.

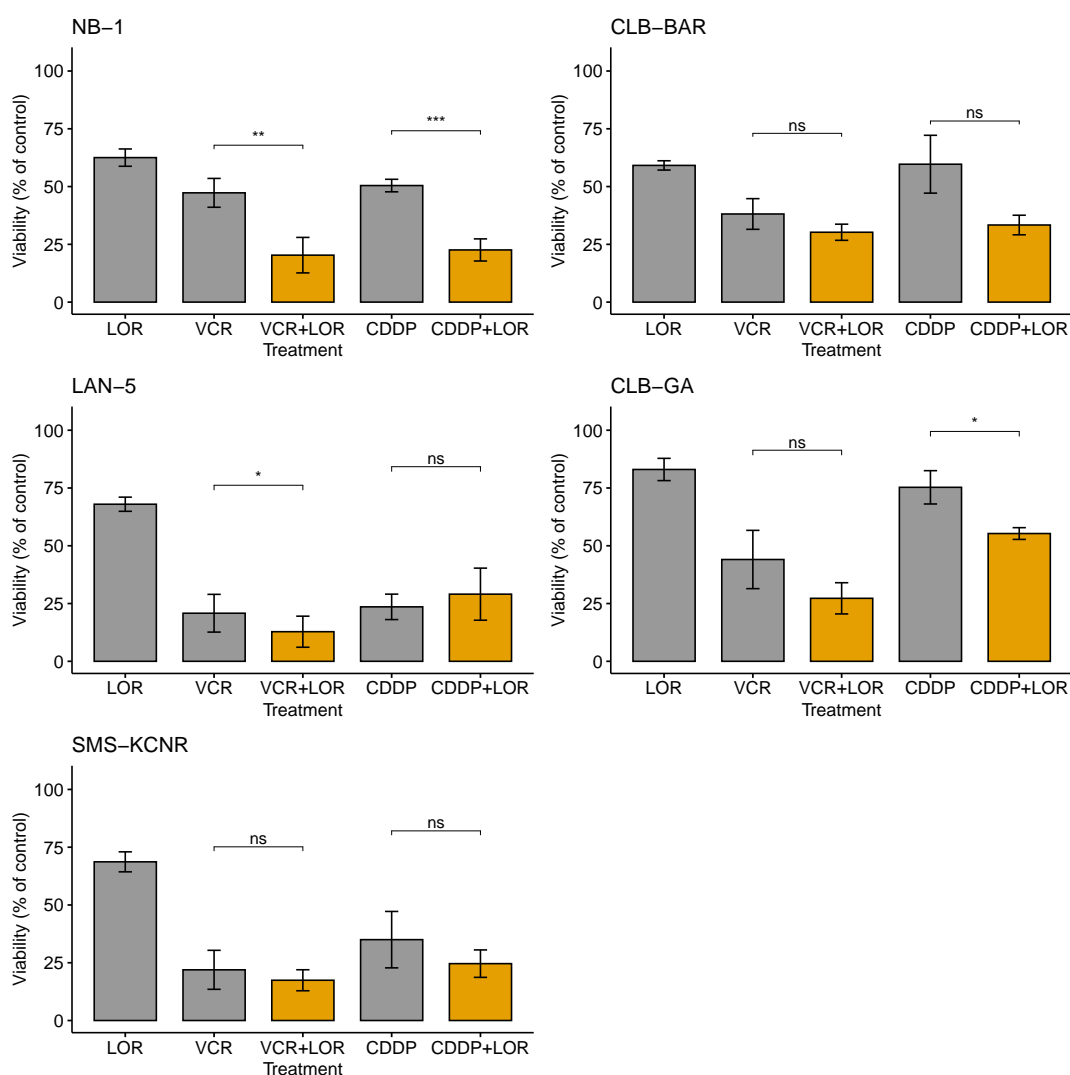


Figure 27: ALK-addicted cells benefit from combination treatment. LOR-sensitive cell lines were treated with their cell line specific EC50 concentrations of LOR, VCR and CDDP in a mono- and combination therapy. Cell viability was measured with the CTB assay after five days of treatment. Gray - monotherapy, orange - combination treatment. Mean \pm SD. $n=3$. Statistical analysis was performed with an unpaired t-test, ns: $p > 0.05$, *: $p < 0.05$, **: $p < 0.01$, ***: $p < 0.001$.

3.5 Validation of combination therapy in NB-1 spheroids

Preclinical testing of potential chemotherapeutics and targeted drugs are important in drug development. Drug candidates are initially analyzed in a two-dimensional (2D) *in vitro* setting before subsequent three-dimensional (3D) studies *in vitro* and *in vivo*. In order to test inhibitors in a more biological surrounding, much effort has been made to develop more advanced 3D *in vitro* tissue cultures, such as multicellular tumor spheroids or organoids, which mimic their corresponding *in vivo* organ. In the present study, tumor spheroids were chosen as 3D tissue culture system.

3.5.1 Establishment of neuroblastoma spheroid tissue culture

There are several approaches to grow tumor spheroids in tissue culture. In the normal monolayer culture, cells attach to the polystyrene bottom of tissue culture plates. In multicellular spheroid culture however, cells are prevented from attaching. For this purpose, cells can be grown either in a scaffold/matrix or in a scaffold-free cellular suspension. Concerning the scaffold/matrix technique, cells are either seeded onto a matrix or dispersed into a liquid matrix which becomes solid by polymerization. Scaffold-free methods include liquid overlay, hanging drop or agitation based techniques. Here, the liquid overlay technique was used, Figure 28.

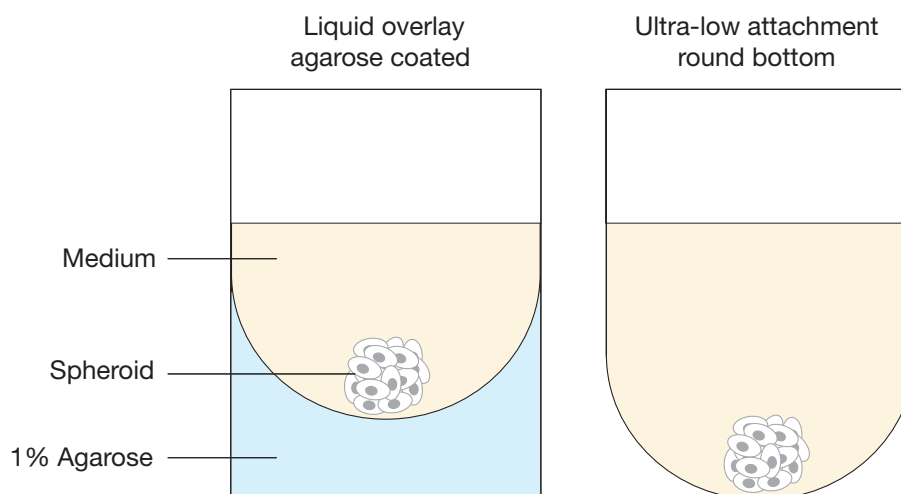


Figure 28: Two techniques to culture multicellular spheroids. Two commonly used techniques to culture multicellular spheroids are liquid overlay (left) and the use of ultra-low attachment (ULA) plates (right). In the liquid overlay technique, the well is covered with a 1% agarose solution to form a non-adhesive round bottom comparable to the round bottom of ULA plates.

This method forces the growth of tumor spheroids in suspension by adding a non-adhesive coating to the surface of the tissue culture plate. This can be achieved by manually coating the plates with a 1% agarose solution, to which the cells cannot attach. Similar, cells can be grown in ultra-low attachment (ULA) plates. These plates are coated with an ultra hydrophilic polymer that enables spontaneous spheroid formation. The techniques are similar, but have different advantages. Ultra-low attachment plates are very comparable within the wells of a plate and between different plates, while the agarose coating can be quite diverse already within one plate. On the other hand, the agarose coating is less expensive.

To test whether NB cell lines form spheroids spontaneously, the liquid overlay technique was tested on four different cell lines: IMR-5/75, KELLY, NBL-S and SK-N-DZ. For this purpose, flat bottom 96-well plates were coated with a 1% agarose solution to form a U-shaped non-adhesive well bottom. Cell suspension with 500 or 5000 cells, respectively, was applied to each well and plates were kept in the incubator overnight without movement to allow spheroid formation. Spheroids were cultured in normal growth medium which was changed every three days. Images of the spheroids were taken on day one, three, five, six, and nine after seeding and the area, width and height were determined with ImageJ.

For both 500 and 5000 cells, all four cell lines formed multicellular tumor spheroids spontaneously, Figure 29,30. At normal growth conditions, loose cell aggregates started to form after one day of incubation and became more dense throughout the course of the experiment. This was in accordance with the measured area, width and height of spheroids, Figure 31. KELLY and NBL-S spheroids had a decrease in area from day one to three, while the area of IMR-5/75 and SK-N-DZ spheroids slightly increased between the first two time points. From day three on, the spheroid area of all four cell lines increased. A similar observation was made for width and height of the spheroids. Although all cell lines were seeded at the same density, the area of spheroids differed between the cell lines. This was due to different sizes of the cells themselves.

Interestingly only three of the four cell lines (SK-N-DZ, IMR-5/75 and NBL-S) grew in spheres. KELLY cells did not grow in round spheroids, but rather as cell aggregates with multiple edges. This was the case for both 500 and 5000 cell spheroids. A similar observation was made in other NB cell lines, such as SK-N-FI and SH-SY5Y, see appendix Figure 60.

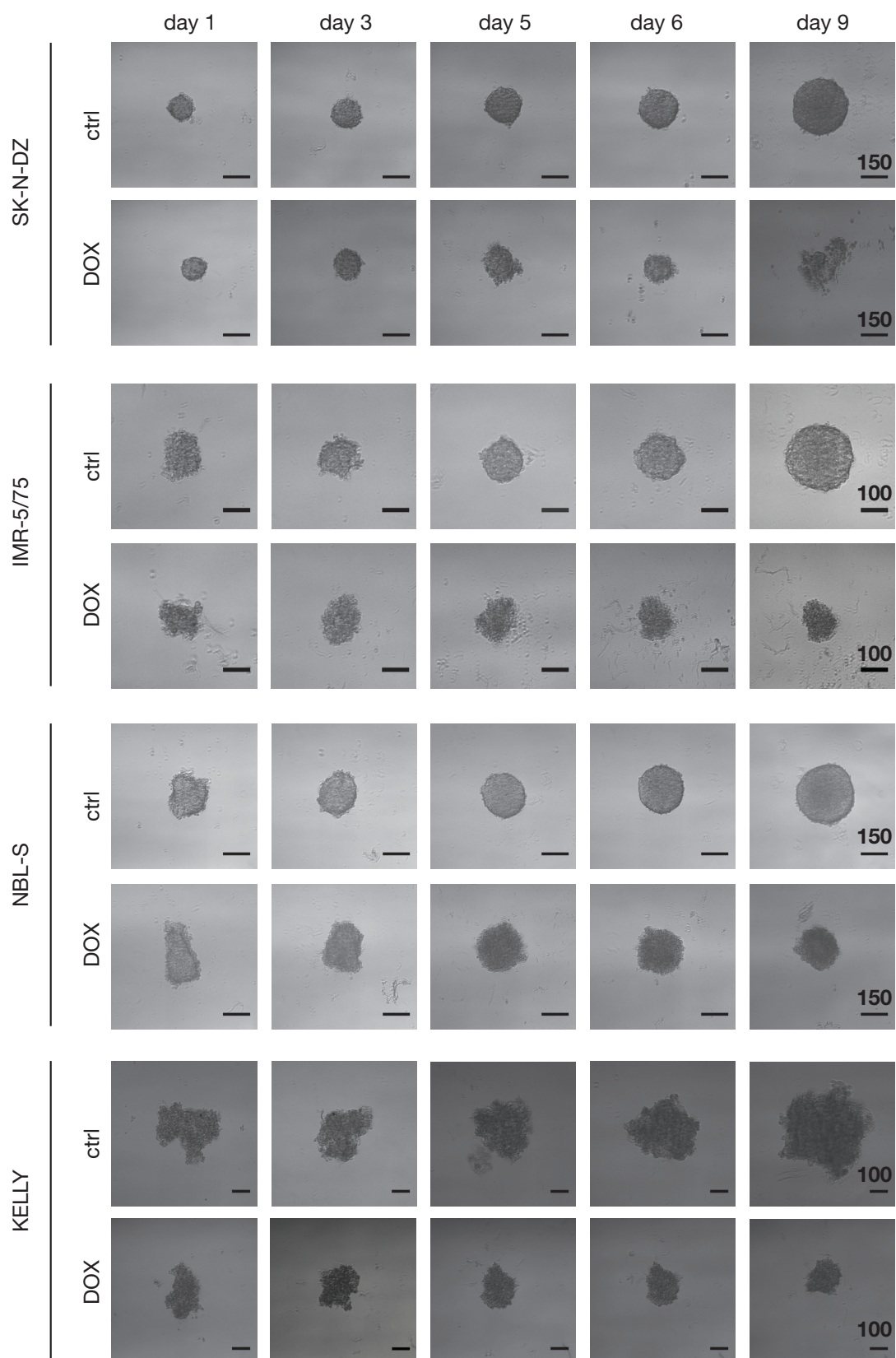


Figure 29: Normal growth of 500-cell spheroids and the effect of chemotherapy on their 3D structure. 500 cells of the respective cell lines were seeded into agarose coated 96-well plates and treated with $0.1 \mu\text{g}/\mu\text{l}$ DOX (KELLY, NBL-S, SK-N-DZ) or $0.05 \mu\text{g}/\mu\text{l}$ DOX (IMR-5/75) after 48h. Images were acquired on day one, three (24h DOX), five (72h DOX), six (96h DOX) and nine (168h DOX) after seeding. DOX - doxorubicin. Scale bar: μm . $n=3$.

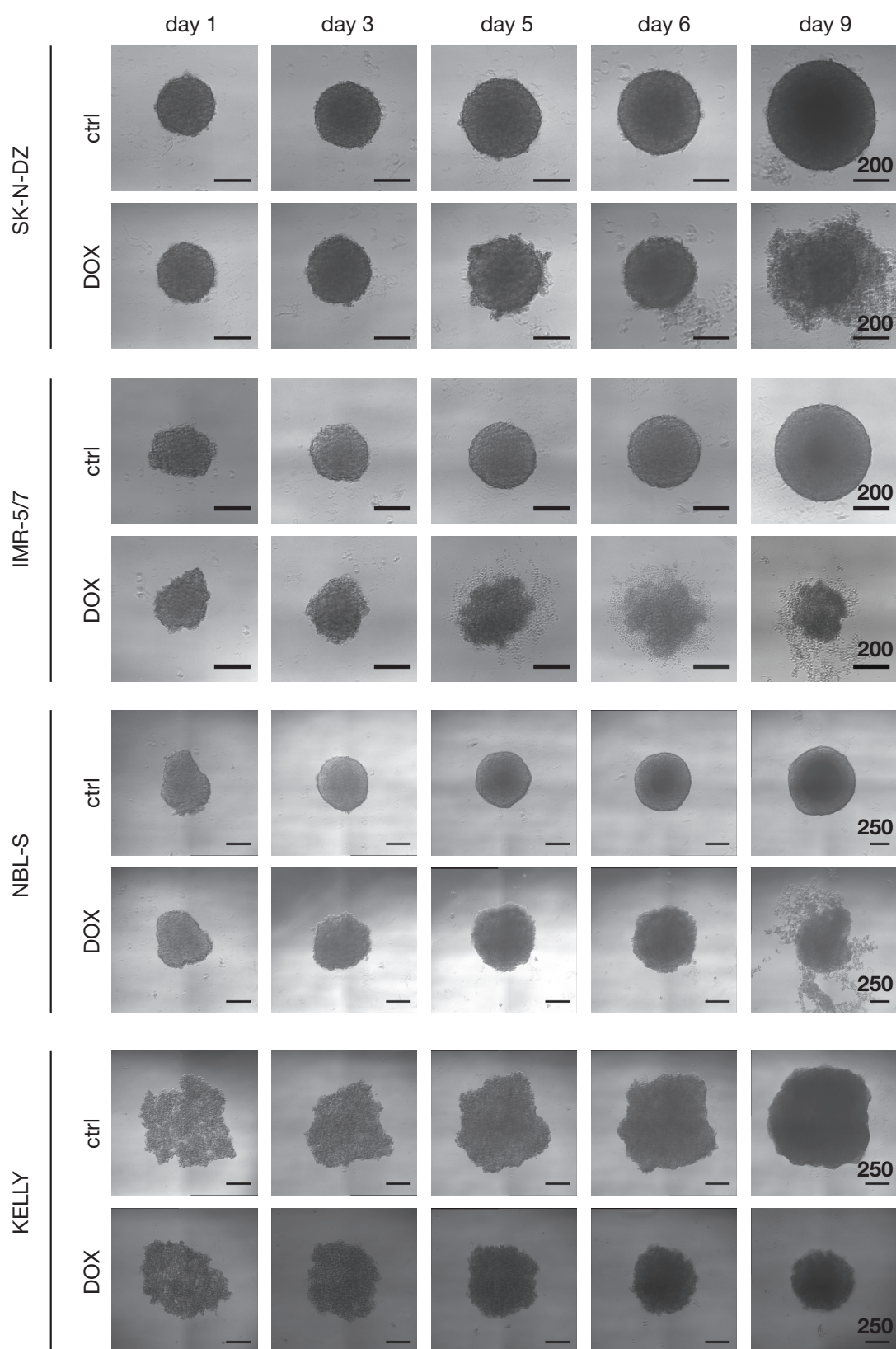


Figure 30: Normal growth of 5000-cell spheroids and the effect of chemotherapy on their 3D structure. 5000 cells of the respective cell lines were seeded into agarose coated 96-well plates and treated with $0.1 \mu\text{g}/\mu\text{l}$ DOX (KELLY, NBL-S, SK-N-DZ) or $0.05 \mu\text{g}/\mu\text{l}$ DOX (IMR-5/75) after 48h. Images were acquired on day one, three (24h DOX), five (72h DOX), six (96h DOX) and nine (168h DOX) after seeding. Scale bar: μm . $n=3$.

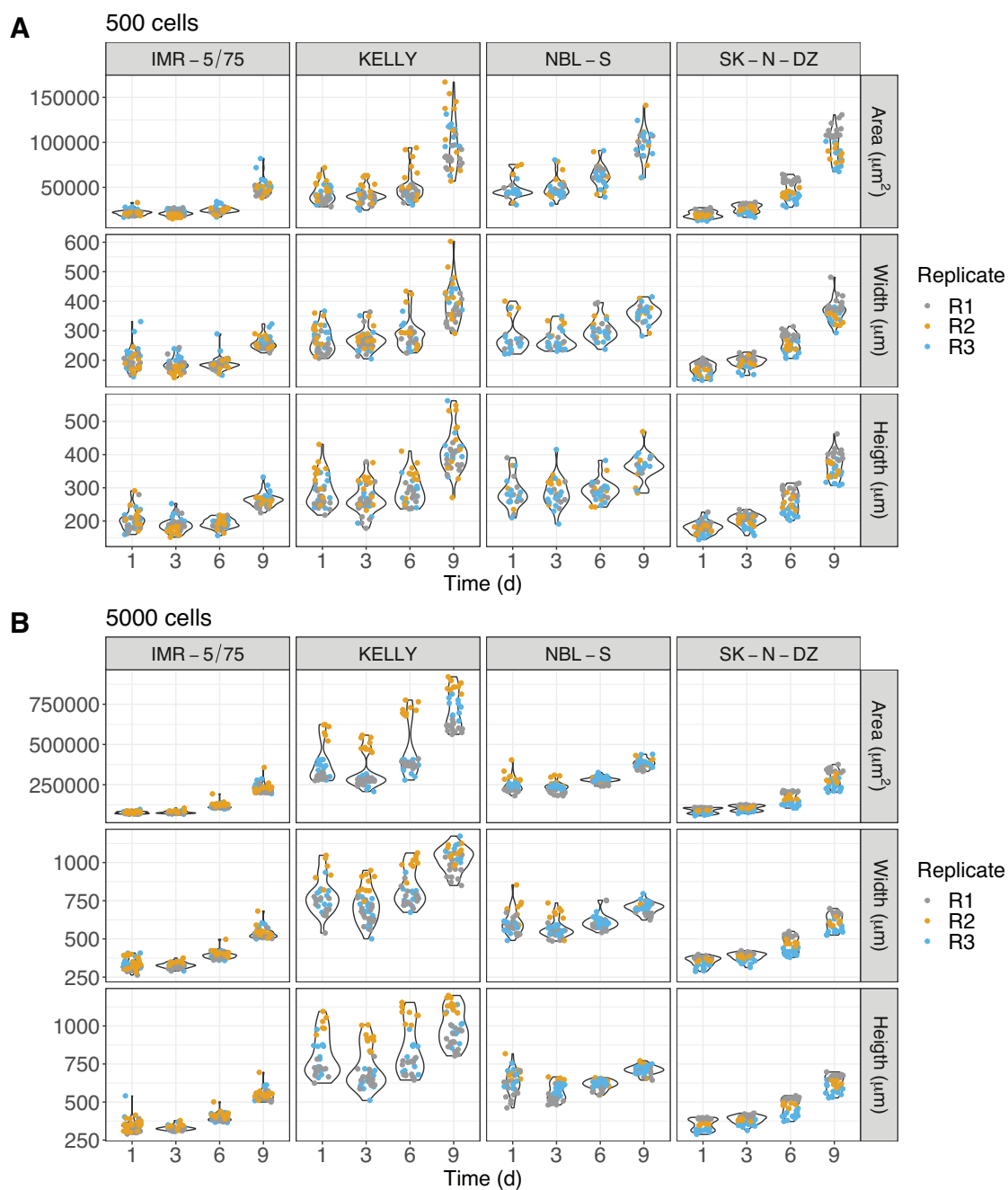


Figure 31: Growth behavior of NB-1 spheroids. Area, width and height of **A** 500-cell spheroids and **B** 5000-cell spheroids grown at control conditions (Figure 29,30) were determined with ImageJ. $n=3$.

One feature of multicellular tumor spheroids is the division into three different zones: an outer proliferation layer and a necrotic core in the center with a quiescent viable cell layer in between. These different layers are mainly observed in larger spheroids. Due to their larger diameter there are varying levels of diffusion in the different zones, which lead to a lack of oxygen and nutrients in the center, while CO_2 and waste accumulates. In the tested cell lines, a necrotic core was observed only in the larger 5000-cell spheroids. Especially in NBL-S spheres, the necrotic core was visible already at day five and represented a large part of the spheroid after nine days of incubation, Figure 32. For IMR-5/75 and SK-N-DZ, a necrotic core was observed, too. However, relative to the total sphere, the area of the necrotic core was smaller. In KELLY spheroids, no necrotic core was visible.

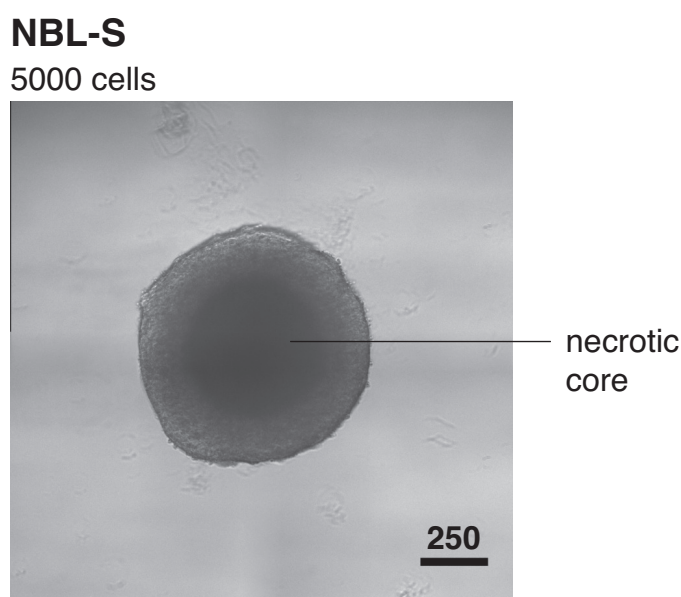


Figure 32: Exemplary NBL-S spheroid with a necrotic core. 5000-cell spheroid of NBL-S cells with visible necrotic core after nine days of incubation. Scale bar: μm .

To examine the response of spheroids to chemotherapy, spheroids were treated with the first-line chemotherapeutic doxorubicin (DOX) at a concentration of $0.1 \mu\text{g}/\mu\text{l}$ (KELLY, NBL-S, SK-N-DZ) or $0.05 \mu\text{g}/\mu\text{l}$ (IMR-5/75), respectively. DOX was applied after 48h of spheroid formation and images acquired on day three (24h DOX), day five (72h DOX), day six (96h DOX) and day nine (168h DOX) of the experiment, Figure 29,31. In general, DOX treatment prevented growth of spheroids, which can be seen in a decrease in size during the course of the treatment. The spheres were not only smaller than the spheroids grown in normal growth medium, but also decreased in size compared to the initial condition at day one. Interestingly, especially the larger 5000-cell spheroids tended to loosen their dense structure, releasing an outer layer of dead cells. This was mainly observed for SK-N-DZ, NBL-S and IMR5-/75 cells. In contrast, the cells in the KELLY spheroids stayed dense in the spheroid.

3.5.2 NB-1 cells are equally sensitive to lorlatinib in 2D and 3D tissue culture

NB-1 cells were highly sensitive to treatment with the ALK inhibitor lorlatinib in the classical 2D tissue culture. To see, whether these cells respond differently in a 3D tissue culture setting, both NB-1 spheroids and a normal monolayer culture were treated with different concentrations of LOR and images were acquired every 24h for five days, starting at the time of drug application. The area of spheroids was determined with ImageJ.

A first treatment effect was observed after 24h, at which spheroids treated with concentrations ≥ 5 nM decreased in size compared to those treated with lower concentrations, Figure 33A. Throughout the course of the treatment, the size of these spheroids remained constant, while the other spheroids continued growing. Dying cells stayed attached to the spheroid, similar to what was observed in the DOX treatment of KELLY cells before, section 3.5.1.

Next, growth of spheroids at each concentration was compared to the monolayer culture. For this purpose, the percentage of covered area by a spheroid in an image was compared to the 2D cell confluence, Figure 34. With approximately 20% covered area in both 2D and 3D settings, the initial condition was similar between both techniques. In normal growth medium and the appropriate DMSO control, cells in the monolayer culture grew much faster compared to spheroids. While 2D growing cells reached approximately 75% confluence after five days, spheroids increase the percentage of covered area only to slightly more than 25%. A similar observation was made for LOR concentrations ≤ 5 nM, while no difference was observed at concentrations ≤ 5 nM. This difference between 2D and 3D cultures may be caused by the multi-dimensional growth of spheroids which cannot be captured completely in a 2D image. Additionally, tumor spheroids have a slower growing speed compared to monolayer cultures, as mainly cells in the outer layer proliferate. For this reason, the treatment was normalized by the DMSO control and dose response curves were generated, Figure 33B. Interestingly, there is a high similarity between the curves of the spheroid and monolayer culture. EC50 concentrations calculated from dose response curves shown in Figure 33B were highly similar throughout the course of the treatment for both techniques and varied only slightly between spheroids and monolayer culture, Figure 33D. In addition to cell confluence, cell viability was measured with the CTB assay after five days of LOR treatment and dose response curves were generated, Figure 33C. The reduction in viability with increasing concentrations of LOR was highly similar for both tissue culture techniques.

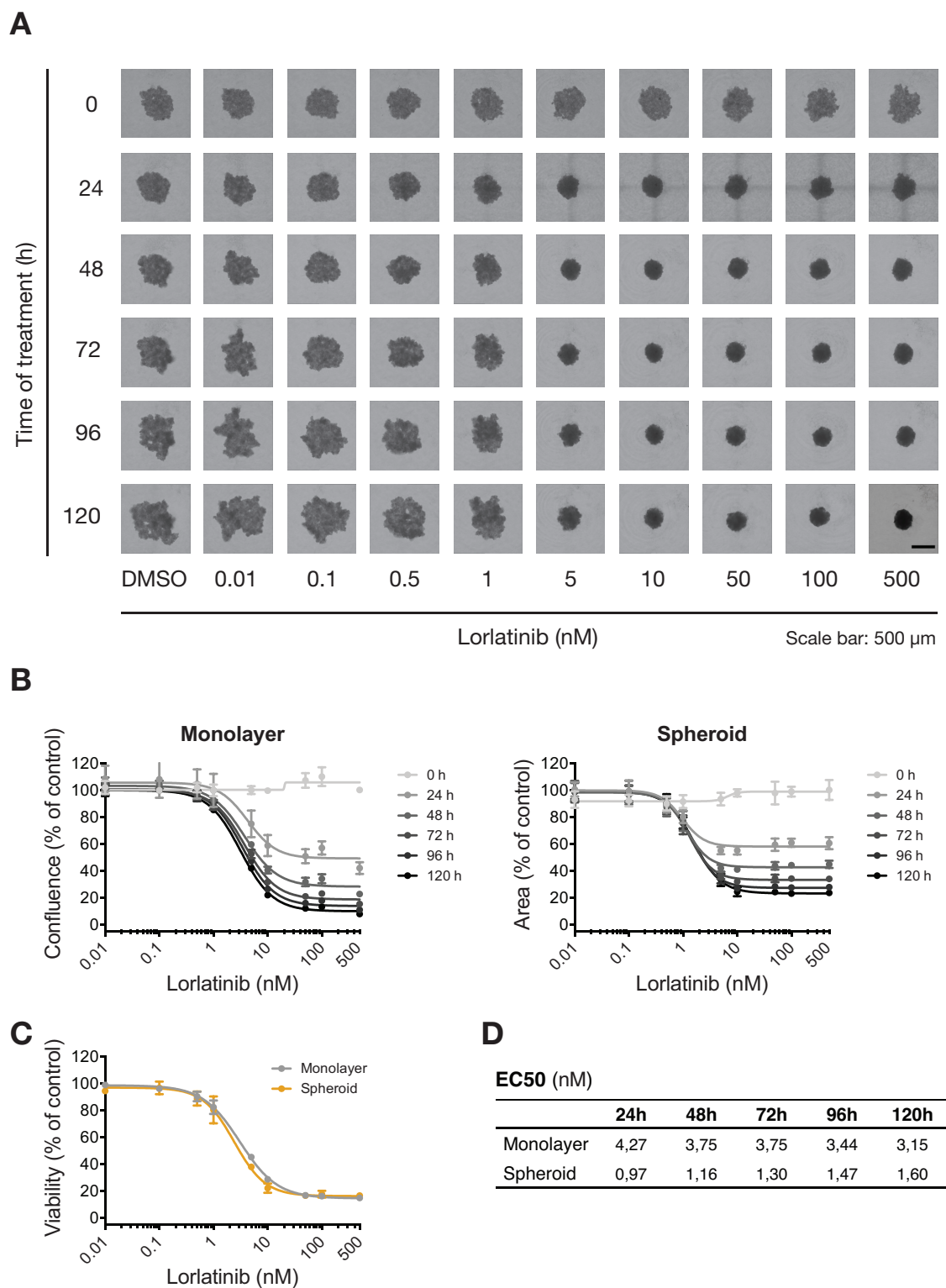


Figure 33: NB-1 cells are equally sensitive to lorlatinib in monolayer and spheroid tissue culture. 5000 NB-1 cells were seeded into ULA and normal 96-well plates and treated with different concentrations of LOR for five days. **A** Spheroid images on day zero to five of LOR treatment. **B** Confluence of monolayer culture and area of spheroids were measured and dose response curves generated with Graphpad Prism. **C** Cell viability was measured with the CTB viability assay on day five of treatment. **D** EC50 values of dose response curves shown in B. Mean \pm SD. n=3.

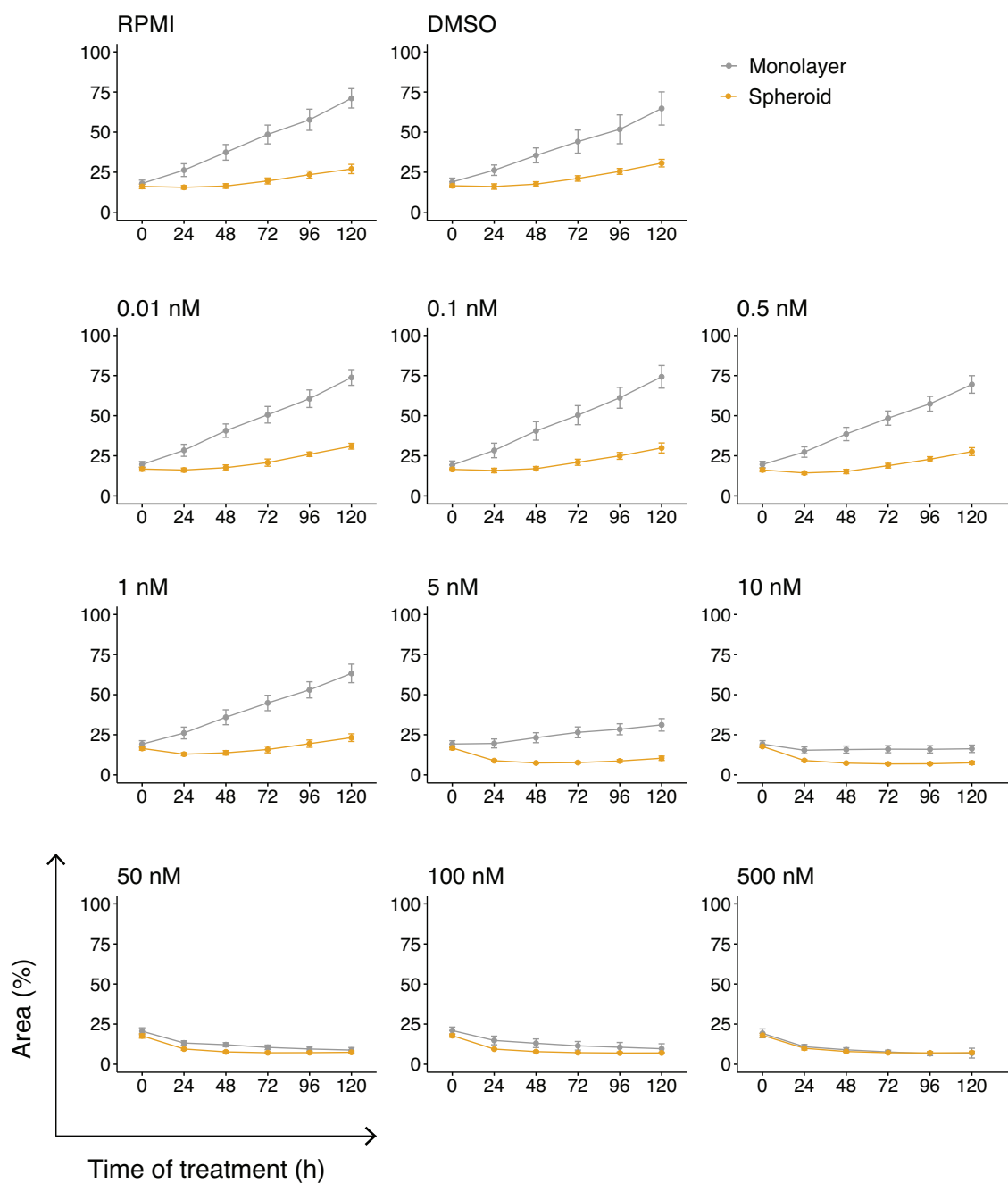


Figure 34: NB-1 cells show similar growth behavior at lorlatinib treatment in monolayer and spheroid tissue culture. Comparison of monolayer and spheroid growth at LOR treatment. 5000 NB-1 cells were seeded into ULA and normal 96-well plates and treated with different concentrations of LOR for five days. Confluence and area of spheroids were determined from data shown in Figure 33. Mean \pm SD. $n=3$.

Taken together, this data illustrates that NB-1 cells respond similar in the classical monolayer and the more advanced multicellular tumor spheroid tissue culture.

3.5.3 NB-1 spheroids respond well to treatment with cisplatin but are more resistant to vincristine

After analyzing the effect of lorlatinib on NB-1 spheroids, the same treatment was performed with the two chemotherapeutics cisplatin and vincristine.

In comparison to LOR, the treatment effect of CDDP was weaker, especially on the first day after drug application. There was no specific concentration at which a clear separation between strong and weak response was seen, Figure 35A. Only at 2.5 μM and 5 μM CDDP the area of the spheroids decreased, while spheroids treated with lower concentrations increased in size throughout the course of the treatment. Spheroids treated with 10 μM had no change of size throughout the treatment and microscopic evaluation indicated that these spheroids consisted dead cells only. Therefore, this concentration was excluded from the dose response analysis, Figure 35B. With each additional day of treatment, reduction of confluence began at lower concentrations for both 2D and 3D cell culture. Furthermore, there was a decrease in EC50 concentrations over time, Figure 35D. In comparison to this, EC50 concentration of LOR hardly changed, while the overall effect increased during the course of the treatment, Figure 33B,D. Similar to LOR, the 2D effect is larger compared to 3D, which may be due to a faster growth in the monolayer culture. However, a comparison of cell viability showed no difference between 2D and 3D cultures, Figure 35C. This data suggests that NB-1 cells are equally sensitive to cisplatin in a monolayer and spheroid setting.

Interestingly, NB-1 spheroids responded differently to treatment with the spindle toxin VCR. Only spheroids treated with the highest concentration (100 nM) showed a clear cytotoxic effect while spheroids treated with all other concentrations continued growing normally, Figure 36A. In the monolayer setting, a large reduction in confluence was obtained additionally for 5 nM and 10 nM LOR. When comparing the dose response of 2D and 3D cultures, this difference was clearly visible, Figure 36B. Similar to the observation made at LOR treatment, the effect size of the dose response changed during the course of the experiment rather than EC50 concentrations, Figure 36D. Similar to the confluence, a reduction in cell viability occurred only at 100 nM VCR in spheroids, while a strong effect was also seen for 5 nM and 10 nM in the 2D culture, Figure 36C.

Taken together, the response of NB-1 spheroids to single agent treatment varied between the different drugs. While LOR and CDDP had the same effect on spheroids compared to the monolayer culture, VCR was less effective in spheroids.

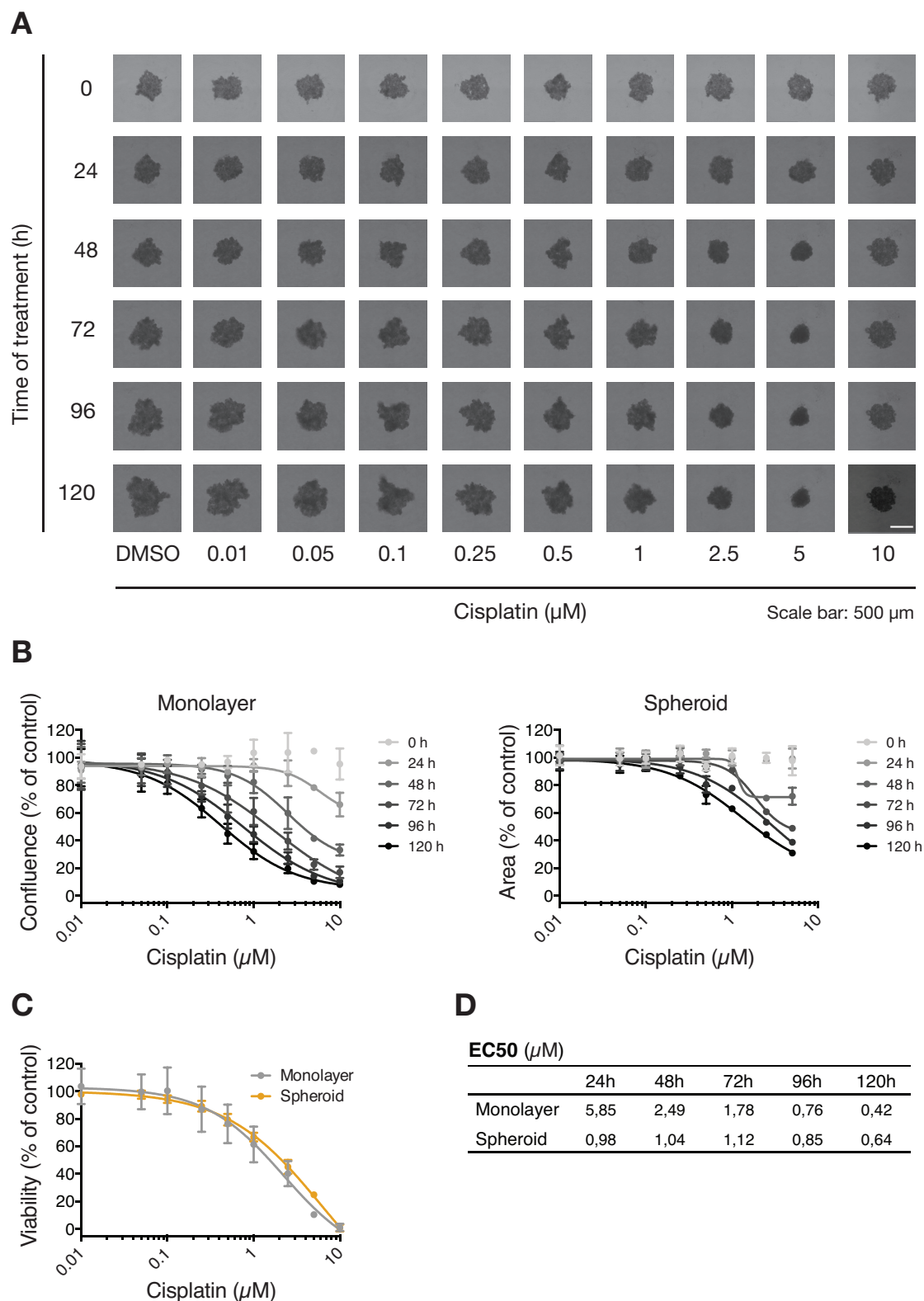


Figure 35: NB-1 cells have similar growth behavior at cisplatin treatment in monolayer and spheroid tissue culture. 5000 NB-1 cells were seeded into ULA and normal 96-well plates and treated with different concentrations of CDDP for five days. **A** Spheroid images on day zero to five of CDDP treatment. **B** Confluence of monolayer culture and area of spheroids were measured and dose response curves calculated with Graphpad Prism. **C** Cell viability was measured with the CTB viability assay on day five of treatment. **D** EC₅₀ values of dose response curves shown in B. Mean \pm SD. n=3.

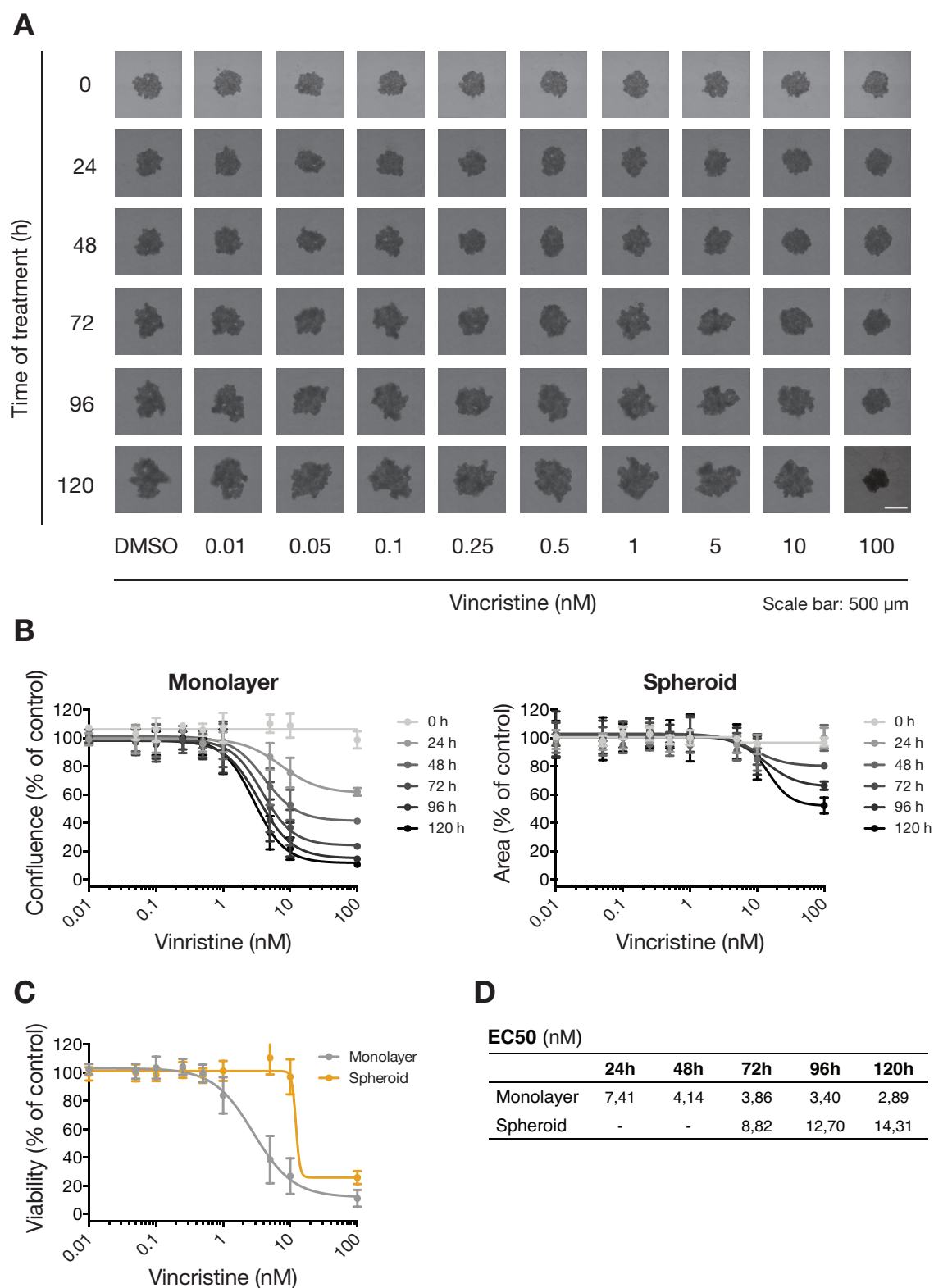


Figure 36: NB-1 cells are more sensitive to vincristine in monolayer tissue culture than spheroid culture. 5000 NB-1 cells were seeded into ULA and normal 96-well plates and treated with different concentrations of VCR for five days. **A** Spheroid images on day zero to five of VCR treatment. **B** Confluence of monolayer culture and area of spheroids were measured and dose response curves calculated with Graphpad Prism. **C** Cell viability was measured with the CTB viability assay on day five of treatment. **D** EC50 values of dose response curves shown in B. Mean \pm SD. n=3.

3.5.4 Combination treatment is more effective than chemotherapy alone

The combination of LOR with both chemotherapeutics was investigated in NB-1 spheroids. For this purpose, cells received the same treatment of CDDP and VCR as described in section 3.5.3. However, in addition to the chemotherapeutics, the EC50 concentration of LOR (2.5 nM) was applied.

For both combinations a first effect was seen already after 24h, which resulted in a reduction of the spheroid area compared to the control spheroids, Figure 37A,38A. The reduction was similar throughout all concentrations, indicating that this was an effect caused by LOR treatment. Throughout the course of the treatment, the relative size of the spheres changed similar to the single agent treatment observed previously in section 3.5.3.

In order to generate dose response curves, the area of spheroids and the confluence of 2D tissue culture was normalized by the DMSO control. This control did not include the additional 2.5 nM LOR. For both chemotherapeutics the relative area and confluence decreased already at low concentration, reaching approximately 50-60% after the five days treatment, Figure 37B,38B. In the single agent treatment, these concentrations, did not cause any reduction in confluence and viability. This suggests that this effect reflects the single agent treatment with 2.5 nM LOR. From day three on 2.5 nM and 5 nM CDDP caused a slightly larger decrease in area of spheroids compared to concentrations ≤ 1 nM. Concerning VCR, the change of area was equal for all concentrations throughout the course of the treatment.

In a next step, cell viability was measured with the CTB assay. Similar to the single agent treatment with chemotherapeutics, CDDP monolayer and spheroid culture had very similar dose response curves for the combination treatment, Figure 37C. Concerning VCR combination, a reduction in viability was observed only for the 100 nM concentration in spheroids, while 5 nM and 10 nM caused a reduction in viability to approximately 20% in the monolayer setting, 38C. This illustrates the different sensitivity of NB-1 cells to VCR dependent on the culture system.

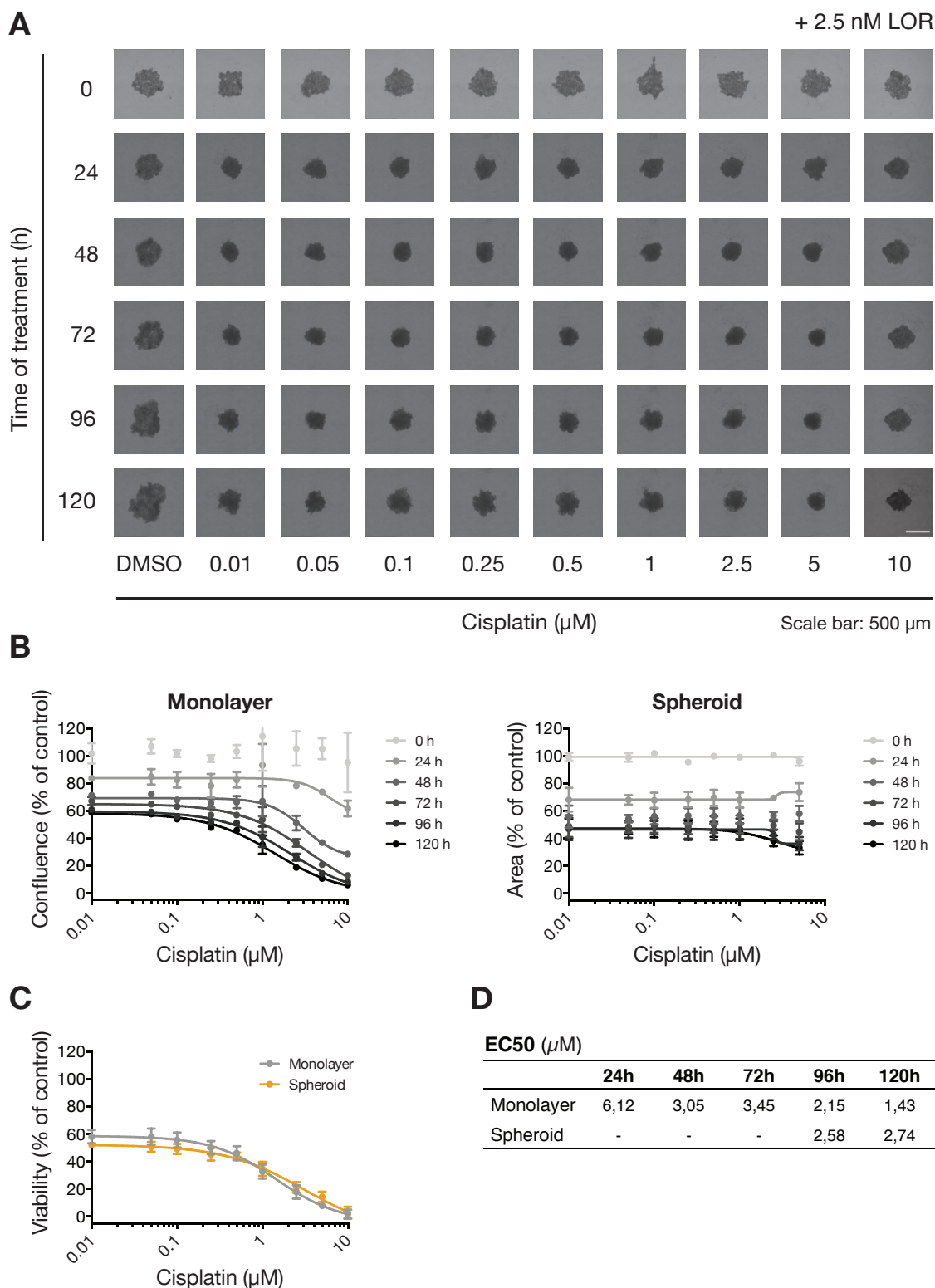


Figure 37: Combination treatment with lorlatinib and cisplatin is similar effective in monolayer and spheroid culture. 5000 NB-1 cells were seeded into ULA and normal 96-well plates and treated with different concentrations of CDDP in combination with the EC50 concentration of for five days. **A** Spheroid images on day zero to five of treatment. **B** Confluence of monolayer culture and area of spheroids were measured and dose response curves calculated with Graphpad Prism. **C** Cell viability was measured with the CTB viability assay on day five of treatment. **D** EC50 values of dose response curves shown in B. Mean \pm SD. n=3.

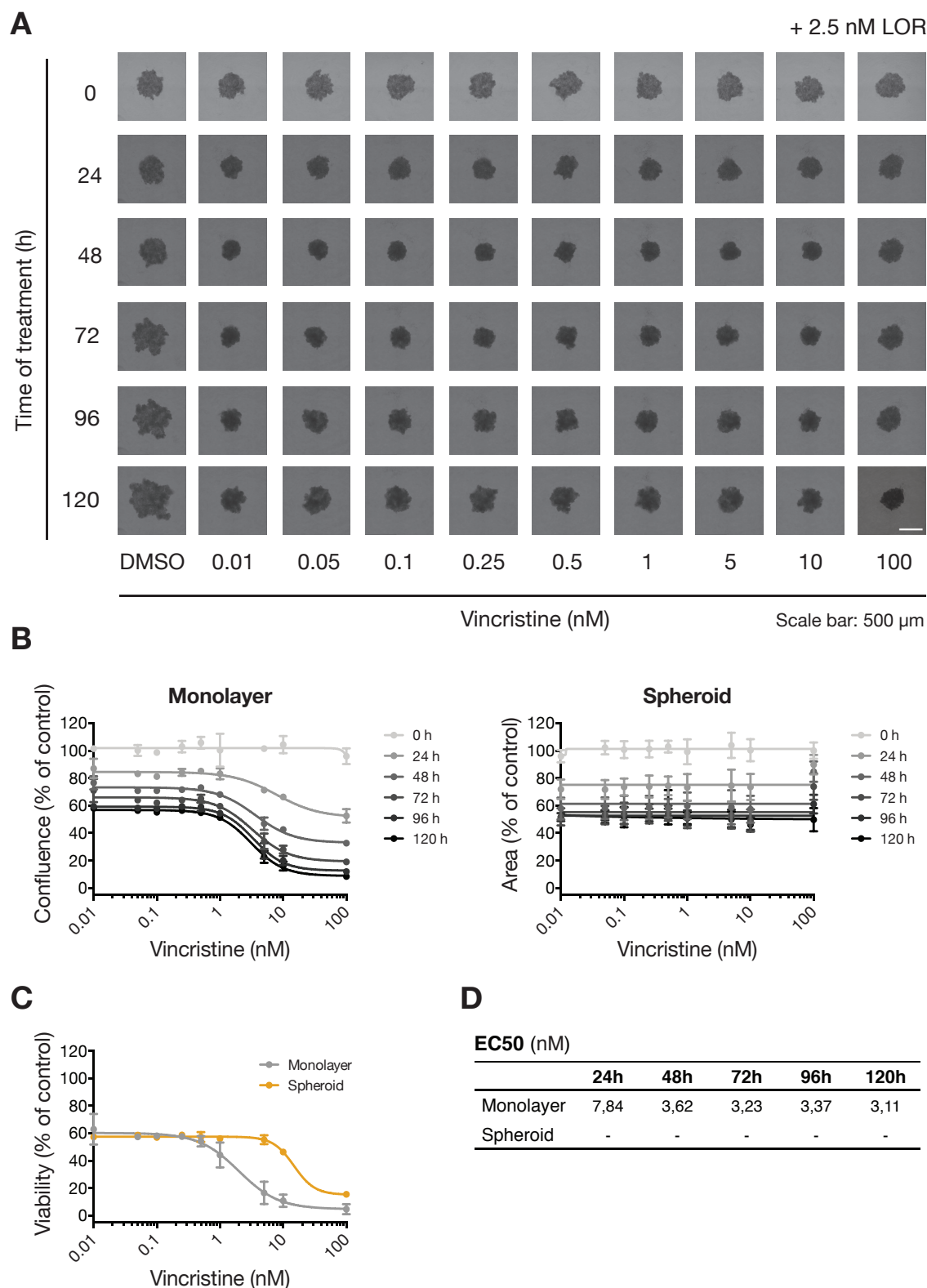
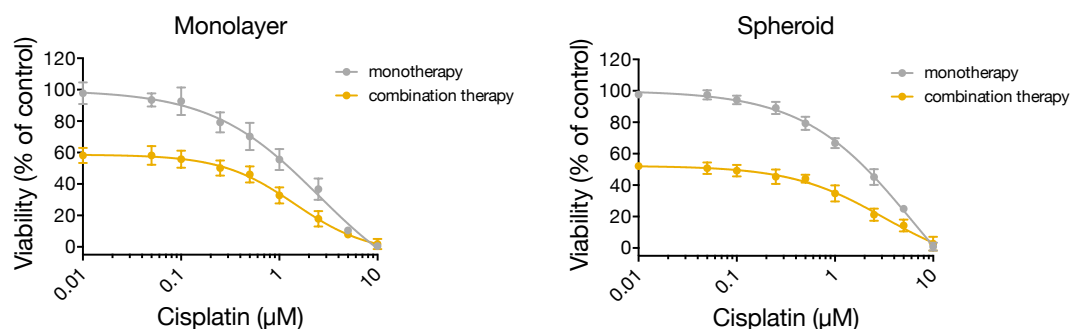


Figure 38: Combination treatment with lorlatinib and vincristine is more effective in monolayer culture than in spheroid culture. 5000 NB-1 cells were seeded into ULA and normal 96-well plates and treated with different concentrations of VCR in combination with the EC₅₀ concentration of LOR for five days. **A** Spheroid images on days zero to five of treatment. **B** Confluence of monolayer culture and area of spheroids were measured and dose response curves calculated with Graphpad Prism. **C** Cell viability was measured with the CTB viability assay on day five of treatment. **D** EC₅₀ values of dose response curves shown in B. Mean \pm SD. n=3.

A comparison of mono- and combination therapy with CDDP between 2D and 3D tissue culture showed that the response of NB-1 cells was similar in both culture systems, Figure 39A. In contrast, NB-1 cells were less sensitive to VCR in spheroids in both mono- and combination treatment, Figure 39B. However, the overall pattern of response was similar in both 2D and 3D cultures. The main difference was that higher concentrations of VCR were needed to achieve a similar response obtained in 2D tissue culture.

A



B

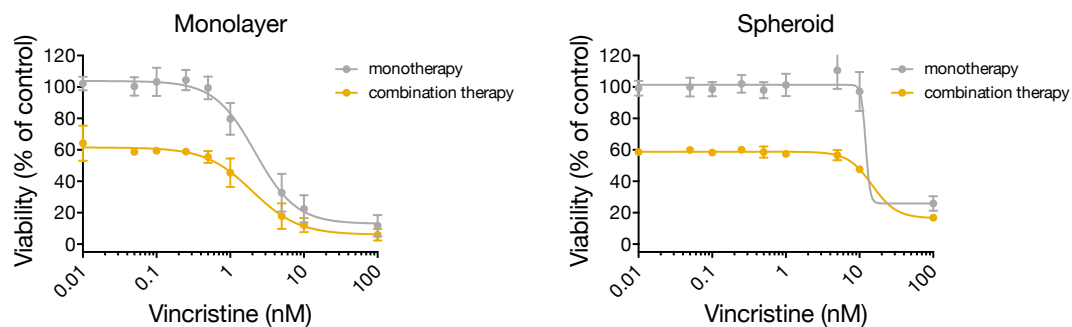


Figure 39: Combination treatment with lorlatinib and cisplatin is more effective than the combination with lorlatinib and vincristine. Dose response curves of monotherapy and combination therapy of LOR with **A** CDDP and **B** VCR in monolayer (left) and spheroid (right) tissue culture. Mean \pm SD. n=3.

3.6 Whole transcriptome analysis to gain insights into the response to lorlatinib

Previous results of the single agent treatment with LOR showed that *ALK* altered cell lines had a different sensitivity to this *ALK* inhibitor. Altogether, NB-1 cells had a much higher sensitivity to LOR compared to all other *ALK*-positive cell lines, even to the second *ALK* amplified cell line CLB-BAR. Interestingly, there was a broad range of response among the F1174L mutated cell lines, which ranged from sensitive (SMS-KCNR) to intermediate sensitive (SH-SY5Y, LAN-1) and resistant (KELLY). These observations led to multiple questions.

- Are there differences in the transcriptome of the cell lines that can explain variations in treatment response?
- Is it possible to predict the response only by the basal gene expression?

This is of special interest, as some patients with an altered *ALK* status do not respond to the therapy with an *ALK* inhibitor while other patients do.

- What makes a responder cell line a responder?
- What is the resistance mechanism of KELLY cells and what causes the high sensitivity of NB-1 cells?
- Is it possible to identify new targets for a novel targeted combination therapy?

This is of particular interest as the combination treatment with classical first-line chemotherapy was not effective in the majority of *ALK*-positive cell lines.

In order to answer these questions, whole transcriptome analysis was performed on the selected cell line panel. Here, the basic gene expression was taken into account. The cell line CLB-BAR was excluded from all analyses as there was no RNAseq data available. Furthermore, the effect of lorlatinib on the transcriptome was investigated in the responder cell line NB-1 and in the non-responder cell line KELLY.

3.6.1 A published ALK gene signature cannot fully explain the difference in sensitivity

A study in 2015 proposed an ALK gene signature consisting of 77 genes (Lambertz et al. 2015). These genes were differentially expressed at the treatment with the ALK inhibitor TAE. In order to determine whether these genes can discriminate the model cell lines according to their treatment response already at a basal gene expression level, a principle component analysis (PCA) was performed, Figure 40. The PCA including the whole cell line panel did not result in a clear clustering according to LOR sensitivity, Figure 40A. There were two smaller clusters consisting of the *ALK* altered cell lines CLB-GA and SH-SY5Y as well as SMS-KCNR and LAN-5, respectively, which did not reflect their response to LOR. Interestingly, the two clusters included cell lines with different *ALK* mutations but the same *MYCN* status, *MYCN* non-amplified or *MYCN* amplified, respectively. Next, *ALK* wild-type cell lines were excluded from the analysis, Figure 40B. Here, SMS-KCNR, LAN-5 and CLB-GA cells formed a cluster, which was in accordance with their similar response to LOR in the viability assay performed previously, section 3.3.2. Intermediate sensitive cell lines SH-SY5Y and LAN-1 did not cluster together. However, KELLY and LAN-1 cells were separated from the rest of the cell lines by principle component 1 (PC1). Thus, the published ALK gene signature can discriminate between different responses to some extent.

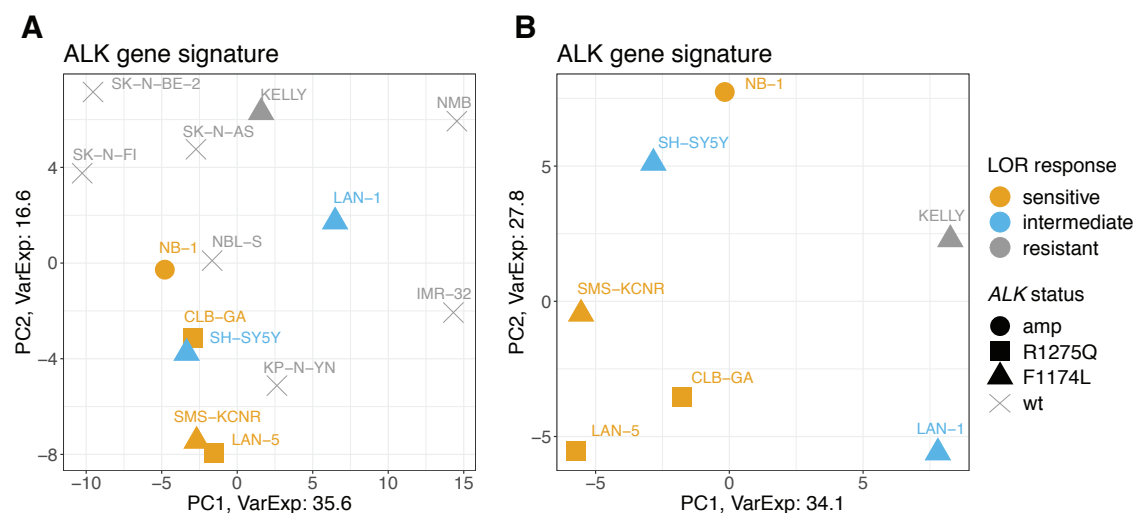


Figure 40: Cell lines do not form clusters of sensitivity based on ALK signature genes. PCA with ALK signature genes on **A** the selected cell line panel and **B** *ALK* altered cell lines.

In order to relate this signature to patient data, the ALK gene signature was used to investigate the basal gene expression of the two patient cohorts described in section

3.1, Figure 41. For both patient cohorts, the gene signature did not discriminate between *ALK* wild-type patients and patients with an altered *ALK* status such as amplification or mutation, Figure 41A,C. Additionally, there were no clear clusters in the PCA of *ALK* altered patients only, Figure 41B,D. Unfortunately, there was no information on which patients were treated with an *ALK* inhibitor and how they responded to the therapy. However, there were no clear clusters visible which indicates that no prediction of treatment response can be made based on the basal gene expression of these signature genes.

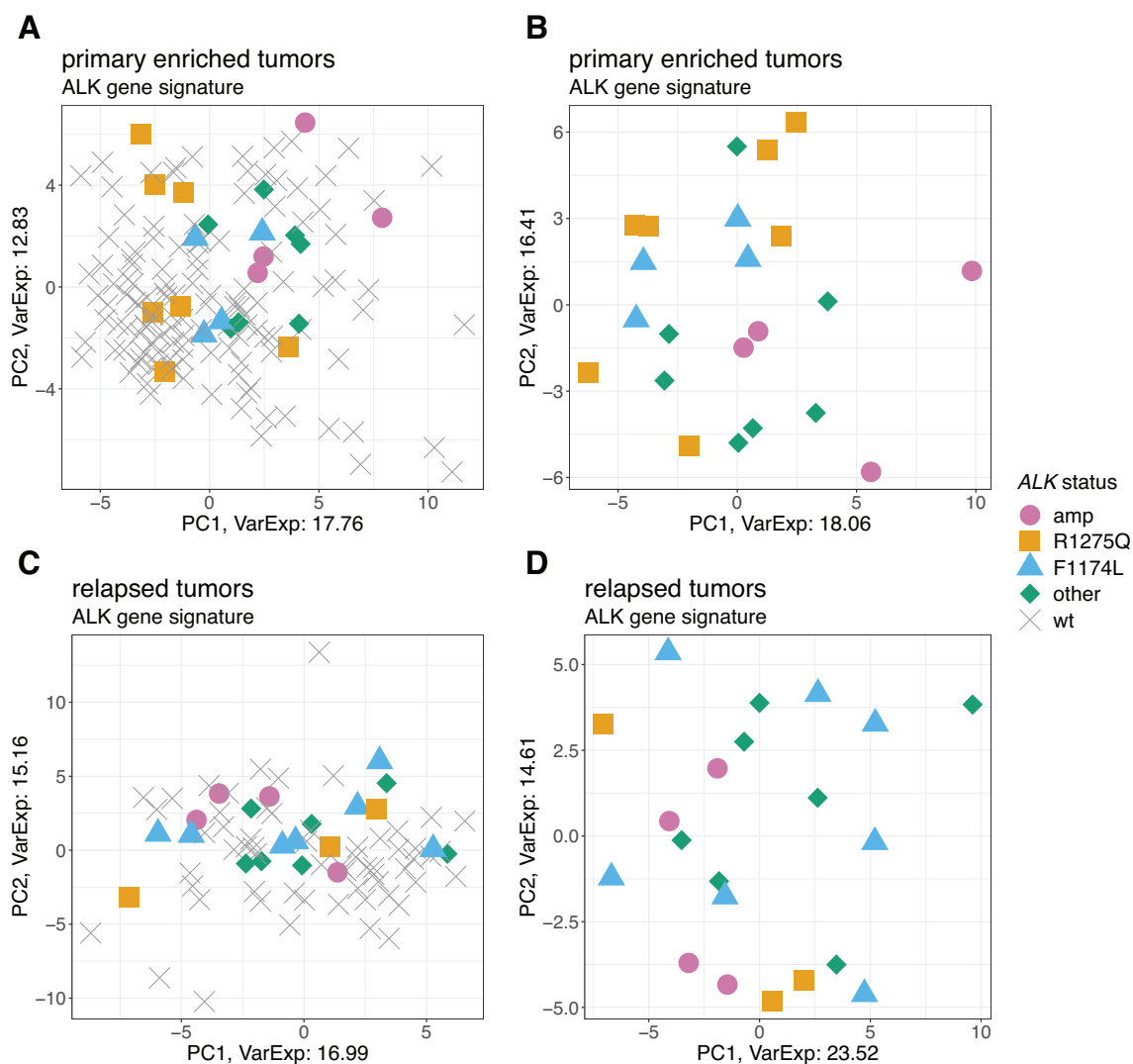


Figure 41: The *ALK* gene signature does not discriminate patients according to their *ALK* status. PCA with *ALK* signature genes on **A** the whole primary enriched tumor cohort, **B** *ALK* altered patients of the primary enriched tumor cohort, **C** the whole relapsed tumor cohort and **D** *ALK* altered patients of the relapsed tumor cohort.

3.6.2 Effect of lorlatinib on the transcriptome of a responder and a non-responder cell line

The published ALK gene signature could not fully capture the response to LOR. Thus, this study was aiming at determining an alternative ALK signature at LOR treatment. For this purpose, RNAseq at LOR treatment was performed for the responder cell line NB-1 and for non-responder KELLY cells.

3.6.2.1 Optimization and experimental design of the RNAseq experiment

To determine optimal conditions for the RNAseq experiment, NB-1 and KELLY cells were treated with 10 nM and 25 nM LOR for 8h, 24h, and 48h and mRNA levels of six genes from the published ALK gene signature were determined with qRT-PCR, Figure 42. While mRNA levels of all six genes changed for both concentrations and time points in NB-1 cells, only the two cell cycle genes *CCNE2* and *CCNG2* as well as the gene encoding the programmed cell death protein 4 (*PDCD4*) were affected in KELLY cells. For most of the genes, a response to both LOR concentrations could be observed already after 8h with a few additional changes after 24h but no further differences at 48h. Concerning the concentrations, effects were seen at both 10 nM and 25 nM. Although 25 nM LOR caused stronger changes in the gene expression, 10 nM is not only more similar to the EC50 concentration of NB-1 cells (EC50: 2.5 nM) but also represents a clinically relevant dose.

To see whether the 10 nM concentration is sufficient to inhibit ALK, phosphorylation at the tyrosine residue 1604 was investigated by western blot, Figure 43. For both cell lines, a reduction of the phosphorylated protein was seen for 10 nM LOR after 6h treatment, indicating that LOR downregulates the activity of ALK in both cell lines.

For these reasons, the RNAseq experiment was performed with a concentration of 10 nM LOR which was applied for 8h and 24h, Figure 44. The experiment was performed in two biological replicates.

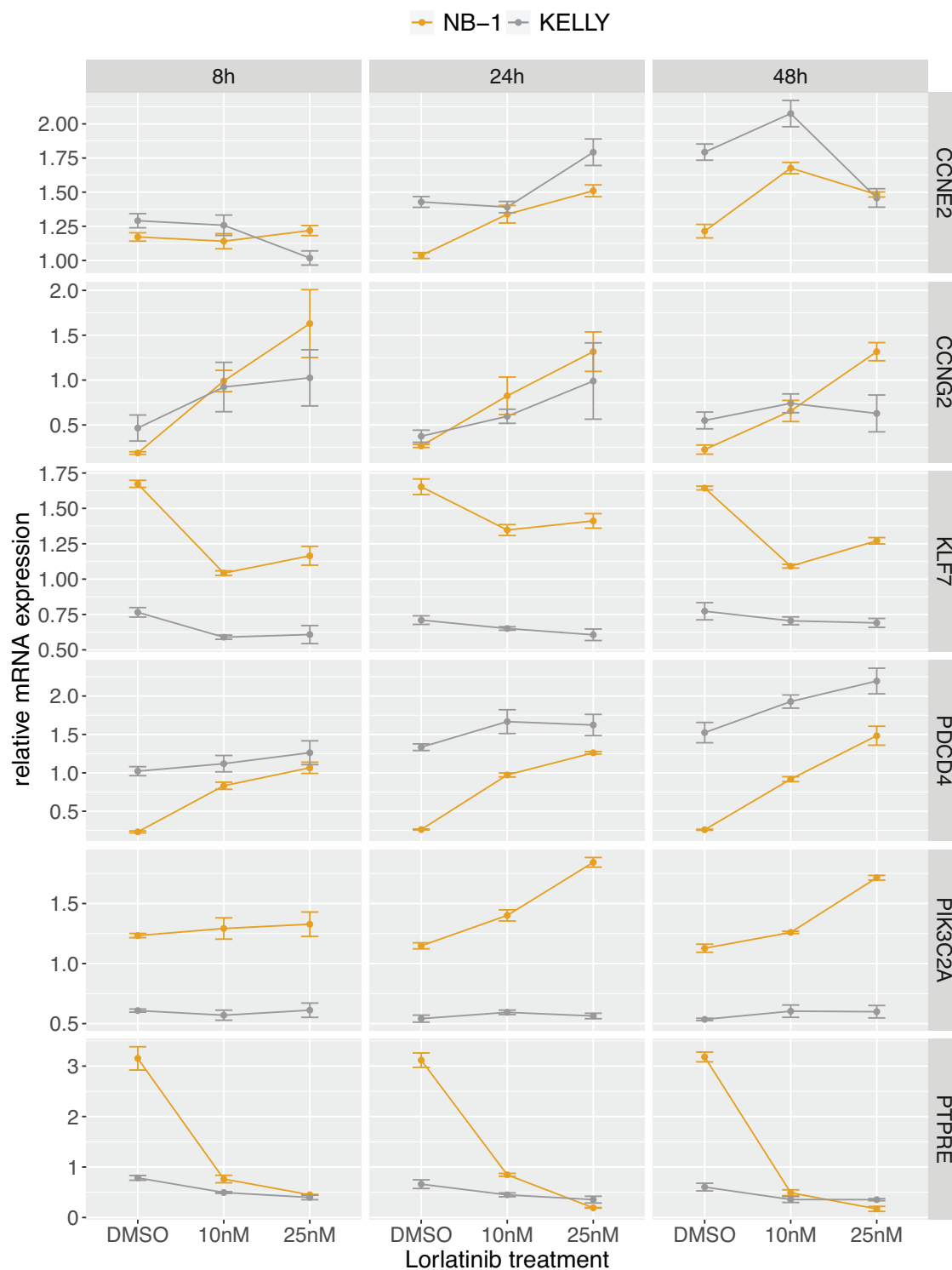


Figure 42: Optimization of concentration and time points for RNA sequencing of lorlatinib treated cell lines. NB-1 and KELLY cells were treated with 10 nM and 25 nM LOR for 8h, 24h and 48h and the expression of six ALK signature genes (*CCNE2*, *CCNG2*, *KLF7*, *PDCD4*, *PIK3D2A* and *PTPRE*) was determined by qRT-PCR. Mean \pm SD of six technical replicates. n=1.

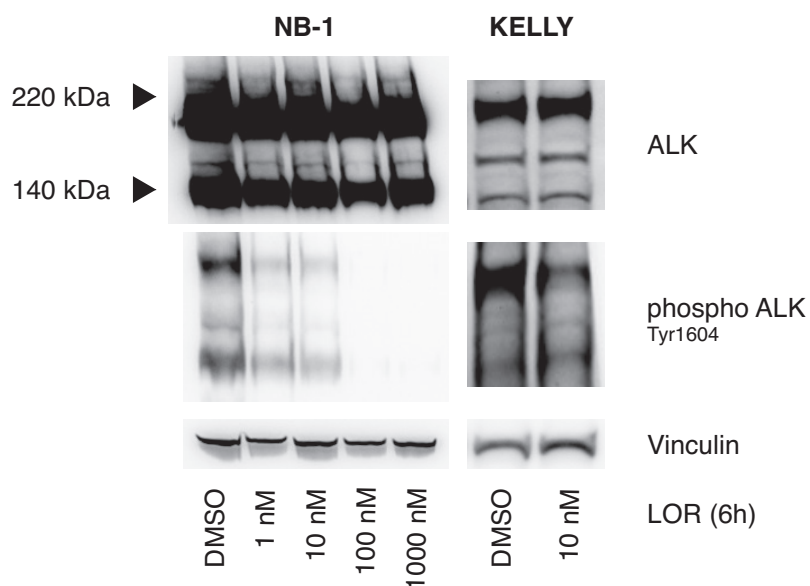


Figure 43: Lorlatinib reduces phosphorylation of ALK. ALK protein expression in NB-1 and KELLY cells at LOR treatment. Cells were treated with indicated LOR concentrations and harvested after 6h. Total protein and phosphorylated protein were analyzed by western blot. n=3. A representative experiment is shown.

Experimental workflow

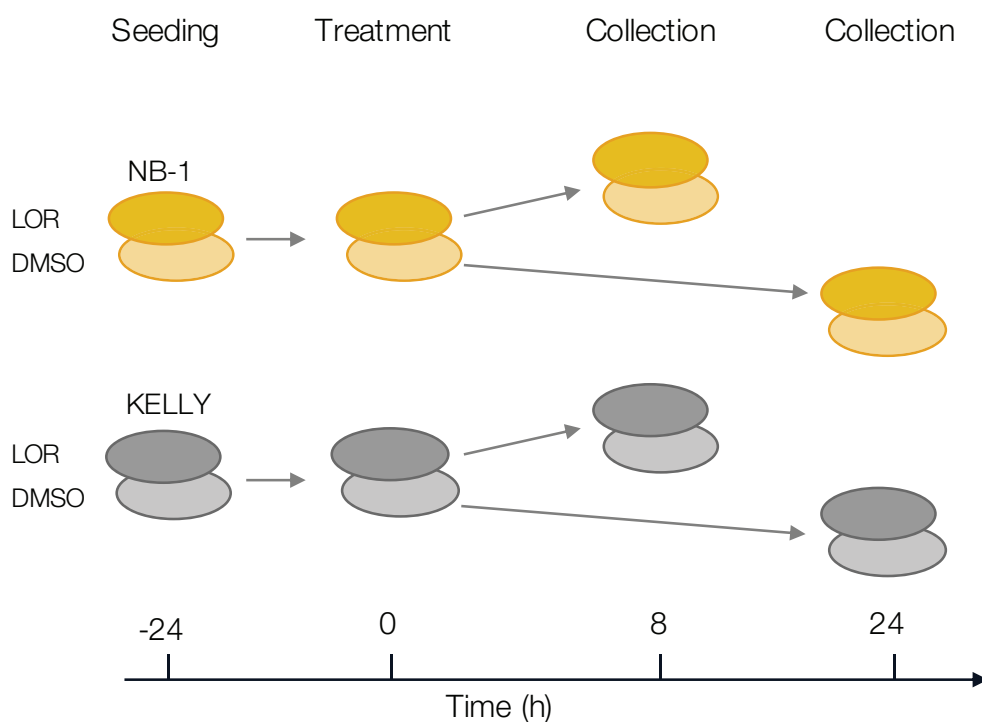


Figure 44: Experimental design of the RNAseq experiment. NB-1 and KELLY cells were treated with 10 nM LOR or a respective DMSO, collected after 8h and 24h and prepared for sequencing. n=2.

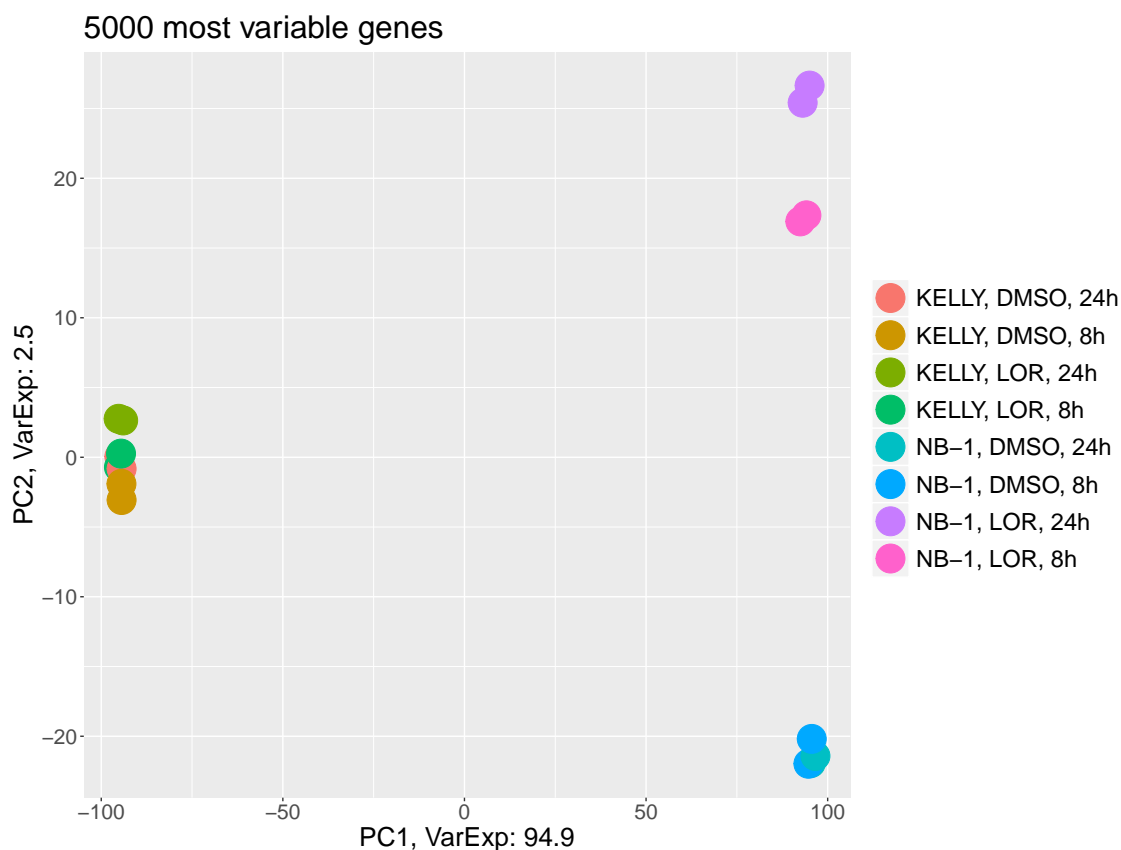


Figure 46: Principle component analysis of RNAseq samples. PCA on the 5000 most variable genes results in a clear separation of the two cell lines NB-1 and KELLY by PC1 and the treatment by PC2.

3.6.2.3 Lorlatinib affects the transcriptome of the responder cell line NB-1 but not of the non-responder KELLY

In order to gain insights into the cellular response to LOR, differential gene expression analysis was performed on both cell lines individually. Treatment of NB-1 cells led to an upregulation of 1042 genes and a downregulation of 1119 genes in total, Figure 47A. While some of these genes were differentially expressed at a specific treatment duration only, approximately a third of all genes were up- or downregulated at both treatment time points. In contrast, LOR treatment of KELLY cells led to a downregulation of four genes only. These four genes were *ETV5* (8h), *SPRY4* (8h and 24h), *DKK1* and *ETV1* (24h), which were also downregulated in NB-1 cells. No upregulated gene was detected, Figure 47B. Despite the partial dephosphorylation of ALK at LOR treatment in KELLY cells, this treatment caused these minor changes in the transcriptome of the cells only.

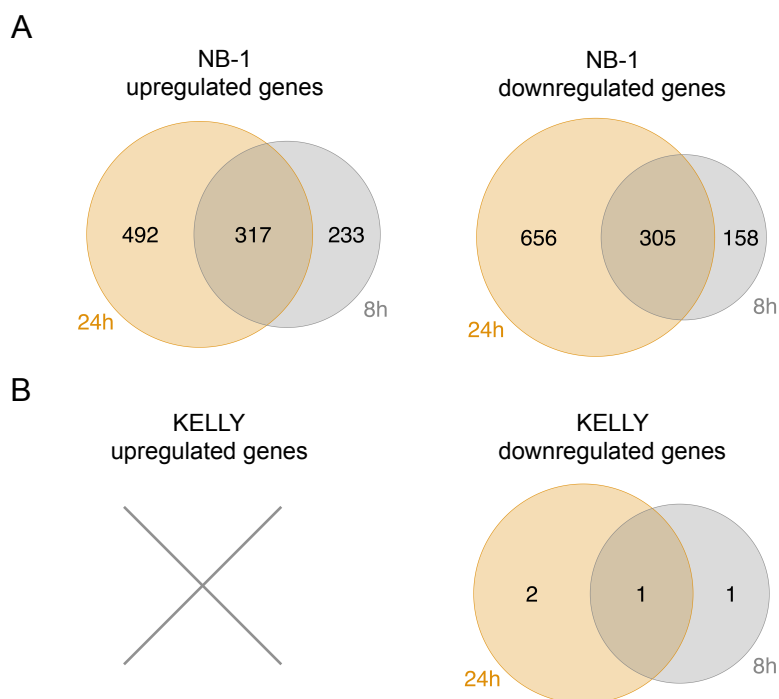


Figure 47: Only NB-1 cells have differentially expressed genes at lorlatinib treatment. Differential gene expression analysis of **A** NB-1 and **B** KELLY cells. Genes with log₂ fold change > 1 and adjusted p-value ≤ 0.05 were considered differentially expressed.

3.6.2.4 Lorlatinib causes cell cycle arrest but not cell death of NB-1 cells

More than 2200 genes were differentially expressed upon LOR treatment in NB-1 cells. To better understand which pathways and biological processes were involved in the response to LOR, gene ontology (GO) enrichment terms were determined, Figure 48. For this purpose, up- and downregulated genes were used for both individual time points and enriched pathways were determined, Figure 48A. For the early 8h time point, MAPK and PI3K-AKT signaling were found among the pathways, confirming the inhibition of these pathways by dephosphorylation of ERK1/2 and AKT observed previously in section 3.3.3. After 24h, LOR caused changes in the expression of genes involved in cell cycle and DNA replication. The 20 most significant biological processes enriched upon treatment included cell division, DNA replication initiation, G₁/S transition and G₂/M transition of mitotic cells, Figure 48B.

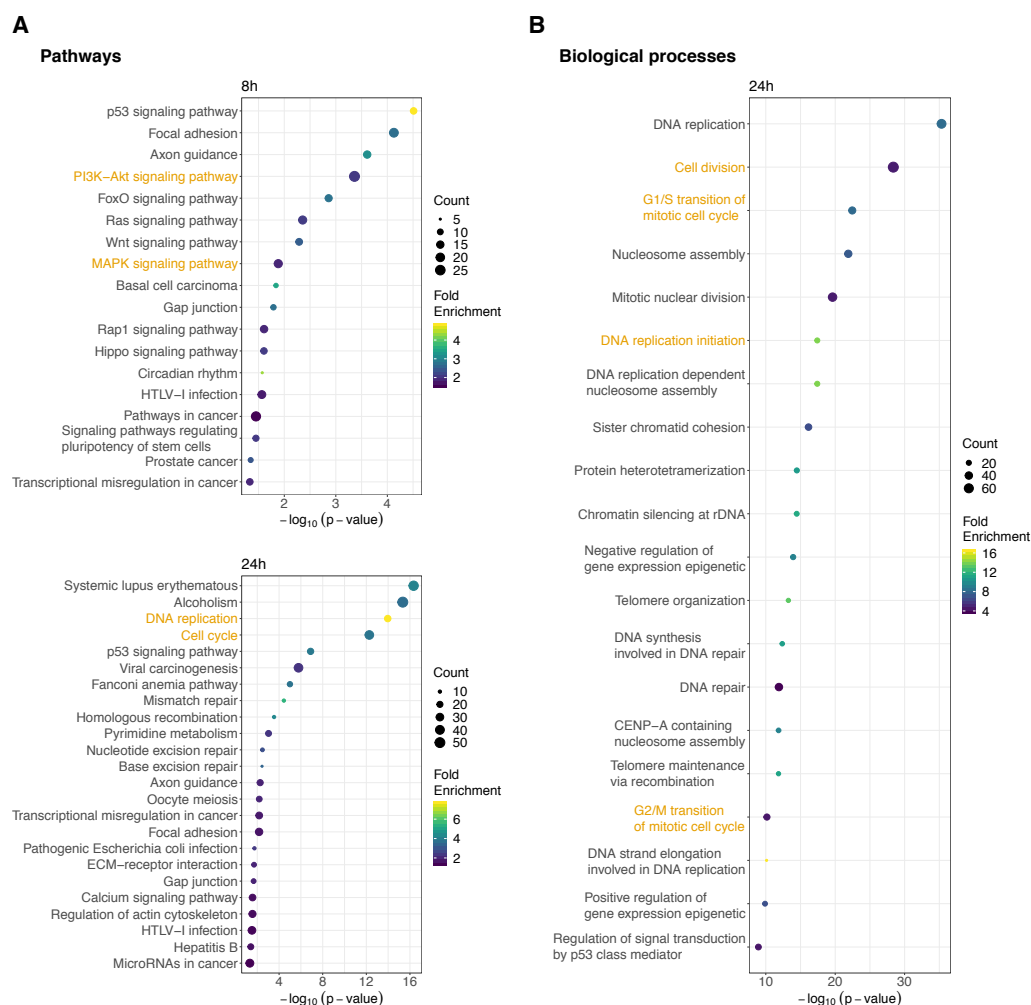
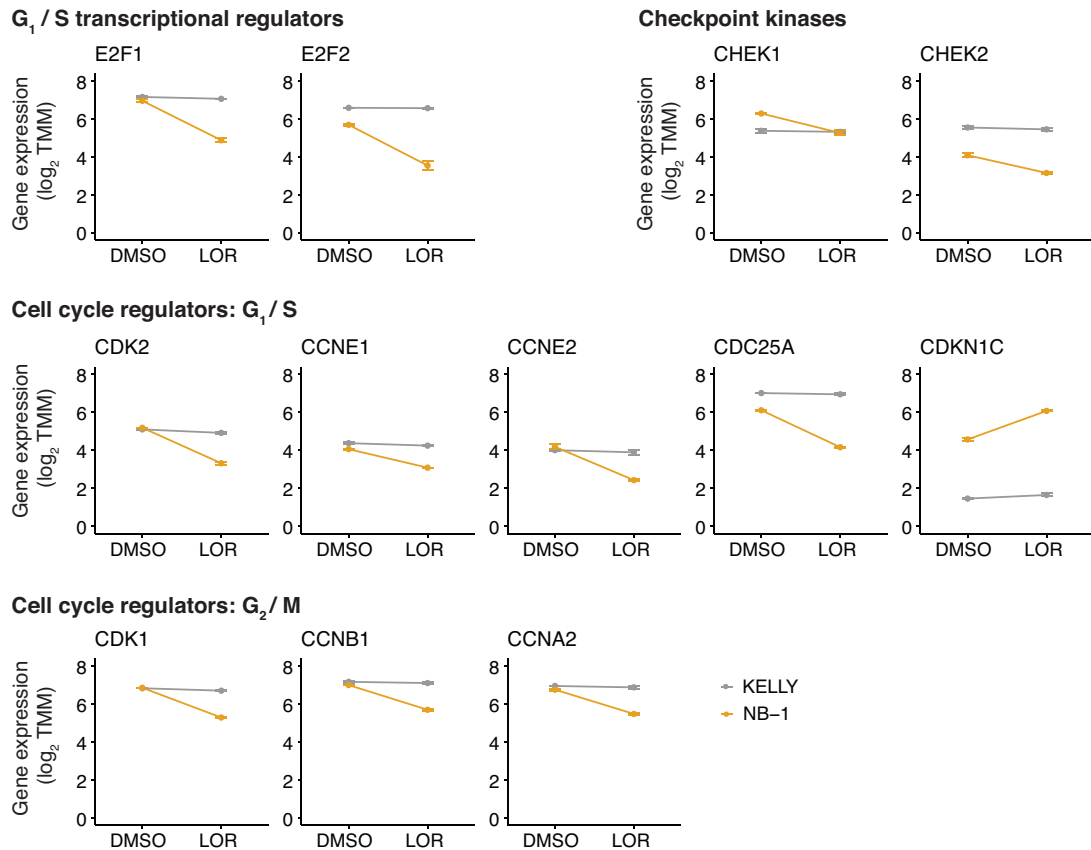


Figure 48: Lorlatinib inhibits cell cycle and ALK downstream pathways in NB-1 cells. Gene ontology enrichment terms of **A** pathways and **B** the 20 most significant biological processes in LOR treated NB-1 cells.

The main effect of LOR treatment was seen in the regulation of genes involved in G_1/S transition and DNA replication initiation, Figure 49A. The expression of both G_1/S transcriptional regulators E2F1 and E2F2 and the cyclin dependent kinase 2 (CDK2) together with its binding partners cyclin E1 and E2 (*CCNE1* and *CCNE2*) were downregulated. Furthermore, the activator and inhibitor of the cyclin E - CDK2 complex, *cdc25a* (*CDC25A*) and *p57* (*CDKN1C*), were down- or upregulated, respectively. Similar, the G_2/M transition regulators cyclin dependent kinase 1 (CDK1) and its binding partners cyclin B1 and A2 (*CCNB1*, *CCNA2*) were downregulated. Furthermore, the gene expression of both checkpoint kinases Chk1 and Chk2 (*CHEK1* and *CHEK2*) decreased. Several other genes involved in cell cycle regulation as well as DNA replication initiation, such as *CDC 6*, *7* and *45*, *MCM 2-7*, *OCR1* and *DBF4*, were downregulated, see appendix Figure 61. Cell cycle arrest suggested by the transcriptome was confirmed by flow cytometry, Figure 49B. The S-Phase population of LOR-treated NB-1 cells completely vanished after

24h, followed by the G2 population after 48h. Both populations slowly started to recover after 96h of LOR treatment. In contrast to NB-1, no effect on the different cell cycle phases was seen in KELLY cells.

A



B

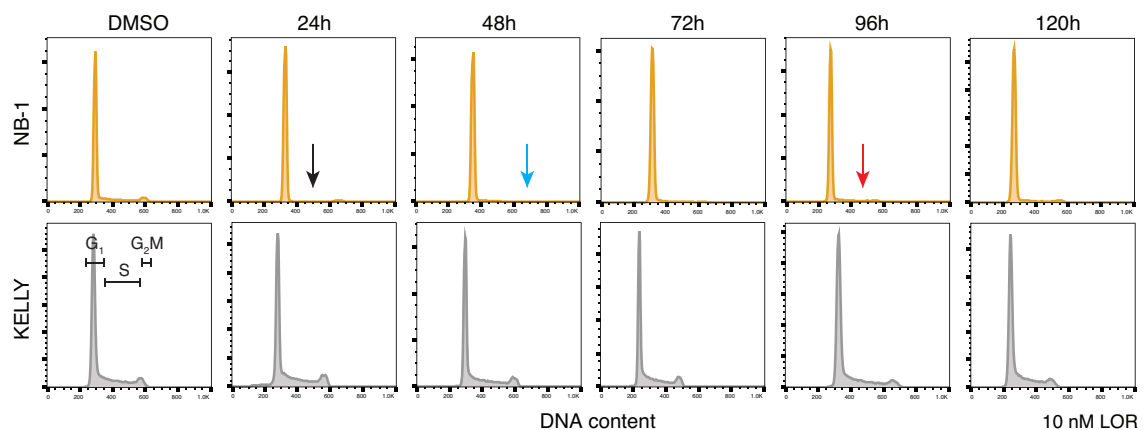


Figure 49: Lorlatinib inhibits cell cycle of NB-1 cells. **A** RNAseq expression of selected cell cycle regulator genes at 24h LOR treatment. Mean \pm SD. $n=2$. **B** Cell cycle of NB-1 and KELLY cells treated with 10 nM LOR at different time points measured by flow cytometry. Arrows indicate loss of S-phase population (black) and G2/M-phase population (blue) as well as the recovery of both populations (red). $n=3$. A representative experiment is shown.

Following the investigation of the cell cycle, the effect of LOR on apoptosis was analyzed. Differential gene expression analysis of NB-1 cells treated with 10 nM LOR for 24h revealed a downregulated of four genes involved in apoptosis, Figure 50A. This includes the executioner caspase 3 (*CASP3*) but not the executioner caspase 7 (*CASP7*), Figure 50B. This suggests that LOR does not induce apoptosis mediated by caspase 3 and caspase 7.

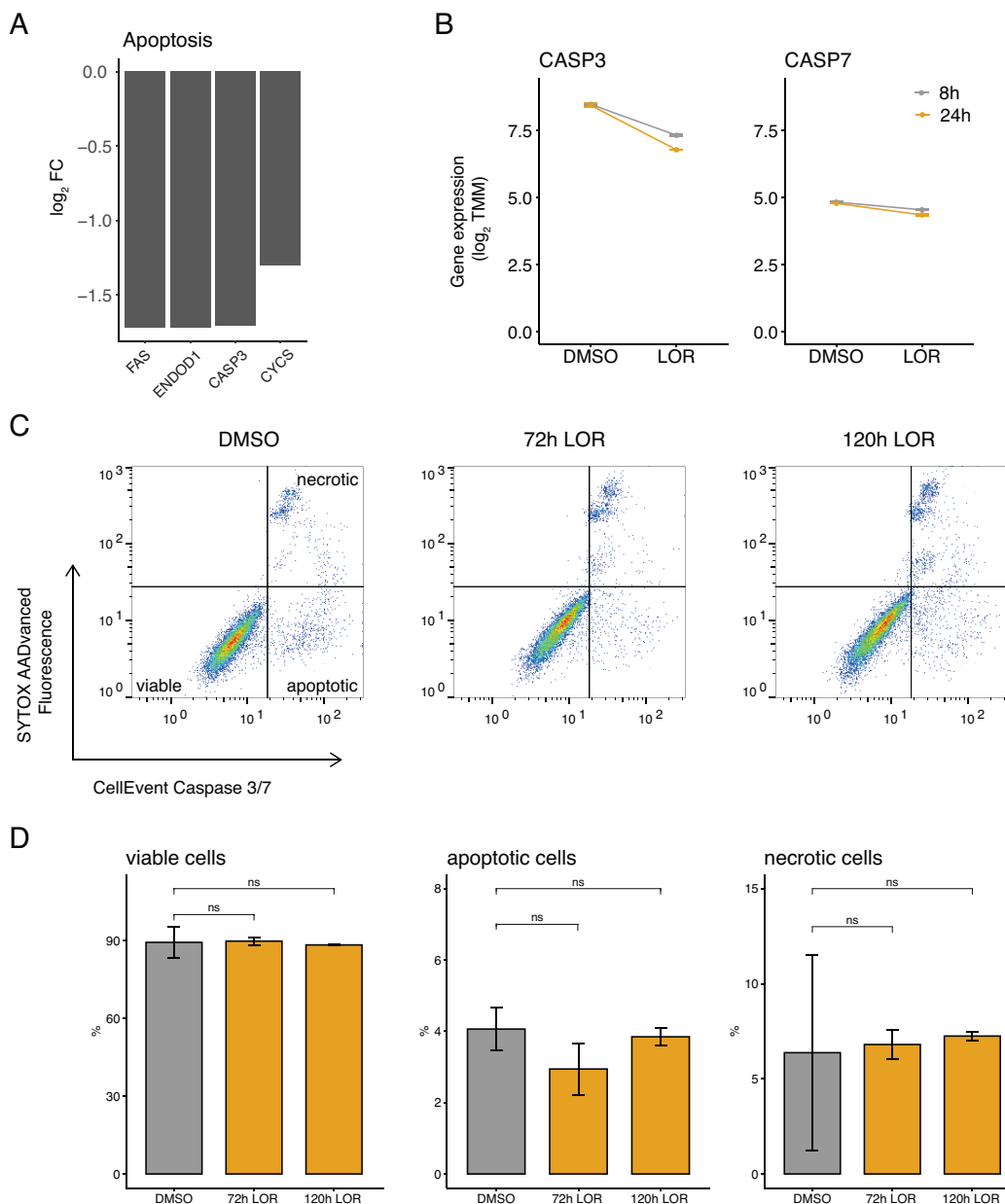


Figure 50: Lortlatinib does not cause cell death mediated by caspase 3 and caspase 7. **A** Differentially expressed genes of the apoptotic pathway of NB-1 cells treated with 10 nM LOR for 24h. **B** RNAseq expression of *CASP3* and *CASP7*. Mean \pm SD. $n=2$. **C** Flow cytometry analysis of NB-1 cells treated with 10 nM LOR for 72h and 120h. Viable, apoptotic and necrotic cells were determined with a caspase 3/7 staining. $n=3$. A representative experiment is shown. **D** Fraction of viable, apoptotic and necrotic cells. Mean \pm SD. $n=3$. Statistical analysis was performed with an unpaired t-test, ns: $p > 0.05$, *: $p < 0.05$, **: $p < 0.01$, ***: $p < 0.001$. FC = fold change.

In order to validate this finding during the course of the LOR treatment, NB-1 cells were treated with 10 nM LOR for 72h and 120h and the fraction of apoptotic and necrotic cells were determined by flow cytometry, Figure 50C,D. There was no significant increase of apoptotic or necrotic cells at LOR treatment for both time points, confirming the RNAseq results.

To further investigate both cell cycle arrest and cell death on the single cell level, live-cell imaging was performed on NB-1 cells. For this purpose, cells were treated with different concentrations of LOR for five days and images were acquired every 20min, Figure 51.

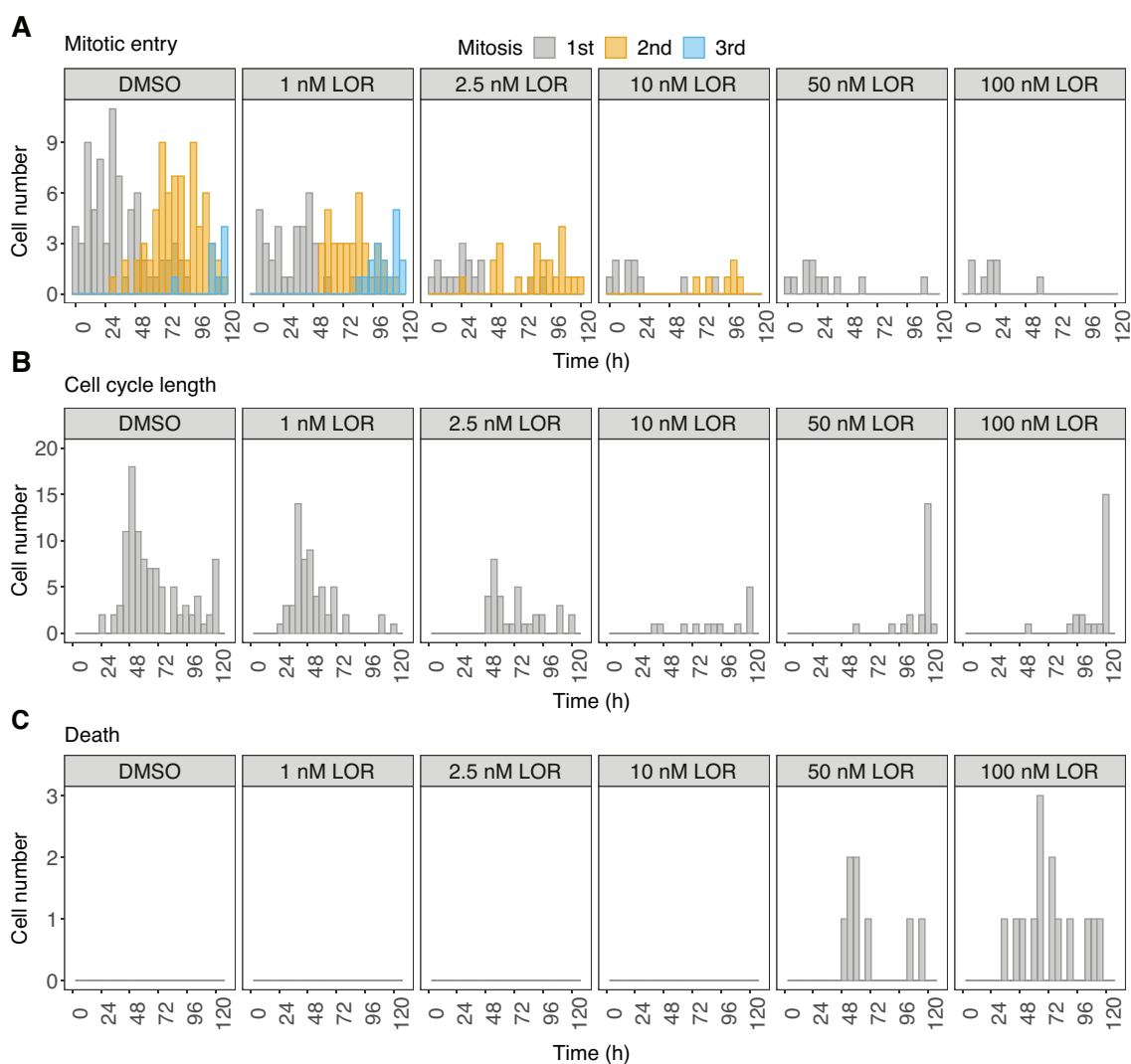


Figure 51: Lorlatinib causes cell cycle arrest. Live cell imaging of NB-1 cells treated with different concentrations of LOR for five days. **A** Time of mitotic entry. **B** Cell cycle length. **C** Time of death. Images were acquired every 20min.

At control conditions, NB-1 cells had a cell cycle length of approximately 48h and divided two to three times within the course of the experiment. There were also a few cells that did not divide within these five days. Cells treated with 1 nM LOR showed a similar behavior, which is in line with the low reduction in viability observed in section 3.3.2. 2.5 nM and 10 nM LOR caused an increased in cell cycle length resulting in a maximum of two divisions during the course of treatment. Furthermore, some cells did not divide at all. The two highest concentrations 50 nM and 100 nM led to an increase in cell cycle length. The high number of cells with a cell cycle length of 120h, the duration of the total treatment, indicates a cell cycle arrest upon a large fraction of the cells. Cell divisions occurred mainly within the first 24h of the treatment and no second divisions were observed. In addition to the cell cycle arrest, these two concentrations caused cell death, Figure 51C. In general, the single cell data confirmed the cell cycle arrest detected in the RNAseq experiment and the cell cycle analysis by flow cytometry.

3.6.2.5 An alternative ALK gene signature determined by lorlatinib treatment

Differential gene expression analysis revealed changes in the transcriptome of the responder cell line NB-1 only. Therefore, control and treated samples of NB-1 cells were used to determine the 100 most variable genes across all NB-1 samples, Figure 52. Similar to what was seen in the PCA on all samples, the samples separated into a treatment and a control cluster. While the treatment cluster was split into two separate clusters by time points, all four control samples were highly similar. Among these 100 genes, there were several genes that belonged to an early response at 8h and genes that were up- or downregulated after 24h. There was an overlap of 22 genes with the published ALK gene signature. These 100 genes were then used as a new gene signature to investigate whether these genes can better discriminate between the treatment response of cell lines. Similar to the published ALK gene signature, there was no clustering of cell lines by their LOR sensitivity in the PCA on the whole cell line panel, Figure 53A. When wild-type cell lines were excluded from the analysis, the three cell lines SMS-KCNR, LAN-5 and CLB-GA formed a cluster, which was observed in the analysis with the published signature as well. Additionally, LAN-1 and KELLY cells clustered together, which was also seen before, Figure 53B. In a next step, a PCA was performed on both patient cohorts, Figure 54. Same as seen with the published signature, there was no clustering based on the *ALK* status for both tumor cohorts when wild-type patients were included, Figure 54A,C, as well as excluded from the analysis, Figure 54B,C. In summary,

these results suggest that the basal gene expression cannot be used to predict the response of cell lines or patients to the treatment with an ALK inhibitor.

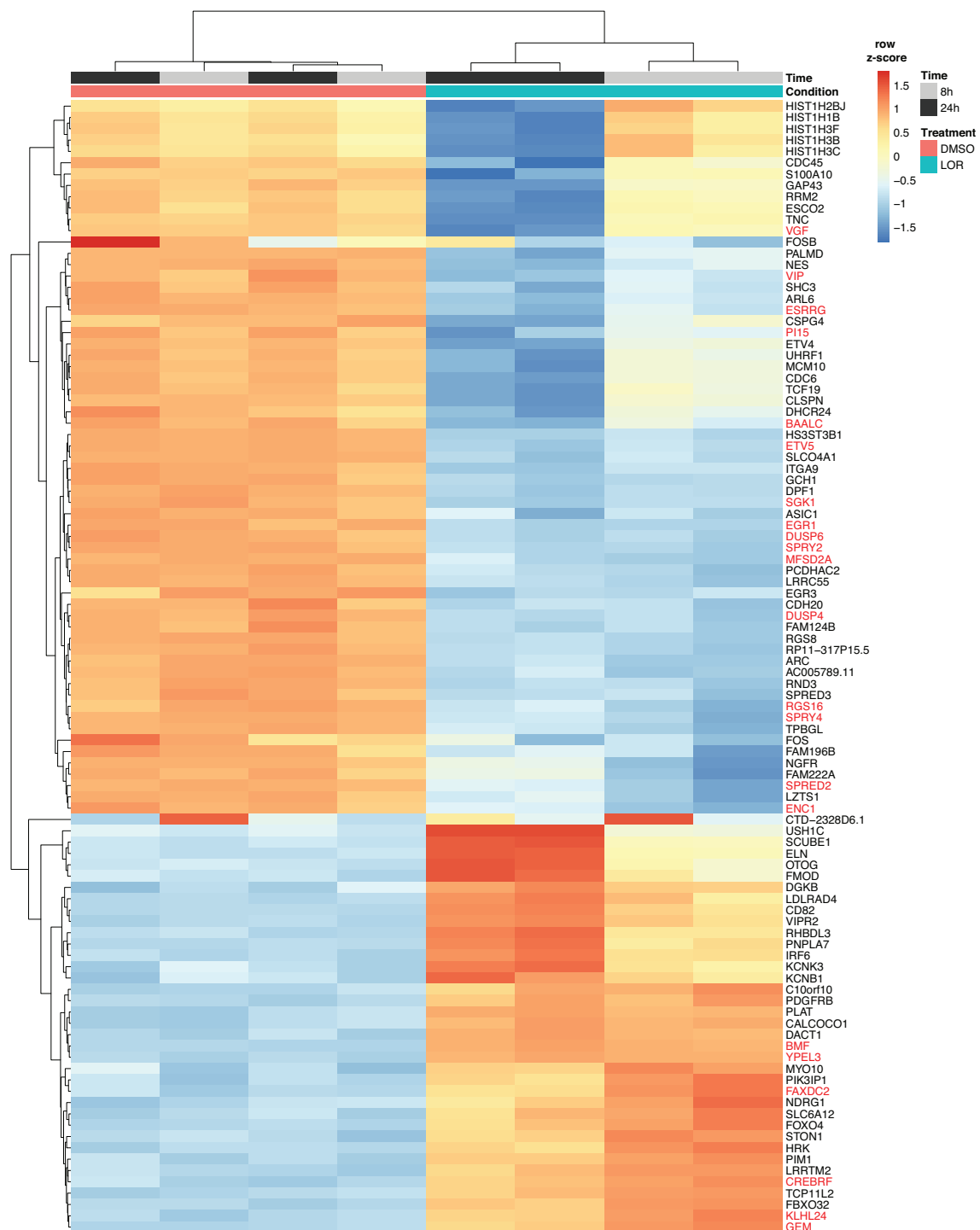


Figure 52: Lorlatinib causes early and late transcript responses in NB-1 cells. Heatmap showing the 100 most variable genes across all NB-1 samples. Genes marked in red overlap with the published ALK signature.

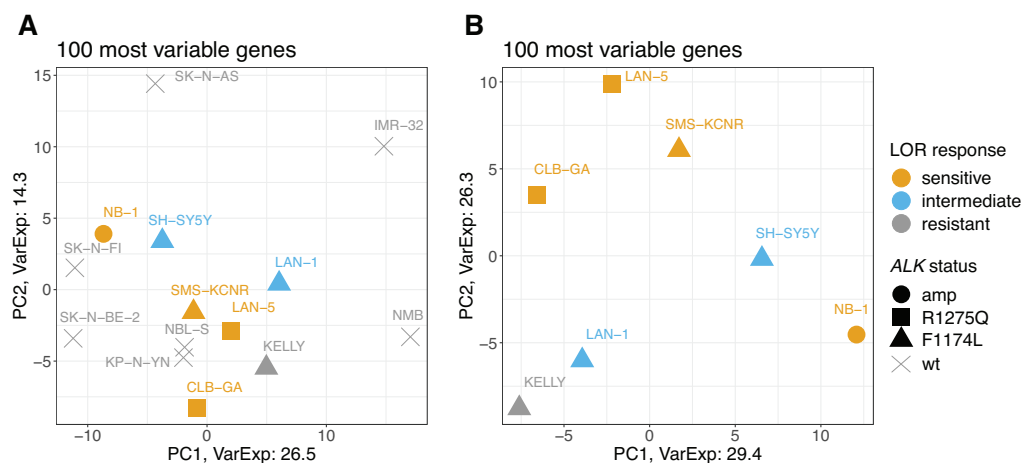


Figure 53: Cell lines do not form clusters of sensitivity based on the 100 most variable genes. PCA of the 100 most variable genes on **A** the selected cell line panel and **B** *ALK* altered cell lines.

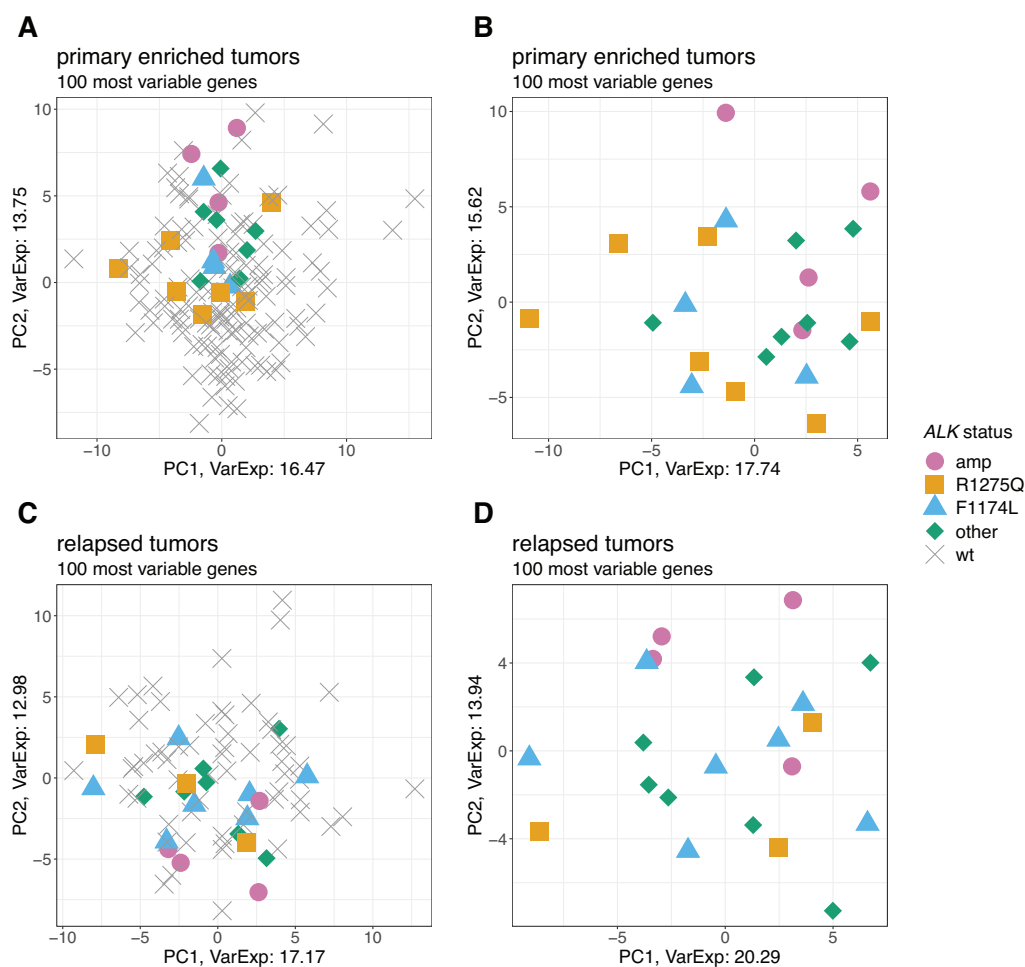


Figure 54: The 100 most variable genes from lorlatinib treatment do not discriminate patients according to their *ALK* status. PCA with the 100 most variable genes at LOR treatment on **A** the primary enriched tumor cohort, **B** *ALK* altered patients of the primary enriched tumor cohort, **C** the relapsed tumor cohort and **D** *ALK* altered patients of the relapsed tumor cohort.

3.6.3 Examination of a possible target gene for ALK combination therapy

Whole transcriptome analysis of LOR treated NB-1 and KELLY cells showed that only NB-1 cells responded to the treatment, suggesting a resistance mechanism of

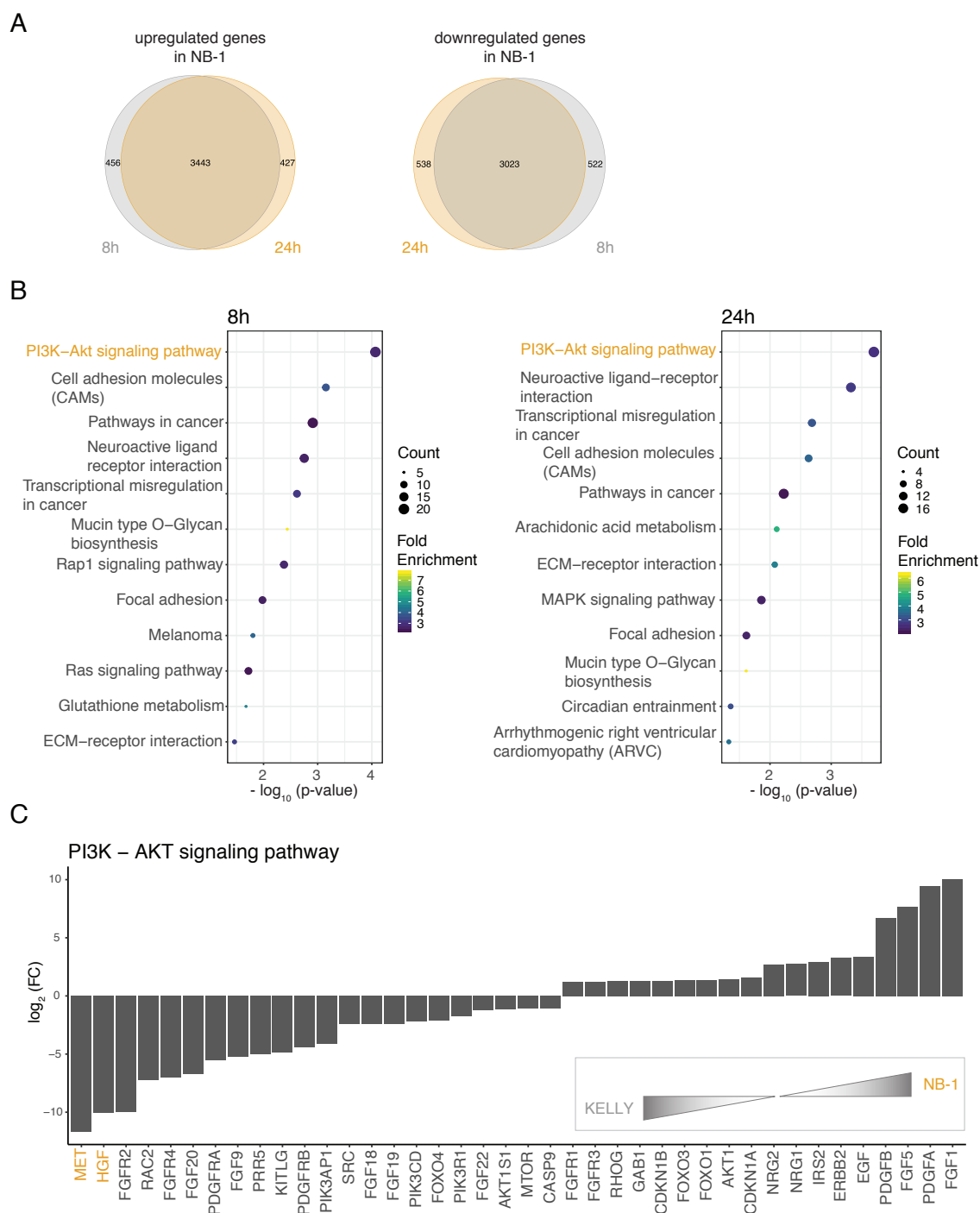


Figure 55: Components of the PI3K-AKT signaling pathway are differentially expressed in responder and non-responder cells. A Differentially expressed genes between NB-1 and KELLY cells at control conditions. **B** Gene ontology enrichment terms determined with genes from A. The 500 genes with the largest absolute \log_2 fold change (FC) were selected. **C** \log_2 FC of genes of the PI3K-AKT signaling pathway. Cutoff: adjusted p-value < 0.05.

KELLY cells. In order to investigate this, basal gene expression of both cell lines were compared by performing a differential gene expression analysis on the control samples, Figure 55A. In total, more than 4000 genes were up- or downregulated in NB-1 cells compared to KELLY cells at normal cell culture conditions. To gain insights into these differences, GO enrichment analysis was performed on the 500 most differentially expressed genes considering changes in the absolute \log_2 FC, Figure 55B. Interestingly, PI3K-AKT signaling, an ALK downstream pathway, was among the enriched pathways. This pathway has several upstream membrane receptors that can cause an activation, such as the tyrosine-protein kinase MET, also known as hepatocyte growth factor receptor (HGFR). Expression of *MET* and its ligand *HGF* were upregulated in the non-responder cell line KELLY, Figure 55C. The expression of both genes were not effected by LOR treatment in both NB-1 and KELLY cells, Figure 56A,B top. A comparison with the rest of the model cell lines revealed a high expression of *MET* also in the intermediate sensitive cell lines LAN-1 and SH-SY5Y as well as sensitive CLB-GA cells, Figure 56A bottom. Similar, *HGF* expression was also higher in SH-SY5Y cells but lower in CLB-GA and LAN-1 cells, Figure 56B bottom. This suggests that signaling via MET could be a bypass mechanism in KELLY cells to decrease their sensitivity to LOR by activating ALK downstream signaling by other membrane receptors.

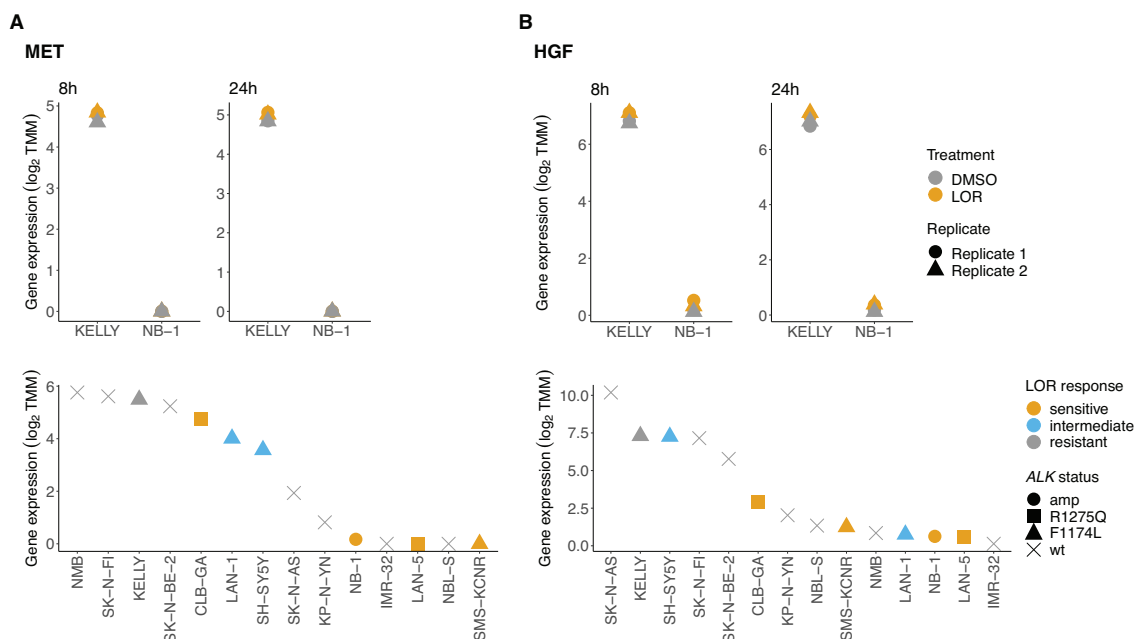


Figure 56: *MET* and *HGF* expression in model cell lines. RNAseq expression of **A** *MET* and **B** *HGF* of LOR- or DMSO-treated NB-1 and KELLY cells (top) and the model cell line panel (bottom).

In order to test whether inhibition of MET can increase the sensitivity to LOR in resistant KELLY and intermediate sensitive SH-SY5Y and LAN-1 cells, the selective MET inhibitor tepotinib (TEP) was applied as single agent and in combination with LOR. *ALK* altered and F1174L mutated SH-EP cells were treated with different concentrations of TEP alone or with the cell line specific EC50 of LOR for five days, viability was measured with the CTB assay and dose response curves were generated, Figure 57. SH-EP and KELLY cells were treated with 1 μM LOR.

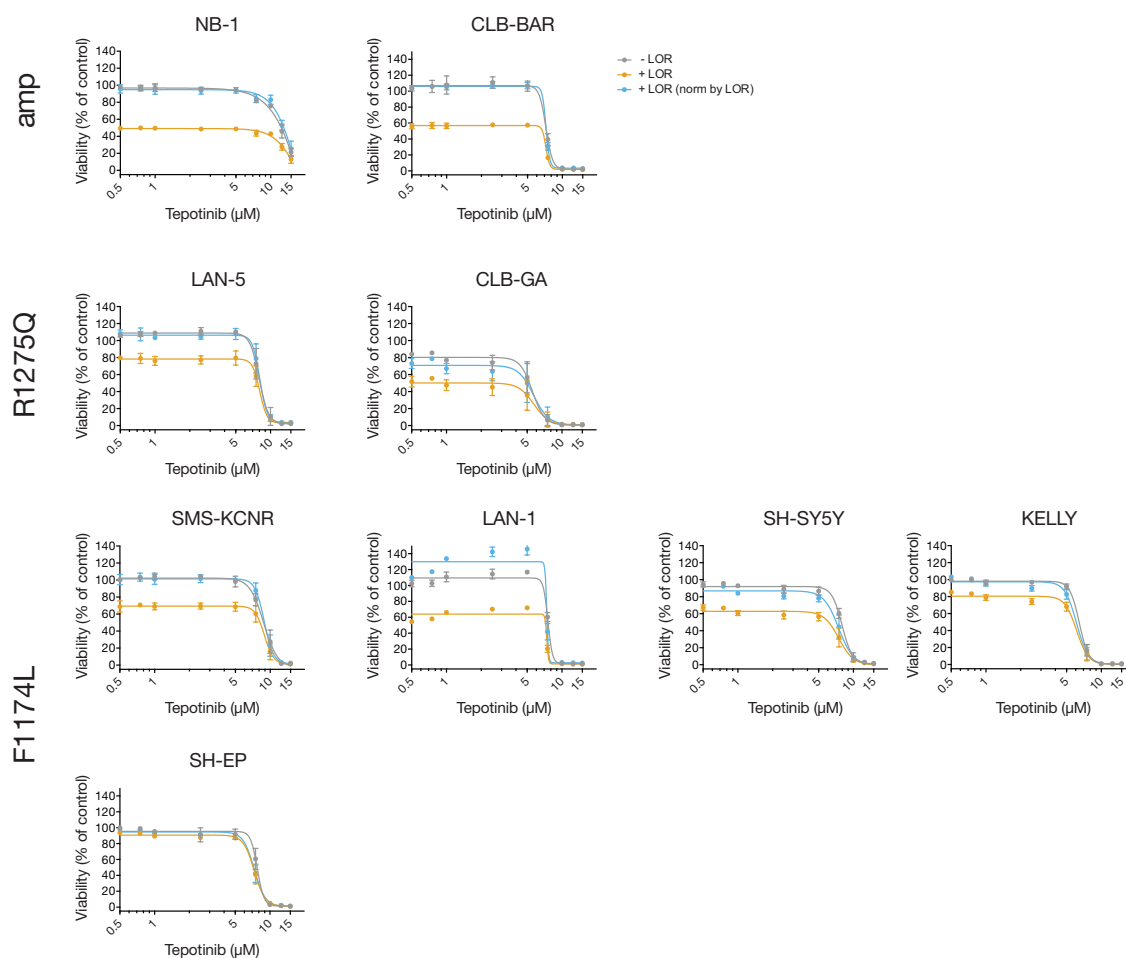


Figure 57: NB cell lines do not respond to the selective MET inhibitor tepotinib. *ALK* amplified and mutated cell lines were treated with different concentrations of TEP alone or together with cell line specific concentrations of LOR for five days and cell viability was measured with the CTB viability assay. GraphPad Prism was used to generate dose response curves. Gray - TEP alone, orange - TEP + EC50 LOR (normalized by ctrl), blue - TEP + EC50 LOR (normalized by EC50 LOR). Mean \pm SD. n=3.

In general, TEP caused a reduction in viability at concentrations $> 5 \mu\text{M}$ for each cell line (gray curve). The addition of LOR caused a reduction in viability at TEP concentrations $< 5 \mu\text{M}$ (orange curve). However, this effect corresponded to LOR single agent treatment of the cells. This could be illustrated by normalizing to treatment with LOR only instead of the DMSO control (blue curve). In this case,

both dose response curves completely overlapped for all cell lines. In general, LOR reduced EC50 values of TEP by several hundred nanomolar, Table 18. Altogether, the selective MET inhibitor TEP was not effective in NB cell lines in clinically relevant doses.

Table 18: EC50 concentrations of tepotinib in mono- and combination therapy with lorlatinib in *ALK* altered cell lines.

Cell line	TEP (μM)	TEP + LOR (μM) (normalized by DMSO)	TEP + LOR (μM) (normalized by LOR)
NB-1	20.51	17.08	16.91
CLB-BAR	7.21	7.22	7.22
LAN-5	7.99	8.07	8.07
CLB-GA	5.55	5.70	5.68
SMS-KCNR	8.78	8.91	8.88
LAN-1	7.56	7.40	7.40
SH-SY5Y	7.98	7.46	7.45
KELLY	6.44	6.10	6.10
SH-EP	7.77	7.32	7.31

In order to determine whether MET has an impact on the general vitality of cells, *MET* was knocked down in the two *ALK* F1174L mutated cell lines KELLY and SH-EP. SH-EP cells were chosen due to their high *MET* expression and their *ALK* mutation status, Figure 58A,B. *MET* was knocked down with three different siRNAs for 120h as a single treatment and in combination with 10 nM LOR. In SH-EP cells, all three siRNAs could fully abolish MET protein expression, Figure 58C. In comparison, in KELLY cells that express much lower levels of MET protein, only siRNA #3 could completely knock down *MET*, Figure 58C. After assessment of protein knock-down, cell viability and cell confluence were determined with the CTB assay and Giemsa staining, respectively, Figure 58D,E. For both cell lines, siRNA knock-down alone could not reduced cell viability or confluence compared to the two non-targeting siRNAs. Next, cell viability and confluence after *MET* knock-down alone and in combination with LOR treatment were analyzed. While the combination with LOR could significantly reduce both viability and confluence in KELLY cells compared to the siRNA knock-down alone, no difference was observed in SH-EP cells.

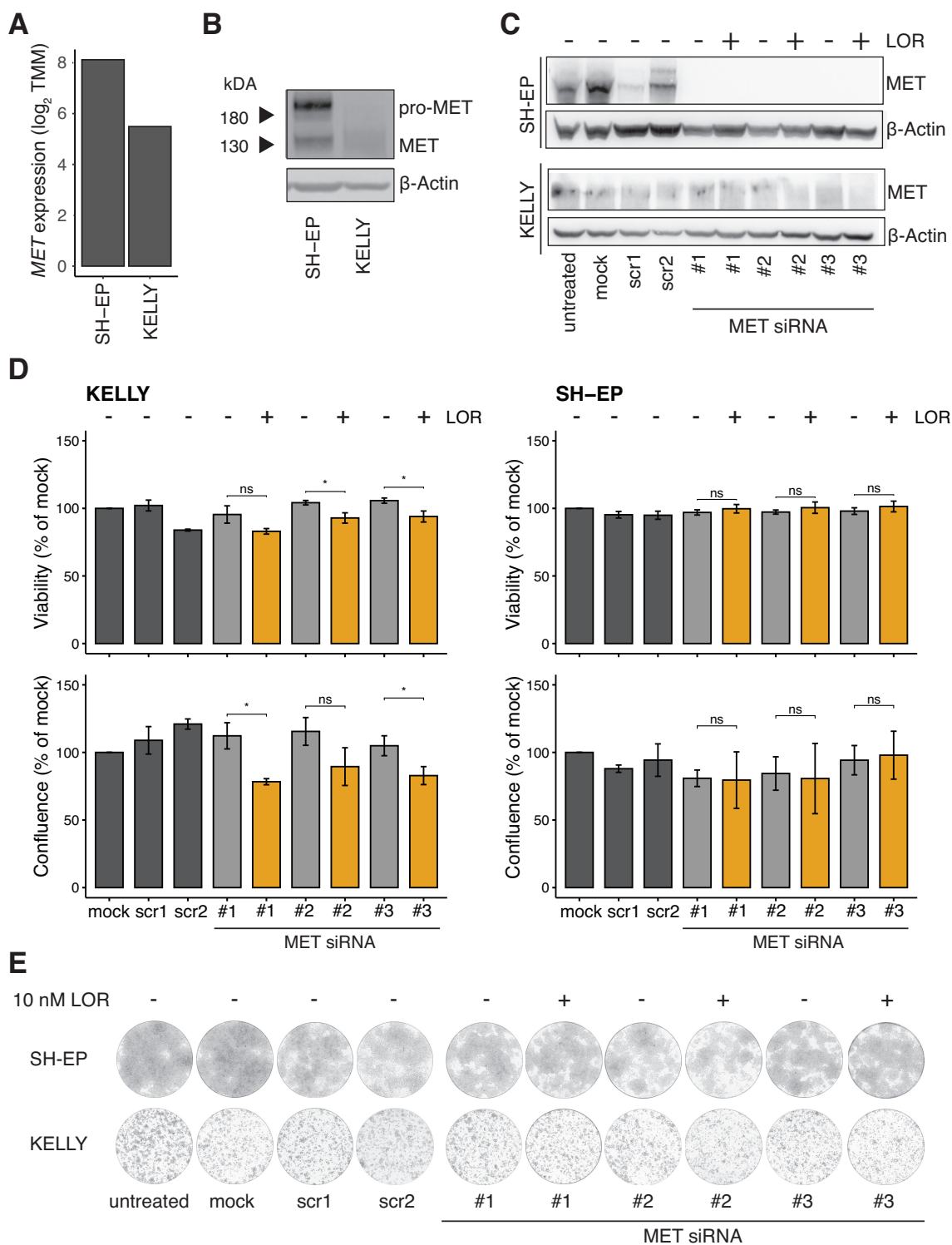


Figure 58: MET knock-down does not effect cell viability and confluence. **A** RNAseq expression and **B** protein expression of MET in SH-EP and KELLY cells. MET was knocked down in both cell lines with three different siRNAs and compared to two non-targeting scrambled siRNAs (scr1/2). In addition to MET knock-down, cells were treated with 10 nM LOR for 120h. **C** MET protein expression upon knock-down was determined by western blot. **D** Cell viability was measured with the CTB assay and Giemsa staining was performed to determine cell confluence. Mean \pm SD. $n=3$. **E** Giemsa staining of one exemplary experiment.

4 Discussion

Neuroblastoma is a highly heterogeneous childhood cancer both from a clinical and biological point of view. There is a large biological diversity of patients which is accompanied by a varying clinical treatment outcome. Therapy with classical chemotherapeutics and radiotherapy cannot eradicate tumors in about half of the high-risk cases, thus novel treatment strategies need to be established. Therefore, the main focus of clinical and pharmaceutical research in the past years has been on the development of small molecule inhibitors that can be used against specific targets that are altered in cancer cells. Unlike cytotoxic chemotherapeutic agents, these drugs target primarily the cancer cells. In the case of neuroblastoma, only a limited number of tractable targets have been determined. *ALK* is the most recurrently mutated gene in NB and as a kinase ALK is also druggable in clinical therapy. To date, several small molecule inhibitors targeting ALK have been developed, some of which are currently used in the care of NB patients and also other ALKomas. However, patients often acquire secondary mutations that cause resistance against the ALK inhibitor used. Thus, these patients often relapse after an initial treatment success, suggesting that the application of ALK inhibitors alone are insufficient. While some patients initially respond well but gain resistance, others do not respond to the treatment at all. Therefore, this study examined a combinatorial therapy approach. In addition, gene expression profiles of patients were analyzed in order to determine whether they can predict the response to ALK inhibition.

4.1 ALK in neuroblastoma patients

ALK is the most recurrently mutated gene in NB with alterations in 6-8% of all NB patients. Approximately 85% of these mutations occur in the three hotspots R1275 (43-49%), F1174 (30-35%) and F1245 (6-12%) (Bresler et al. 2011, De Brouwer et al. 2010). In the present study, RNAseq data of two patient cohorts were analyzed, the primary enriched tumor cohort and the relapsed tumor cohort. While the primary enriched tumor cohort consisted predominantly of primary NBs, the relapsed tumor cohort included only relapse cases. Interestingly, in comparison to published data,

both cohorts had a higher percentage of *ALK* altered patients with 15% and 26%, respectively. The 182 patients of the primary enriched tumor cohort belonged to larger patient cohorts. However, the *ALK* status could only be determined for this subset, due to the lack of accessible data. Therefore, this difference could be explained by subsampling of the patient cohort. Concerning the relapsed tumors, especially the F1174L, as well as further mutations other than R1275Q, increased in this cohort. This could be explained by the high frequency of co-occurrence of the F1174L mutations and *MYCN* amplification causing an unfavorable clinical outcome and thus a relapse disease as well as the gain of secondary resistance mutations (De Brouwer et al. 2010).

4.2 *ALK* in neuroblastoma cell lines

Besides the analysis of RNAseq data from patients, the main focus of this study was the investigation of novel combination therapies including *ALK* inhibitors and standard chemotherapeutics or other targeted drugs, respectively. For this purpose, model cell lines with varying genetic background were selected. To date, more than 30 different *ALK* mutations have been reported, making a reasonable comparison difficult when using too many different alterations (Janoueix-Lerosey et al. 2008, Hallberg and Palmer 2013). Thus, the analysis in this work was restricted to the two main hotspot mutations F1174L and R1275Q. Cell lines with these mutations were compared to *ALK* amplified and wild-type cell lines, which were used as treatment controls. It was found that *ALK* alterations occur at similar frequencies in favorable (INSS 1, 2 and 4S) and unfavorable (INSS 3 and 4) NB (De Brouwer et al. 2010) and one key difference between low-, intermediate- and high-risk NBs is the *MYCN* status (Cohn et al. 2009). To include cell lines that represent the different risk stages, *MYCN* amplified and non-amplified cell lines were chosen for each *ALK* alteration. *ALK* amplification was an exception as there was no *ALK* amplified cell line that was *MYCN* non-amplified. Besides *ALK* and *MYCN* status, the gene expression level of cell lines were determined from RNAseq data and compared to *ALK* expression levels of the two patient cohorts. Expression levels of the different *ALK* subgroups were comparable and thus, cell lines with a broad expression level were included in the analysis. This is especially the case for wild-type cell lines, for which cells with intermediate and low gene expression levels were chosen. Overall, the selected cell lines were a good representation of the total NB cell line panel as they had no specific gene expression profiles compared to the non-selected cell lines.

4.3 Therapeutic targeting of ALK

A total of 15 cell lines were chosen to investigate treatment with ALK inhibitors in NB. In order to find a tissue culture assay that determines the response to ALK inhibitors in a comparable way between the cells, growth behavior of all cell lines was investigated. Overall, NB cell lines were highly heterogeneous in their morphology and growth behavior. While some cells grew in a single layer, other cell lines had the tendency to grow three-dimensional already in the classical 2D tissue culture system. Measuring cell confluence after treatment is a common approach used for drug testing, as it indicates the number of surviving cells. This works particularly well when cells grow in a single layer because the covered area relates to the cell number. In the case of the 15 cell line panel however, this was not possible for all cell lines. Therefore, this method was not suitable for the analysis in the present study. Thus, a cell viability assay was chosen to determine the effect of all agents used. However, this assay does not reflect the actual number of cells surviving the treatment but represents the metabolic activity. First steps were made at a more detailed characterization of all fates during treatment using time-lapse microscopy, see section 3.6.2.4, which may serve as a starting point for future work.

In recent years, several *in vitro* and *in vivo* studies with different ALK inhibitors were performed to reveal their effect on ALK-positive cancer cells (Schonherr et al. 2011, Guan et al. 2016, Infarinato et al. 2016, Cervantes-Madrid et al. 2019). A particular focus was on the effect on viability, survival and how ALK inhibition affects ALK signaling. Especially the two first generation inhibitors crizotinib and NVP-TAE684 (TAE) were extensively studied to determine changes in transcriptome and phosphoproteome upon ALK inhibition (Lambertz et al. 2015, Emdal et al. 2018, Eynden et al. 2018). After studies on these first generation inhibitors, second and third generation ALK inhibitors that were primarily developed for other ALKomas were extensively studied in neuroblastoma in recent years. Here, a first generation ALK inhibitor NVP-TAE684 and a third generation inhibitor lorlatinib (LOR) were tested in six of the 15 selected cell lines. In general, all cell lines were more sensitive to TAE than LOR, also the *ALK* wild-type cell lines SK-N-BE(2C) and SK-N-FI. This is in accordance with previous studies that revealed a high overall toxicity of TAE, which led to the development of the less toxic derivate ceritinib (Schonherr et al. 2011). Thus, in comparison to the selective ALK inhibitor LOR, TAE had strong off-target effects and was therefore excluded from the present study. Cell viability analysis of LOR treatment revealed different sensitivities of cell lines depending on the *ALK* status. The variation in viability reduction was large, ranging from approximately 25% to 85%. This was also reflected in large differences in AUC

values. The combination of both EC50 and AUC showed that cells were sensitive to LOR in clinically relevant doses, but could not be completely eradicated by the treatment. In general, these findings were in accordance with previous studies from other groups (Infarinato et al. 2016, Wang et al. 2017). However, the effect on some cell lines such as KELLY, SH-SY5Y and LAN-5 were stronger in the study performed by Infarinato et al. compared to Wang et al. and the present study. One reason for this difference could be alternative cell numbers in the seeding process. In the former study, all cell lines were seeded in 3000 cells while in the present study, cell numbers were adjusted by the doubling time of cell lines to reach similar confluence at the end of the treatment. Furthermore, KELLY cells had a reduction of viability by only 5-10% in the latter studies, while the study by Infarinato et al. had a reduction by more than 50%. In this case however, seeding numbers were the same. One explanation for the different response of KELLY cells could be the long-term culture of cell lines in different laboratories. This could lead to variations in newly acquired mutations that may cause a resistance to the treatment, due to cultivation over decades.

Based on EC50 and AUC values, five of the selected cell lines (NB-1, CLB-BAR, LAN-5, CLB-GA and SMS-KCNR) were considered LOR-sensitive and had the lowest EC50 and AUC values. For these cell lines, LOR caused a partial dephosphorylation of the ALK downstream targets ERK1/2 and AKT, which was observed by other groups for LOR and other ALK inhibitors (Wang et al. 2017, Cervantes-Madrid et al. 2019, Emdal et al. 2018, Eynden et al. 2018). Interestingly, the largest effect was observed in the *ALK* amplified cell line NB-1. This may be due to much higher expression levels of ALK protein in these cells compared to all other LOR-sensitive cell lines suggesting that NB-1 cells are highly dependent on ALK signaling. One explanation for the weaker response in the other cell lines could be the activation of other upstream membrane receptors activating the Ras-MAPK and PI3K-AKT signaling pathways. One example of an alternative pathway is MET signaling which will be discussed in more detail in section 4.6.

NB-1 cells showed an exceptional response to LOR with a complete inhibition of ALK signaling which had a large effect on the overall vitality of the cells. However, patients are usually treated with such inhibitors over a longer period of time. In a Phase I clinical trial conducted by the New Approaches to Neuroblastoma Therapy Consortium (NCT03107988), patients with ALK-driven relapsed or refractory NBs receive one dose of LOR daily continuously in 28-day cycles. To mimic this long-term treatment with LOR on the super-responder cell line NB-1, cells were continuously treated with low doses (1 nM, 2.5 nM and 5 nM) of LOR for four weeks. These NB-1-R cells showed different responses to the normal five day treatment with 2.5

nM LOR, the EC50 of parental NB-1 cells. Cells with a long-term treatment of 2.5 nM (EC50) or 5 nM LOR were effected significantly less by the normal five day treatment with 2.5 nM LOR compared to cells with a long-term treatment of 1 nM LOR. These data suggest that NB-1 cells become resistance to LOR when treated for an extended period of time, as performed in the clinics. In order to determine the mechanism responsible for the gain in drug resistance, whole transcriptome or phosphoproteome approaches of NB-1-R cells could be taken into consideration for future studies.

Altogether, the findings suggest that single agent treatment with this ALK inhibitor may not be sufficient for the treatment of *ALK* altered NB patients, both due to limited killing of tumor cells and development of resistance. Together with the data on *ALK* mutated cell lines, these results emphasize the need to develop effective combination therapies with ALK inhibitors.

4.4 ALK addicted cells benefit from combination treatment of lorlatinib with chemotherapeutics

Crizotinib was the first ALK inhibitor introduced to the clinical care of adult patients in 2011 and was only shortly thereafter investigated in a clinical trial including NB patients (Mosse et al. 2013). Although patients initially respond well to therapy with crizotinib, they often develop resistance mutations (Choi et al. 2010). In adults, this secondary acquired resistance can be overcome by treatment with the second generation ALK inhibitor ceritinib (Friboulet et al. 2014, Shaw et al. 2014). In NB patients however, the cytotoxic effect of ceritinib was too high in children which illustrated the need to introduce a third generation ALK inhibitor to clinical therapy of NB patients (Janoueix-Lerosey et al. 2018). Therefore, a phase I/II study that is still ongoing was initiated by the New Approaches to Neuroblastoma Therapy consortium in 2015 (NCT03107988). Despite improvement of clinical therapy of NB patients due to the introduction of ALK inhibitors, preclinical and clinical studies showed that the single agent treatment with ALK inhibitors is often not sufficient and needs to be further developed into combinatorial approaches. This observation was confirmed by the present study, as some of the *ALK* F1174L-mutated cell lines only had a weak response to LOR (SH-SY5Y) or did not respond at all (KELLY). Furthermore, the overall response in *ALK* mutated cell lines was relatively weak and therefore provided a rationale for combination treatments. To date, several preclinical studies as well as phase I clinical trials were conducted to test possible combinations of ALK inhibitors with chemotherapeutics or other targeted drugs. These include

the following combinations: crizotinib + topotecan/cyclophosphamide, crizotinib + temsirolimus, ceritinib + ribociclib, ceritinib + NVP-CGM097 and lorlatinib + topotecan/cyclophosphamide (Krytska et al. 2016, Berry et al. 2012, Moore et al. 2014, Wood et al. 2017, Wang et al. 2017, NCT01606878, NCT02559778, NTR5584, NCT02780128, NCT03107988). The present study is the first approach of a combination treatment with the third generation ALK inhibitor lorlatinib and the cytotoxic agents vincristine (VCR) and cisplatin (CDDP). Similar to topotecan and cyclophosphamide, VCR and CDDP are part of the first-line therapy of NB patients (Pinto et al. 2015). The two chemotherapeutics were chosen due to their different mode of action especially on the cell cycle of cancer cells. As a spindle toxin, VCR causes a predominant G2 arrest, while the DNA intercalating agent CDDP forces G1 arrest upon treatment. Combination therapy was tested on all *ALK* altered cell lines and the two *ALK* wild-type cell lines SK-N-BE(2C) and SK-N-FI both in a dose dependent manner and in the combination of EC50 values only. Although a general reduction in cell viability at combination therapy compared to single agent treatment was observed, this was only significant in the super-responder cell line NB-1 for both combinatorial approaches. This is in contrast to observations made by other groups, who could show synergistic effects upon combination therapy also in *ALK* mutated cell lines and patient derived xenografts (PDX) or mouse models (Krytska et al. 2016). However, in the present study, the focus was placed on the combination of EC50 values. In future studies, the synergism of these drug combinations could be determined by using a dose against dose viability assay. Furthermore, the combination was evaluated in a simultaneous application regimen only. An alternative approach could be a deferred application of the drugs, such as pretreatment with LOR followed by therapy with a chemotherapeutic or vice versa. Additionally, a pulsed treatment schedule could also be an option for further investigation. This was found to be more effective than a continuous drug application in the treatment of SH-EP Tet21N cells with the cytostatic agent doxorubicine (DOX) at low concentrations, see appendix Figure 59. Interestingly, the time interval between different treatments had an influence on the treatment efficacy. In contrast, when using higher concentrations of DOX, a continuous treatment was more effective than a pulsed treatment regimen. Altogether, these data suggested that the combination of LOR with the chemotherapeutic agents VCR and CDDP could be beneficial for *ALK* altered cell lines or patients with high ALK protein expression when the concentration and schedule is optimized individually. Nonetheless, the data suggested that NB-1 cells profit from the combination with the tested schedule and drug concentrations. For this reason, the combination treatment was validated in NB-1 tumor spheroids, that more closely mimics a solid tissue.

4.5 Validation of combination therapy in NB-1 spheroids

The first step in drug development is the evaluation of agents in a normal 2D tissue culture setting with conventional cell lines. If the drug shows a promising cytotoxic effect, the next step is to test this agent in appropriate *in vivo* models. However, due to the lack of accessibility of these *in vivo* systems in some laboratories and other limitations of cell and animal models, alternative systems have been developed in the past years. These include 3D tissue culture systems such as multicellular tumor spheroids or more advanced organoids, which can be grown from cell lines and tumor tissue of patients. 3D cultures were first introduced in 1970 and only shortly thereafter tumor spheroids were developed and used in NB research (Inch, McCredie, and Sutherland 1970, Robert M. Sutherland 1971). These tissue culture systems were not only used to study the potency of chemotherapeutic agents on cancer cells and their resistance mechanisms but were also used to investigate the effect of radiotherapy (Russell et al. 1989, Weichselbaum et al. 1984). Russell et al. for example investigated the different treatment outcome of cisplatin and its analogues carboplatin and iproplatin on NCSLC and NB spheroids generated from primary tumor tissue. They found that cisplatin can delay the regrowth of spheroids at a similar level compared to carboplatin and iproplatin but at a much lower dose suggesting to use cisplatin in the clinical care of patients. However, not only single agent treatment but also combination therapies were investigated in 3D culture systems. One example is the combination of the reactive oxygen species (ROS) inducing agent fentretinib (4HPR) with buthionine sulfoximine (BSO), an inhibitor of glutathione synthesis (Cuperus et al. 2011). Here, an astonishing reduction of cell viability by 90% was reached in the combination therapy compared to control spheroids, while the agents alone reduced cell viability only by 20%.

In the present study, mono - and combination therapies were investigated in a 3D tissue culture system. Therefore, NB cell line spheroids were grown with the liquid-overlay technique described by Metzger et al. or by using ULA tissue culture plates (Metzger et al. 2011). While some cell lines grew in almost perfect spheres (NBL-S, IMR5/75, SK-N-DZ) other cell lines formed cellular aggregates without a smooth surface (KELLY, SH-SY5Y, SK-N-FI). To avoid this phenotype, matrigel can be applied to the growth medium. However, the perfect sphere-like shape was not crucial for the normal growth or therapy response and therefore spheroids were grown in normal growth medium only. The established spheroid culture protocol was used to test the single agent LOR, VCR and CDDP treatments as well as the combination of LOR with VCR or CDDP, respectively, in NB-1 spheroids. Interestingly,

NB-1 spheroids responded similar to the 2D culture when treated with LOR and CDDP. Concerning VCR, much higher concentrations compared to the 2D culture had to be applied in order to induce the same cytotoxic effect on NB-1 spheroids. This phenomenon was in accordance with observations of a study from 1980 (Wibe 1980). Wibe showed that the human cervix carcinoma cell line NHIK 3025 is less sensitive to VCR in a 3D setting compared to a 2D culture, while no such difference was observed at DOX treatment. One possible reason for this discrepancy could be the division of spheroids in zones with different proliferative properties. These zones include an outer proliferative layer, an inner necrotic core consisting of dying cells, and a quiescent viable cell layer in between. As a spindle toxin, VCR affects dividing cells in particular, while CDDP also affects quiescent cells by causing DNA damage. Thus, a smaller fraction of cells is susceptible to VCR treatment, making the spheroids more resistant to the treatment. Furthermore, differences in drug uptake, metabolism of cells in a tissue, intracellular communication, insufficient penetration to the inner core or resistance of hypoxic cells could be possible reasons for the varying response. Strikingly, 2D and 3D effects of the combination therapy with LOR and CDDP were similar, suggesting further evaluation of this treatment in *in vivo* models. The tendency for LOR and VCR was similar in spheroids, although one has to keep in mind that spheroids need a higher concentration of VCR to produce the same cytotoxic effect. In a next step, it could be tested whether other drug concentrations or schedules would work better for this drug combination. However, one disadvantage of the liquid overlay technique is that spheroids are not attached to the plate but move freely in the growth medium. Thus, a complete washout of therapeutic agents by medium change is not possible. Therefore, other 3D culture systems would need to be taken into consideration, e.g. by embedding the spheroids in a collagen matrix.

In the last decade, culture of NB organoids has been established and optimized by several groups (Redden and Doolin 2011, Redden et al. 2014, Fusco et al. 2019). Fusco et al. were the first to generate patient derived organoids (PDO) from stage M high-risk NB patients exhibiting self-renewal properties. This approach is more advanced than tumor spheroids because it mimics the actual tumor in greater detail and more realistically than spheroids, while the techniques of cultivating both 3D systems are similar. In a time when personalized medicine becomes extremely important in clinical therapy of cancer patients, PDOs could provide a huge advantage over the classical treatment regimens. PDOs grown from tumor tissue of each patient could be used to test different treatment options within a short period of time. Combination therapies that could significantly reduce organoid growth may be discussed in the tumor board as a possible treatment strategy for individual

patients.

In summary, the combination therapy of LOR with the chemotherapeutics CDDP and VCR was effective in ALK addicted NB-1 cells in both the classical monolayer and the more advanced spheroid tissue culture systems. Although the proliferation of tumor cells could not be completely prohibited, a significant reduction in cell viability and proliferation was observed. This suggests that the doses of these chemotherapeutics may be reduced in the presence of LOR in the treatment of ALK-positive NB patients.

4.6 Whole transcriptome analysis to gain insights into the response to lorlatinib

The combination treatment performed in this work did not result in a favorable response of the majority of *ALK* altered cell lines. Indeed, the combination therapy was effective only in the *ALK* amplified cell line NB-1. To find other possible drug targets for a targeted combination therapy, RNA sequencing was performed on LOR treated NB-1 and KELLY cells. This provided the opportunity to compare changes in the transcriptome of a responder and a non-responder cell line.

4.6.1 KELLY cells may be resistant to lorlatinib through activation of bypass signaling pathways

The different response of NB-1 and KELLY cells to LOR treatment observed in the viability assays was validated by the analysis of the transcriptome at LOR treatment. A first indication of the resistance of KELLY cells to LOR was the formation of a single KELLY cluster compared to different treatment clusters of NB-1 cells at LOR treatment. This discrepancy on a global level was confirmed by differential gene expression analysis, where LOR treatment effected gene expression only in NB-1 cells. Here, more than 2000 genes were up- or downregulated, while only four genes were downregulated in KELLY cells. Interestingly, these four genes included the transcription factor ETV5, which was reported to be a target of activated ALK in NB (Lopez-Delisle et al. 2018, Mus et al. 2020). This suggests that the ERK-ETV5-RET pathway is primarily activated by ALK in KELLY cells, rather than the typical ALK pathways Ras-MAPK or PI3K-AKT. In order to confirm this, further analyses on ETV5 and RET mRNA and protein expression need to be conducted. Despite the partial dephosphorylation of ALK in KELLY cells, only four genes were

differentially expressed. The downregulation of this neglectable number of genes however, may also be generated by chance, rather than being an actual effect of the treatment. Nonetheless, the absence of differentially expressed genes was in line with the lack of reduction in cell viability at LOR treatment in KELLY cells. The presented data suggest that KELLY cells have a bypass signaling pathway that can compensate for the inhibition of ALK. One of these possible bypass pathways includes the hepatocyte growth factor receptor MET, which was found to be differentially expressed between NB-1 and KELLY cells already at basic growth condition. In addition, RNAseq expression of *MET* was also upregulated in the intermediate sensitive cell lines SH-SY5Y and LAN-1. Together, this data suggested that MET inhibition in these cell lines could overcome the resistance or low sensitivity to LOR. Interestingly, treatment with the dual ALK/MET inhibitor crizotinib was effective also in NB cell lines that had a low sensitivity to LOR, indicating to act via both ALK and MET (Shen et al. 2018, Bresler et al. 2014). In ALK-positive NSCLC, inhibition of MET by metformin reduced HGF-induced resistance to alectinib treatment (Chen et al. 2020). Altogether, this suggested to test a combination of LOR with a MET inhibitor. Treatment with the selective MET inhibitor tepotinib (TEP) caused reduction in cell viability only at concentrations in the low micromolar range. This finding confirmed a previous study, in which similar EC50 values were reported (Scorsone et al. 2014). Although TEP could cause a full reduction in cell viability, the concentrations to achieve these results were not in a clinically relevant range. It is therefore more likely that off-target effects caused by a MET-independent toxicity were observed. In addition to MET inhibition by small molecule inhibitors, knock-down experiments with siRNAs were performed on KELLY cells and SH-EP cells, which express high levels of MET mRNA and protein. In both cases, knock-down of *MET* did not have an effect on the general vitality of the cells. This indicates that MET is not the bypass signaling pathway through which KELLY or SH-EP cells gain resistance to LOR treatment. Furthermore, these results demonstrate that gene expression may not be the right type of data to determine bypass signaling pathways, as protein levels define the signaling intensity rather than mRNA levels. Therefore, proteomics or phosphoproteomics approaches may be a better option to find active bypass pathways. In general, the genetic background of NB patients and cell lines is highly versatile, which makes it extremely difficult to find common bypass signaling pathways that are active in many different individuals. To overcome this, one possible option could be the inhibition of ALK downstream targets such as ERK1/2 or AKT directly, which may lead to a synergistic effect together with LOR.

4.6.2 Lorlatinib causes cell cycle arrest rather than cell death

Other than resistant KELLY cells, NB-1 cells responded extremely well to ALK inhibition. This could be seen by a complete dephosphorylation of the main ALK downstream targets ERK1/2 and AKT at LOR treatment which could not be detected in any other tested cell line. This was confirmed by the deregulation of the PI3K-AKT and Ras-MAPK signaling pathways determined by GO term analysis of the RNAseq data. In general, these results were in accordance with many previous studies on ALK inhibition by small molecule inhibitors (Wang et al. 2017, Cervantes-Madrid et al. 2019, Emdal et al. 2018, Eynden et al. 2018). Additionally, GO term analysis revealed deregulation of cell division, G₁/S and G₂/M transition as well as DNA replication initiation. Indeed, downregulation of many cell cycle genes resulted in a cell cycle arrest. The predominant G₁ arrest at 24h treatment and loss of S and G₂/M populations suggests that cells in S and G₂/M phases can finish their cell cycle still at LOR treatment and subsequently arrest in G₁ phase. The treatment with this low doses of LOR could only cause cell cycle arrest but not cell death. In the present study, caspase 3 and 7 mediated apoptosis was investigated. Besides apoptosis, other forms of cell death such as ferroptosis, necroptosis or autophagy could be activated, which will need further investigation in future studies. However, a simple way to investigate whether LOR has the capability to induce cell death at all, is the tracking of cells by time-lapse microscopy. This method gives the opportunity to follow individual cells for an extended period of time by taking images at frequent intervals. Here, live-cell imaging revealed that the clinically relevant dose of 10 nM LOR does not cause cell death. Only 50 nM and 100 nM LOR resulted in cell death of a fraction of treated cells, for which the type of cell death has to be determined in future studies. However, the vast majority of cells showed a cell cycle arrest which could be seen in the dose response curve of NB-1, too. Here, no complete reduction in viability to 0% was observed. The finding of LOR induced cell cycle arrest but not cell death is in accordance with a study on the treatment with the ALK inhibitor alectinib (Miyazaki et al. 2018). In this study, Miyazaki et al. showed that alectinib single agent treatment as well as the combination with the first-line chemotherapeutic CDDP of NB-1 cells caused cell cycle arrest but not cell death. This study suggests that the combination of LOR with p53 activators such as nutlin-2 may be an alternative to the combination with classical first-line chemotherapeutics, which is currently tested in a clinical trial (NCT03107988).

4.6.3 Response to the ALK inhibitor lorlatinib cannot be predicted by the transcriptome

Insights into the genetic background of tumors increased in importance in the past years, as the generation of omics data by whole genome or exome sequencing or RNA sequencing became easily accessible and affordable. The availability of these datasets gives the opportunity to analyze the tumor of each patient individually. This could be used to develop a personalized treatment. On the other hand, available data sets can be used to evaluate the response of patients to prior therapies. Here, RNAseq data was used to relate the response of ALK inhibition by LOR to the basal gene expression of the tested cell lines. Gene expression of both the published ALK signature and the generated ALK signature in this study could not discriminate the cell lines into response clusters. Unfortunately, there was no information on ALK treatment and its outcome on the patient cohorts, but both signatures did not discriminate patients according to their *ALK* status. Altogether, these findings suggest that the transcriptome is not the appropriate data to predict clinical outcome of patients treated with small molecule inhibitors. The transcriptome may be used to detect possible bypass pathways that may lead to therapy resistance. However, the analysis of the proteome or the phosphoproteome are necessary to assess whether the determined pathways are also active on the protein level.

4.7 Conclusion and perspective

The use of ALK inhibitors in the clinical care of patients suffering from tumors with *ALK* alterations increased tremendously over the past years. This study focused on the third generation ALK inhibitor lorlatinib, its effect on the different *ALK* alterations detected in NB patients and possible combination therapies.

In this study it was shown that LOR single agent treatment led to varying responses in *ALK* altered NB cell lines. Notably, this finding applies to cell lines with the same *ALK* alteration. This illustrates that ALK protein expression and activation is the key factor of therapy response rather than the *ALK* alteration itself. In particular, the weak response to ALK inhibition of some *ALK* altered cell lines indicates that ALK may not be the driver of some tumors despite the presence of an *ALK* alteration. Thus, the dependency of tumors on ALK signaling should be included in the first examination of patients, together with the determination of the *ALK* status. This could be done by targeted assays such as protein analysis by flow cytometry or western blot for ALK expression and phosphorylation. More generally,

proteomics or phosphoproteomics could also be useful to include for diagnosis. These data may also provide insights into bypass signaling pathways that can compensate the downregulation of ALK targets caused by ALK inhibition. In parallel, PDOs could be used to test if an ALK inhibitor can successfully inhibit the growth of tumor cells from a particular patient. This may provide the basis for a decision of whether the respective ALK inhibitor should be included into the first-line therapy of each patient individually or not.

Similar to the single agent treatment, combination therapy of LOR with CDDP tested in 2D and 3D tissue culture systems was found to be effective only in the ALK addicted cell line NB-1. This provides the basis for a novel combination therapy approach with the ALK inhibitor LOR. However, the efficacy and optimal scheduling of this combination needs further evaluation in PDOs, PDX or *in vivo* models.

Altogether, treatment of NB patients with ALK inhibitors may cause a favorable clinical outcome for a selected group of patients. Our finding in cell lines that high ALK expression is an indicator for combination therapy with ALK inhibitors warrants future investigation.

References

- Amiel, J. et al. (2003). “Polyalanine expansion and frameshift mutations of the paired-like homeobox gene PHOX2B in congenital central hypoventilation syndrome”. In: *Nat Genet* 33.4, pp. 459–61.
- Baker, D. L. et al. (2010). “Outcome after reduced chemotherapy for intermediate-risk neuroblastoma”. In: *N Engl J Med* 363.14, pp. 1313–23.
- Bazigou, E. et al. (2007). “Anterograde Jelly belly and Alk receptor tyrosine kinase signaling mediates retinal axon targeting in *Drosophila*”. In: *Cell* 128.5, pp. 961–75.
- Berry, T. et al. (2012). “The ALK(F1174L) mutation potentiates the oncogenic activity of MYCN in neuroblastoma”. In: *Cancer Cell* 22.1, pp. 117–30.
- Berthold, F. et al. (1997). “The current contribution of molecular factors to risk estimation in neuroblastoma patients”. In: *Eur J Cancer* 33.12, pp. 2092–7.
- Biedler, J. L., L. Helson, and B. A. Spengler (1973). “Morphology and growth, tumorigenicity, and cytogenetics of human neuroblastoma cells in continuous culture”. In: *Cancer Res* 33.11, pp. 2643–52.
- Biedler, J. L. and B. A. Spengler (1976). “A novel chromosome abnormality in human neuroblastoma and antifolate-resistant Chinese hamster cell lines in culture”. In: *J Natl Cancer Inst* 57.3, pp. 683–95.
- Biedler, J. L. et al. (1978). “Multiple neurotransmitter synthesis by human neuroblastoma cell lines and clones”. In: *Cancer Res* 38.11 Pt 1, pp. 3751–7.
- Bilsland, J. G. et al. (2008). “Behavioral and neurochemical alterations in mice deficient in anaplastic lymphoma kinase suggest therapeutic potential for psychiatric indications”. In: *Neuropsychopharmacology* 33.3, pp. 685–700.
- Bossi, R. T. et al. (2010). “Crystal structures of anaplastic lymphoma kinase in complex with ATP competitive inhibitors”. In: *Biochemistry* 49.32, pp. 6813–25.
- Bourdeaut, F. et al. (2012). “ALK germline mutations in patients with neuroblastoma: a rare and weakly penetrant syndrome”. In: *Eur J Hum Genet* 20.3, pp. 291–7.
- Bouzas-Rodriguez, J. et al. (2010). “Neurotrophin-3 production promotes human neuroblastoma cell survival by inhibiting TrkC-induced apoptosis”. In: *J Clin Invest* 120.3, pp. 850–8.

- Bresler, S. C. et al. (2011). “Differential inhibitor sensitivity of anaplastic lymphoma kinase variants found in neuroblastoma”. In: *Sci Transl Med* 3.108, 108ra114.
- Bresler, S. C. et al. (2014). “ALK mutations confer differential oncogenic activation and sensitivity to ALK inhibition therapy in neuroblastoma”. In: *Cancer Cell* 26.5, pp. 682–94.
- Brinkschmidt, C. et al. (1997). “Comparative genomic hybridization (CGH) analysis of neuroblastomas—an important methodological approach in paediatric tumour pathology”. In: *J Pathol* 181.4, pp. 394–400.
- Brodeur, G. M. (2003). “Neuroblastoma: biological insights into a clinical enigma”. In: *Nat Rev Cancer* 3.3, pp. 203–16.
- Brodeur, G. M., G. Sekhon, and M. N. Goldstein (1977). “Chromosomal aberrations in human neuroblastomas”. In: *Cancer* 40.5, pp. 2256–63.
- Brodeur, G. M. et al. (1984). “Amplification of N-myc in untreated human neuroblastomas correlates with advanced disease stage”. In: *Science* 224.4653, pp. 1121–4.
- Brodeur, G. M. et al. (1987). “Consistent N-myc copy number in simultaneous or consecutive neuroblastoma samples from sixty individual patients”. In: *Cancer Res* 47.16, pp. 4248–53.
- Brodeur, G. M. et al. (1988). “International criteria for diagnosis, staging, and response to treatment in patients with neuroblastoma”. In: *J Clin Oncol* 6.12, pp. 1874–81.
- Brodeur, G. M. et al. (1993). “Revisions of the international criteria for neuroblastoma diagnosis, staging, and response to treatment”. In: *J Clin Oncol* 11.8, pp. 1466–77.
- Camidge, D. R. and R. C. Doebele (2012). “Treating ALK-positive lung cancer—early successes and future challenges”. In: *Nat Rev Clin Oncol* 9.5, pp. 268–77.
- Caren, H. et al. (2008). “High incidence of DNA mutations and gene amplifications of the ALK gene in advanced sporadic neuroblastoma tumours”. In: *Biochem J* 416.2, pp. 153–9.
- Cazes, A. et al. (2013). “Characterization of rearrangements involving the ALK gene reveals a novel truncated form associated with tumor aggressiveness in neuroblastoma”. In: *Cancer Res* 73.1, pp. 195–204.
- Cazes, A. et al. (2014). “Activated Alk triggers prolonged neurogenesis and Ret upregulation providing a therapeutic target in ALK-mutated neuroblastoma”. In: *Oncotarget* 5.9, pp. 2688–702.
- Cervantes-Madrid, D. et al. (2019). “Repotrectinib (TPX-0005), effectively reduces growth of ALK driven neuroblastoma cells”. In: *Sci Rep* 9.1, p. 19353.

- Chand, D. et al. (2013). “Cell culture and *Drosophila* model systems define three classes of anaplastic lymphoma kinase mutations in neuroblastoma”. In: *Dis Model Mech* 6.2, pp. 373–82.
- Chen, H. et al. (2020). “Metformin reduces HGF-induced resistance to alectinib via the inhibition of Gab1”. In: *Cell Death Dis* 11.2, p. 111.
- Chen, K. et al. (2016). “Phosphoproteomics reveals ALK promote cell progress via RAS/ JNK pathway in neuroblastoma”. In: *Oncotarget* 7.46, pp. 75968–75980.
- Chen, Y. et al. (2008). “Oncogenic mutations of ALK kinase in neuroblastoma”. In: *Nature* 455.7215, pp. 971–4.
- Cheung, N. K. et al. (2012). “Association of age at diagnosis and genetic mutations in patients with neuroblastoma”. In: *JAMA* 307.10, pp. 1062–71.
- Chiarle, R. et al. (2008). “The anaplastic lymphoma kinase in the pathogenesis of cancer”. In: *Nat Rev Cancer* 8.1, pp. 11–23.
- Choi, Y. L. et al. (2010). “EML4-ALK mutations in lung cancer that confer resistance to ALK inhibitors”. In: *N Engl J Med* 363.18, pp. 1734–9.
- Christensen, J. G. et al. (2007). “Cytoreductive antitumor activity of PF-2341066, a novel inhibitor of anaplastic lymphoma kinase and c-Met, in experimental models of anaplastic large-cell lymphoma”. In: *Mol Cancer Ther* 6.12 Pt 1, pp. 3314–22.
- Cohn, S. L. et al. (1990a). “Analysis of DNA ploidy and proliferative activity in relation to histology and N-myc amplification in neuroblastoma”. In: *Am J Pathol* 136.5, pp. 1043–52.
- Cohn, S. L. et al. (1990b). “Prolonged N-myc protein half-life in a neuroblastoma cell line lacking N-myc amplification”. In: *Oncogene* 5.12, pp. 1821–7.
- Cohn, S. L. et al. (2009). “The International Neuroblastoma Risk Group (INRG) classification system: an INRG Task Force report”. In: *J Clin Oncol* 27.2, pp. 289–97.
- Combaret, V. et al. (1995). “Sensitive detection of numerical and structural aberrations of chromosome 1 in neuroblastoma by interphase fluorescence in situ hybridization. Comparison with restriction fragment length polymorphism and conventional cytogenetic analyses”. In: *Int J Cancer* 61.2, pp. 185–91.
- Cowell, J. K. and H. T. Rupniak (1983). “Chromosome analysis of human neuroblastoma cell line TR14 showing double minutes and an aberration involving chromosome 1”. In: *Cancer Genet Cytogenet* 9.3, pp. 273–80.
- Cuperus, R. et al. (2011). “Promising effects of the 4HPR-BSO combination in neuroblastoma monolayers and spheroids”. In: *Free Radic Biol Med* 51.6, pp. 1213–20.
- Dagogo-Jack, I., A. T. Shaw, and G. J. Riely (2017). “Optimizing treatment for patients with anaplastic lymphoma kinase-positive lung cancer”. In: *Clin Pharmacol Ther* 101.5, pp. 625–633.

- D'Angio, G. J., A. E. Evans, and C. E. Koop (1971). "Special pattern of widespread neuroblastoma with a favourable prognosis". In: *Lancet* 1.7708, pp. 1046–9.
- De Bernardi, B. et al. (2003). "Disseminated neuroblastoma in children older than one year at diagnosis: comparable results with three consecutive high-dose protocols adopted by the Italian Co-Operative Group for Neuroblastoma". In: *J Clin Oncol* 21.8, pp. 1592–601.
- De Bernardi, B. et al. (2008). "Treatment of localised resectable neuroblastoma. Results of the LNESG1 study by the SIOP Europe Neuroblastoma Group". In: *Br J Cancer* 99.7, pp. 1027–33.
- De Bernardi, B. et al. (2009). "Excellent outcome with reduced treatment for infants with disseminated neuroblastoma without MYCN gene amplification". In: *J Clin Oncol* 27.7, pp. 1034–40.
- De Brouwer, S. et al. (2010). "Meta-analysis of neuroblastomas reveals a skewed ALK mutation spectrum in tumors with MYCN amplification". In: *Clin Cancer Res* 16.17, pp. 4353–62.
- Donti, E. et al. (1988). "Cytogenetic and molecular study of two human neuroblastoma cell lines". In: *Cancer Genet Cytogenet* 30.2, pp. 225–31.
- Duijkers, F. A. et al. (2011). "Anaplastic lymphoma kinase (ALK) inhibitor response in neuroblastoma is highly correlated with ALK mutation status, ALK mRNA and protein levels". In: *Cell Oncol (Dordr)* 34.5, pp. 409–17.
- (2012). "High anaplastic lymphoma kinase immunohistochemical staining in neuroblastoma and ganglioneuroblastoma is an independent predictor of poor outcome". In: *Am J Pathol* 180.3, pp. 1223–31.
- Eklof, O. et al. (1983). "Spontaneous regression of stage IV neuroblastoma". In: *Acta Paediatr Scand* 72.3, pp. 473–6.
- El-Badry, O. M. et al. (1989). "Autonomous growth of a human neuroblastoma cell line is mediated by insulin-like growth factor II". In: *J Clin Invest* 84.3, pp. 829–39.
- Eleveld, T. F. et al. (2015). "Relapsed neuroblastomas show frequent RAS-MAPK pathway mutations". In: *Nat Genet* 47.8, pp. 864–71.
- Emdal, K. B. et al. (2018). "Integrated proximal proteomics reveals IRS2 as a determinant of cell survival in ALK-driven neuroblastoma". In: *Sci Signal* 11.557.
- Englund, C. et al. (2003). "Jeb signals through the Alk receptor tyrosine kinase to drive visceral muscle fusion". In: *Nature* 425.6957, pp. 512–6.
- Evans, A. E., G. J. D'Angio, and J. Randolph (1971). "A proposed staging for children with neuroblastoma. Children's cancer study group A". In: *Cancer* 27.2, pp. 374–8.

- Eynden, J. Van den et al. (2018). “Phosphoproteome and gene expression profiling of ALK inhibition in neuroblastoma cell lines reveals conserved oncogenic pathways”. In: *Sci Signal* 11.557.
- Falini, B. et al. (1999). “ALK+ lymphoma: clinico-pathological findings and outcome”. In: *Blood* 93.8, pp. 2697–706.
- Farooqi, A. S. et al. (2014). “Alternative lengthening of telomeres in neuroblastoma cell lines is associated with a lack of MYCN genomic amplification and with p53 pathway aberrations”. In: *J Neurooncol* 119.1, pp. 17–26.
- Fiorillo, A. et al. (1982). “Prolonged survival of a patient with disseminated neuroblastoma”. In: *J Pediatr* 101.4, pp. 564–6.
- Fong, C. T. et al. (1989). “Loss of heterozygosity for the short arm of chromosome 1 in human neuroblastomas: correlation with N-myc amplification”. In: *Proc Natl Acad Sci U S A* 86.10, pp. 3753–7.
- Franks, L. M. et al. (1997). “Neuroblastoma in adults and adolescents: an indolent course with poor survival”. In: *Cancer* 79.10, pp. 2028–35.
- Fransson, S. et al. (2015). “Intragenic anaplastic lymphoma kinase (ALK) rearrangements: translocations as a novel mechanism of ALK activation in neuroblastoma tumors”. In: *Genes Chromosomes Cancer* 54.2, pp. 99–109.
- Friboulet, L. et al. (2014). “The ALK inhibitor ceritinib overcomes crizotinib resistance in non-small cell lung cancer”. In: *Cancer Discov* 4.6, pp. 662–673.
- Fusco, P. et al. (2019). “Patient-derived organoids (PDOs) as a novel in vitro model for neuroblastoma tumours”. In: *BMC Cancer* 19.1, p. 970.
- Gainor, J. F. et al. (2016). “Molecular Mechanisms of Resistance to First- and Second-Generation ALK Inhibitors in ALK-Rearranged Lung Cancer”. In: *Cancer Discov* 6.10, pp. 1118–1133.
- Galkin, A. V. et al. (2007). “Identification of NVP-TAE684, a potent, selective, and efficacious inhibitor of NPM-ALK”. In: *Proc Natl Acad Sci U S A* 104.1, pp. 270–5.
- Gambacorti Passerini, C. et al. (2014). “Crizotinib in advanced, chemoresistant anaplastic lymphoma kinase-positive lymphoma patients”. In: *J Natl Cancer Inst* 106.2, djt378.
- Gansler, T. et al. (1986). “Flow cytometric DNA analysis of neuroblastoma. Correlation with histology and clinical outcome”. In: *Cancer* 58.11, pp. 2453–8.
- George, R. E. et al. (2008). “Activating mutations in ALK provide a therapeutic target in neuroblastoma”. In: *Nature* 455.7215, pp. 975–8.
- Gouzi, J. Y. et al. (2005). “Role of the subcellular localization of ALK tyrosine kinase domain in neuronal differentiation of PC12 cells”. In: *J Cell Sci* 118.Pt 24, pp. 5811–23.
- Guan, J. et al. (2015). “FAM150A and FAM150B are activating ligands for anaplastic lymphoma kinase”. In: *Elife* 4, e09811.

- Guan, J. et al. (2016). “The ALK inhibitor PF-06463922 is effective as a single agent in neuroblastoma driven by expression of ALK and MYCN”. In: *Dis Model Mech* 9.9, pp. 941–52.
- Guan, J. et al. (2018). “Clinical response of the novel activating ALK-I1171T mutation in neuroblastoma to the ALK inhibitor ceritinib”. In: *Cold Spring Harb Mol Case Stud* 4.4.
- Hallberg, B. and R. H. Palmer (2013). “Mechanistic insight into ALK receptor tyrosine kinase in human cancer biology”. In: *Nat Rev Cancer* 13.10, pp. 685–700.
- (2016). “The role of the ALK receptor in cancer biology”. In: *Ann Oncol* 27 Suppl 3, pp. iii4–iii15.
- Hayflick, L. (1965). “The Limited in Vitro Lifetime of Human Diploid Cell Strains”. In: *Exp Cell Res* 37, pp. 614–36.
- Heath, J. A. et al. (2018). “Good clinical response to alectinib, a second generation ALK inhibitor, in refractory neuroblastoma”. In: *Pediatr Blood Cancer* 65.7, e27055.
- Hero, B. et al. (2008). “Localized infant neuroblastomas often show spontaneous regression: results of the prospective trials NB95-S and NB97”. In: *J Clin Oncol* 26.9, pp. 1504–10.
- Heukamp, L. C. et al. (2012). “Targeted expression of mutated ALK induces neuroblastoma in transgenic mice”. In: *Sci Transl Med* 4.141, 141ra91.
- Huang, H. (2018). “Anaplastic Lymphoma Kinase (ALK) Receptor Tyrosine Kinase: A Catalytic Receptor with Many Faces”. In: *Int J Mol Sci* 19.11.
- Ignatius Ou, S. H. et al. (2014). “Next-generation sequencing reveals a Novel NSCLC ALK F1174V mutation and confirms ALK G1202R mutation confers high-level resistance to alectinib (CH5424802/RO5424802) in ALK-rearranged NSCLC patients who progressed on crizotinib”. In: *J Thorac Oncol* 9.4, pp. 549–53.
- Inch, W. R., J. A. McCredie, and R. M. Sutherland (1970). “Growth of nodular carcinomas in rodents compared with multi-cell spheroids in tissue culture”. In: *Growth* 34.3, pp. 271–82.
- Infarinato, N. R. et al. (2016). “The ALK/ROS1 Inhibitor PF-06463922 Overcomes Primary Resistance to Crizotinib in ALK-Driven Neuroblastoma”. In: *Cancer Discov* 6.1, pp. 96–107.
- Ishihara, T. et al. (2002). “HEN-1, a secretory protein with an LDL receptor motif, regulates sensory integration and learning in *Caenorhabditis elegans*”. In: *Cell* 109.5, pp. 639–49.
- Iwahara, T. et al. (1997). “Molecular characterization of ALK, a receptor tyrosine kinase expressed specifically in the nervous system”. In: *Oncogene* 14.4, pp. 439–49.

- Janoueix-Lerosey, I. et al. (2008). “Somatic and germline activating mutations of the ALK kinase receptor in neuroblastoma”. In: *Nature* 455.7215, pp. 967–70.
- Janoueix-Lerosey, I. et al. (2018). “The ALK receptor in sympathetic neuron development and neuroblastoma”. In: *Cell Tissue Res* 372.2, pp. 325–337.
- Johnsen, J. I. et al. (2009). “Embryonal neural tumours and cell death”. In: *Apoptosis* 14.4, pp. 424–38.
- Kaneko, Y. et al. (1987). “Different karyotypic patterns in early and advanced stage neuroblastomas”. In: *Cancer Res* 47.1, pp. 311–8.
- Kaneko, Y. et al. (1999). “Disomy 1 with terminal 1p deletion is frequent in mass-screening-negative/late-presenting neuroblastomas in young children, but not in mass-screening-positive neuroblastomas in infants”. In: *Int J Cancer* 80.1, pp. 54–9.
- Katayama, R. et al. (2014). “Two novel ALK mutations mediate acquired resistance to the next-generation ALK inhibitor alectinib”. In: *Clin Cancer Res* 20.22, pp. 5686–96.
- Keshelava, N. et al. (1998). “Drug resistance patterns of human neuroblastoma cell lines derived from patients at different phases of therapy”. In: *Cancer Res* 58.23, pp. 5396–405.
- Kodityal, S. et al. (2016). “A novel acquired ALK F1245C mutation confers resistance to crizotinib in ALK-positive NSCLC but is sensitive to ceritinib”. In: *Lung Cancer* 92, pp. 19–21.
- Kohler, J. A. et al. (2013). “Treatment of children over the age of one year with unresectable localised neuroblastoma without MYCN amplification: results of the SIOPEN study”. In: *Eur J Cancer* 49.17, pp. 3671–9.
- Kramer, M. et al. (2016). “Proliferation and Survival of Embryonic Sympathetic Neuroblasts by MYCN and Activated ALK Signaling”. In: *J Neurosci* 36.40, pp. 10425–10439.
- Krytska, K. et al. (2016). “Crizotinib Synergizes with Chemotherapy in Preclinical Models of Neuroblastoma”. In: *Clin Cancer Res* 22.4, pp. 948–60.
- Kwak, E. L. et al. (2010). “Anaplastic lymphoma kinase inhibition in non-small-cell lung cancer”. In: *N Engl J Med* 363.18, pp. 1693–703.
- Lamant, L. et al. (2000). “Expression of the ALK tyrosine kinase gene in neuroblastoma”. In: *Am J Pathol* 156.5, pp. 1711–21.
- Lambertz, I. et al. (2015). “Upregulation of MAPK Negative Feedback Regulators and RET in Mutant ALK Neuroblastoma: Implications for Targeted Treatment”. In: *Clin Cancer Res* 21.14, pp. 3327–39.
- Lasek, A. W. et al. (2011). “Alk is a transcriptional target of LMO4 and ERalpha that promotes cocaine sensitization and reward”. In: *J Neurosci* 31.40, pp. 14134–41.

- Lastowska, M. et al. (1997). “Comparative genomic hybridization study of primary neuroblastoma tumors. United Kingdom Children’s Cancer Study Group”. In: *Genes Chromosomes Cancer* 18.3, pp. 162–9.
- Lee, C. C. et al. (2010). “Crystal structure of the ALK (anaplastic lymphoma kinase) catalytic domain”. In: *Biochem J* 430.3, pp. 425–37.
- Lee, H. H. et al. (2003). “Jelly belly protein activates the receptor tyrosine kinase Alk to specify visceral muscle pioneers”. In: *Nature* 425.6957, pp. 507–12.
- Li, R. and S. W. Morris (2008). “Development of anaplastic lymphoma kinase (ALK) small-molecule inhibitors for cancer therapy”. In: *Med Res Rev* 28.3, pp. 372–412.
- Liao, E. H. et al. (2004). “An SCF-like ubiquitin ligase complex that controls presynaptic differentiation”. In: *Nature* 430.6997, pp. 345–50.
- Limpt, V. van et al. (2004). “The Phox2B homeobox gene is mutated in sporadic neuroblastomas”. In: *Oncogene* 23.57, pp. 9280–8.
- Lin, J. J., G. J. Riely, and A. T. Shaw (2017). “Targeting ALK: Precision Medicine Takes on Drug Resistance”. In: *Cancer Discov* 7.2, pp. 137–155.
- Livak, K. J. and T. D. Schmittgen (2001). “Analysis of relative gene expression data using real-time quantitative PCR and the 2(-Delta Delta C(T)) Method”. In: *Methods* 25.4, pp. 402–8.
- London, W. B. et al. (2005). “Evidence for an age cutoff greater than 365 days for neuroblastoma risk group stratification in the Children’s Oncology Group”. In: *J Clin Oncol* 23.27, pp. 6459–65.
- Look, A. T. et al. (1984). “Cellular DNA content as a predictor of response to chemotherapy in infants with unresectable neuroblastoma”. In: *N Engl J Med* 311.4, pp. 231–5.
- Look, A. T. et al. (1991). “Clinical relevance of tumor cell ploidy and N-myc gene amplification in childhood neuroblastoma: a Pediatric Oncology Group study”. In: *J Clin Oncol* 9.4, pp. 581–91.
- Lopez-Delisle, L. et al. (2018). “Activated ALK signals through the ERK-ETV5-RET pathway to drive neuroblastoma oncogenesis”. In: *Oncogene* 37.11, pp. 1417–1429.
- Loren, C. E. et al. (2001). “Identification and characterization of DAlk: a novel *Drosophila melanogaster* RTK which drives ERK activation in vivo”. In: *Genes Cells* 6.6, pp. 531–44.
- Loren, C. E. et al. (2003). “A crucial role for the Anaplastic lymphoma kinase receptor tyrosine kinase in gut development in *Drosophila melanogaster*”. In: *EMBO Rep* 4.8, pp. 781–6.
- Louis, C. U. and J. M. Shohet (2015). “Neuroblastoma: molecular pathogenesis and therapy”. In: *Annu Rev Med* 66, pp. 49–63.
- Lutz, W. et al. (1996). “Conditional expression of N-myc in human neuroblastoma cells increases expression of alpha-prothymosin and ornithine decarboxylase and

- accelerates progression into S-phase early after mitogenic stimulation of quiescent cells". In: *Oncogene* 13.4, pp. 803–12.
- Marini, P. et al. (1999). "SiMa, a new neuroblastoma cell line combining poor prognostic cytogenetic markers with high adrenergic differentiation". In: *Cancer Genet Cytogenet* 112.2, pp. 161–4.
- Maris, J. M. (2010). "Recent advances in neuroblastoma". In: *N Engl J Med* 362.23, pp. 2202–11.
- Maris, J. M. et al. (2007). "Neuroblastoma". In: *Lancet* 369.9579, pp. 2106–20.
- Martinsson, T. et al. (2011). "Appearance of the novel activating F1174S ALK mutation in neuroblastoma correlates with aggressive tumor progression and unresponsiveness to therapy". In: *Cancer Res* 71.1, pp. 98–105.
- Mathivet, T., P. Mazot, and M. Vigny (2007). "In contrast to agonist monoclonal antibodies, both C-terminal truncated form and full length form of Pleiotrophin failed to activate vertebrate ALK (anaplastic lymphoma kinase)?" In: *Cell Signal* 19.12, pp. 2434–43.
- Matthay, K. K. et al. (1999). "Treatment of high-risk neuroblastoma with intensive chemotherapy, radiotherapy, autologous bone marrow transplantation, and 13-cis-retinoic acid. Children's Cancer Group". In: *N Engl J Med* 341.16, pp. 1165–73.
- McDermott, U. et al. (2008). "Genomic alterations of anaplastic lymphoma kinase may sensitize tumors to anaplastic lymphoma kinase inhibitors". In: *Cancer Res* 68.9, pp. 3389–95.
- Mena, M. A. et al. (1989). "Biochemical properties of monoamine-rich human neuroblastoma cells". In: *Brain Res* 486.2, pp. 286–96.
- Metzger, W. et al. (2011). "The liquid overlay technique is the key to formation of co-culture spheroids consisting of primary osteoblasts, fibroblasts and endothelial cells". In: *Cytotherapy* 13.8, pp. 1000–12.
- Miyake, I. et al. (2002). "Activation of anaplastic lymphoma kinase is responsible for hyperphosphorylation of ShcC in neuroblastoma cell lines". In: *Oncogene* 21.38, pp. 5823–34.
- Miyake S. Shimo T., Kitamura Y. Nojyo T. Nakamura S. Imashuka S. Abe T. (1973). "Characteristics of continuous and functional cell line NB-I, derived from a human neuroblastoma." In: *Jiritsu Shinkei* 10, pp. 115–120.
- Miyazaki, M. et al. (2018). "The p53 activator overcomes resistance to ALK inhibitors by regulating p53-target selectivity in ALK-driven neuroblastomas". In: *Cell Death Discov* 4, p. 56.
- Molenaar, J. J. et al. (2012). "Sequencing of neuroblastoma identifies chromothripsis and defects in neuritogenesis genes". In: *Nature* 483.7391, pp. 589–93.
- Monclair, T. et al. (2009). "The International Neuroblastoma Risk Group (INRG) staging system: an INRG Task Force report". In: *J Clin Oncol* 27.2, pp. 298–303.

- Montavon, G. et al. (2014). “Wild-type ALK and activating ALK-R1275Q and ALK-F1174L mutations upregulate Myc and initiate tumor formation in murine neural crest progenitor cells”. In: *Oncotarget* 5.12, pp. 4452–66.
- Moog-Lutz, C. et al. (2005). “Activation and inhibition of anaplastic lymphoma kinase receptor tyrosine kinase by monoclonal antibodies and absence of agonist activity of pleiotrophin”. In: *J Biol Chem* 280.28, pp. 26039–48.
- Moore, N. F. et al. (2014). “Molecular rationale for the use of PI3K/AKT/mTOR pathway inhibitors in combination with crizotinib in ALK-mutated neuroblastoma”. In: *Oncotarget* 5.18, pp. 8737–49.
- Morris, S. W. et al. (1994). “Fusion of a kinase gene, ALK, to a nucleolar protein gene, NPM, in non-Hodgkin’s lymphoma”. In: *Science* 263.5151, pp. 1281–4.
- Morris, S. W. et al. (1997). “ALK, the chromosome 2 gene locus altered by the t(2;5) in non-Hodgkin’s lymphoma, encodes a novel neural receptor tyrosine kinase that is highly related to leukocyte tyrosine kinase (LTK)”. In: *Oncogene* 14.18, pp. 2175–88.
- Morse, D. L. et al. (2005). “Determining suitable internal standards for mRNA quantification of increasing cancer progression in human breast cells by real-time reverse transcriptase polymerase chain reaction”. In: *Anal Biochem* 342.1, pp. 69–77.
- Mosse, Y. P. et al. (2004). “Germline PHOX2B mutation in hereditary neuroblastoma”. In: *Am J Hum Genet* 75.4, pp. 727–30.
- Mosse, Y. P. et al. (2008). “Identification of ALK as a major familial neuroblastoma predisposition gene”. In: *Nature* 455.7215, pp. 930–5.
- Mosse, Y. P. et al. (2013). “Safety and activity of crizotinib for paediatric patients with refractory solid tumours or anaplastic large-cell lymphoma: a Children’s Oncology Group phase 1 consortium study”. In: *Lancet Oncol* 14.6, pp. 472–80.
- Mosse, Y. P. et al. (2017). “Targeting ALK With Crizotinib in Pediatric Anaplastic Large Cell Lymphoma and Inflammatory Myofibroblastic Tumor: A Children’s Oncology Group Study”. In: *J Clin Oncol* 35.28, pp. 3215–3221.
- Moyzis, R. K. et al. (1988). “A highly conserved repetitive DNA sequence, (TTAGGG)_n, present at the telomeres of human chromosomes”. In: *Proc Natl Acad Sci U S A* 85.18, pp. 6622–6.
- Murray, P. B. et al. (2015). “Heparin is an activating ligand of the orphan receptor tyrosine kinase ALK”. In: *Sci Signal* 8.360, ra6.
- Mus, L. M. et al. (2020). “The ETS transcription factor ETV5 is a target of activated ALK in neuroblastoma contributing to increased tumour aggressiveness”. In: *Sci Rep* 10.1, p. 218.

- Nuchtern, J. G. et al. (2012). “A prospective study of expectant observation as primary therapy for neuroblastoma in young infants: a Children’s Oncology Group study”. In: *Ann Surg* 256.4, pp. 573–80.
- Okubo, J. et al. (2012). “Aberrant activation of ALK kinase by a novel truncated form ALK protein in neuroblastoma”. In: *Oncogene* 31.44, pp. 4667–76.
- Olovnikov, A. M. (1971). “[Principle of marginotomy in template synthesis of polynucleotides]”. In: *Dokl Akad Nauk SSSR* 201.6, pp. 1496–9.
- Oppedal, B. R. et al. (1989). “N-myc amplification in neuroblastomas: histopathological, DNA ploidy, and clinical variables”. In: *J Clin Pathol* 42.11, pp. 1148–52.
- Padovan-Merhar, O. M. et al. (2016). “Enrichment of Targetable Mutations in the Relapsed Neuroblastoma Genome”. In: *PLoS Genet* 12.12, e1006501.
- Passoni, L. et al. (2009). “Mutation-independent anaplastic lymphoma kinase overexpression in poor prognosis neuroblastoma patients”. In: *Cancer Res* 69.18, pp. 7338–46.
- Peifer, M. et al. (2015). “Telomerase activation by genomic rearrangements in high-risk neuroblastoma”. In: *Nature* 526.7575, pp. 700–4.
- Perez-Pinera, P. et al. (2007). “Anaplastic lymphoma kinase is activated through the pleiotrophin/receptor protein-tyrosine phosphatase beta/zeta signaling pathway: an alternative mechanism of receptor tyrosine kinase activation”. In: *J Biol Chem* 282.39, pp. 28683–90.
- Pietsch, T. et al. (1988). “Characterization of a continuous cell line (MHH-NB-11) derived from advanced neuroblastoma”. In: *Anticancer Res* 8.6, pp. 1329–33.
- Pinto, N. R. et al. (2015). “Advances in Risk Classification and Treatment Strategies for Neuroblastoma”. In: *J Clin Oncol* 33.27, pp. 3008–17.
- Plantaz, D. et al. (2001). “Comparative genomic hybridization (CGH) analysis of stage 4 neuroblastoma reveals high frequency of 11q deletion in tumors lacking MYCN amplification”. In: *Int J Cancer* 91.5, pp. 680–6.
- Powers, C. et al. (2002). “Pleiotrophin signaling through anaplastic lymphoma kinase is rate-limiting for glioblastoma growth”. In: *J Biol Chem* 277.16, pp. 14153–8.
- Pritchard, J. and J. A. Hickman (1994). “Why does stage 4s neuroblastoma regress spontaneously?” In: *Lancet* 344.8926, pp. 869–70.
- Pugh, T. J. et al. (2013). “The genetic landscape of high-risk neuroblastoma”. In: *Nat Genet* 45.3, pp. 279–84.
- Pulford, K. et al. (1997). “Detection of anaplastic lymphoma kinase (ALK) and nucleolar protein nucleophosmin (NPM)-ALK proteins in normal and neoplastic cells with the monoclonal antibody ALK1”. In: *Blood* 89.4, pp. 1394–404.

- Redden, R. A. and E. J. Doolin (2011). “Microgravity assay of neuroblastoma: in vitro aggregation kinetics and organoid morphology correlate with MYCN expression”. In: *In Vitro Cell Dev Biol Anim* 47.4, pp. 312–7.
- Redden, R. A. et al. (2014). “Rotary bioreactor culture can discern specific behavior phenotypes in Trk-null and Trk-expressing neuroblastoma cell lines”. In: *In Vitro Cell Dev Biol Anim* 50.3, pp. 188–93.
- Reiff, T. et al. (2011). “Midkine and Alk signaling in sympathetic neuron proliferation and neuroblastoma predisposition”. In: *Development* 138.21, pp. 4699–708.
- Reshetnyak, A. V. et al. (2015). “Augmentor alpha and beta (FAM150) are ligands of the receptor tyrosine kinases ALK and LTK: Hierarchy and specificity of ligand-receptor interactions”. In: *Proc Natl Acad Sci U S A* 112.52, pp. 15862–7.
- Reynolds, C. P. et al. (1986). “Characterization of human neuroblastoma cell lines established before and after therapy”. In: *J Natl Cancer Inst* 76.3, pp. 375–87.
- Rice, C. et al. (2017). “Structural and functional analysis of the human POT1-TPP1 telomeric complex”. In: *Nat Commun* 8, p. 14928.
- Robert M. Sutherland John A McCredie, W. Rodger Inch (1971). “Growth of Multicell Spheroids in Tissue Culture as a Model of nodular Carcinomas”. In: *JNCI: Journal of the National Cancer Institute* 46.1, pp. 113–120.
- Ross, R. A., B. A. Spengler, and J. L. Biedler (1983). “Coordinate morphological and biochemical interconversion of human neuroblastoma cells”. In: *J Natl Cancer Inst* 71.4, pp. 741–7.
- Rubie, H. et al. (2011). “Excellent outcome with reduced treatment in infants with nonmetastatic and unresectable neuroblastoma without MYCN amplification: results of the prospective INES 99.1”. In: *J Clin Oncol* 29.4, pp. 449–55.
- Rudolph, G. et al. (1991). “Cytogenetic and molecular characterization of a newly established neuroblastoma cell line LS”. In: *Hum Genet* 86.6, pp. 562–6.
- Russell, J. et al. (1989). “The relative effectiveness of analogues of cisplatin in the experimental chemotherapy of human non-small-cell lung cancer and neuroblastoma grown as multicellular spheroids”. In: *Cancer Chemother Pharmacol* 23.2, pp. 111–4.
- Sattu, K. et al. (2013). “Phosphoproteomic analysis of anaplastic lymphoma kinase (ALK) downstream signaling pathways identifies signal transducer and activator of transcription 3 as a functional target of activated ALK in neuroblastoma cells”. In: *FEBS J* 280.21, pp. 5269–82.
- Sausen, M. et al. (2013). “Integrated genomic analyses identify ARID1A and ARID1B alterations in the childhood cancer neuroblastoma”. In: *Nat Genet* 45.1, pp. 12–7.
- Schlesinger, H. R. et al. (1976). “Establishment and characterization of human neuroblastoma cell lines”. In: *Cancer Res* 36.9 pt.1, pp. 3094–100.

- Schmidt, M. L. et al. (2005). “Favorable prognosis for patients 12 to 18 months of age with stage 4 nonamplified MYCN neuroblastoma: a Children’s Cancer Group Study”. In: *J Clin Oncol* 23.27, pp. 6474–80.
- Schonherr, C. et al. (2011). “Activating ALK mutations found in neuroblastoma are inhibited by Crizotinib and NVP-TAE684”. In: *Biochem J* 440.3, pp. 405–13.
- Schramm, A. et al. (2015). “Mutational dynamics between primary and relapse neuroblastomas”. In: *Nat Genet* 47.8, pp. 872–7.
- Schulte, J. H. et al. (2011). “High ALK receptor tyrosine kinase expression supersedes ALK mutation as a determining factor of an unfavorable phenotype in primary neuroblastoma”. In: *Clin Cancer Res* 17.15, pp. 5082–92.
- Schulte, J. H. et al. (2013a). “MYCN and ALKF1174L are sufficient to drive neuroblastoma development from neural crest progenitor cells”. In: *Oncogene* 32.8, pp. 1059–65.
- Schulte, J. H. et al. (2013b). “Targeted Therapy for Neuroblastoma: ALK Inhibitors”. In: *Klin Padiatr* 225.6, pp. 303–8.
- Schwab, Manfred et al. (1983). “Amplified DNA with limited homology to myc cellular oncogene is shared by human neuroblastoma cell lines and a neuroblastoma tumour”. In: *Nature* 305.5931, pp. 245–248.
- Scorsone, K. et al. (2014). “The novel kinase inhibitor EMD1214063 is effective against neuroblastoma”. In: *Invest New Drugs* 32.5, pp. 815–24.
- Seeger, R. C. et al. (1977). “Morphology, growth, chromosomal pattern and fibrinolytic activity of two new human neuroblastoma cell lines”. In: *Cancer Res* 37.5, pp. 1364–71.
- Seeger, R. C. et al. (1982). “Definition of a Thy-1 determinant on human neuroblastoma, glioma, sarcoma, and teratoma cells with a monoclonal antibody”. In: *J Immunol* 128.2, pp. 983–9.
- Seeger, R. C. et al. (1985). “Association of multiple copies of the N-myc oncogene with rapid progression of neuroblastomas”. In: *N Engl J Med* 313.18, pp. 1111–6.
- Shaw, A. T. et al. (2013). “Crizotinib versus chemotherapy in advanced ALK-positive lung cancer”. In: *N Engl J Med* 368.25, pp. 2385–94.
- Shaw, A. T. et al. (2014). “Ceritinib in ALK-rearranged non-small-cell lung cancer”. In: *N Engl J Med* 370.13, pp. 1189–97.
- Shaw, A. T. et al. (2016). “Resensitization to Crizotinib by the Lorlatinib ALK Resistance Mutation L1198F”. In: *N Engl J Med* 374.1, pp. 54–61.
- Shaw, A. T. et al. (2017). “Lorlatinib in non-small-cell lung cancer with ALK or ROS1 rearrangement: an international, multicentre, open-label, single-arm first-in-man phase 1 trial”. In: *Lancet Oncol* 18.12, pp. 1590–1599.

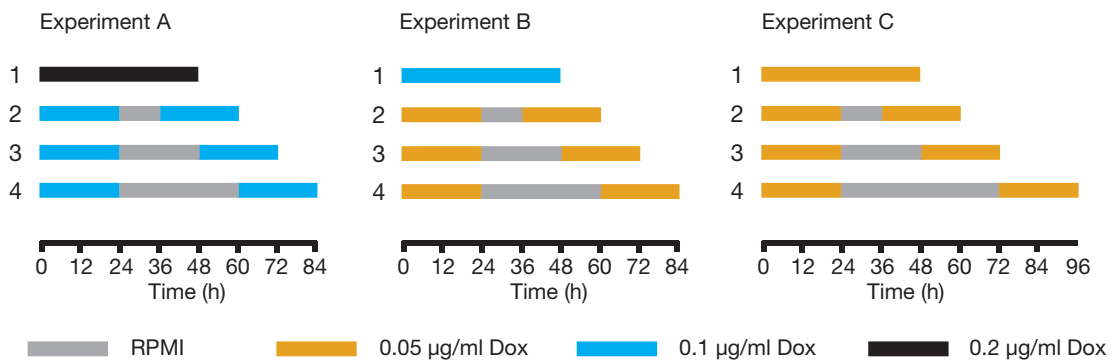
- Shen, J. et al. (2018). “A kinome-wide RNAi screen identifies ALK as a target to sensitize neuroblastoma cells for HDAC8-inhibitor treatment”. In: *Cell Death Differ* 25.12, pp. 2053–2070.
- Shiota, M. et al. (1994). “Hyperphosphorylation of a novel 80 kDa protein-tyrosine kinase similar to Ltk in a human Ki-1 lymphoma cell line, AMS3”. In: *Oncogene* 9.6, pp. 1567–74.
- Shojaei-Brosseau, T. et al. (2004). “Genetic epidemiology of neuroblastoma: a study of 426 cases at the Institut Gustave-Roussy in France”. In: *Pediatr Blood Cancer* 42.1, pp. 99–105.
- Soda, M. et al. (2007). “Identification of the transforming EML4-ALK fusion gene in non-small-cell lung cancer”. In: *Nature* 448.7153, pp. 561–6.
- Solomon, B. J. et al. (2014). “First-line crizotinib versus chemotherapy in ALK-positive lung cancer”. In: *N Engl J Med* 371.23, pp. 2167–77.
- Steensel, B. van, A. Smogorzewska, and T. de Lange (1998). “TRF2 protects human telomeres from end-to-end fusions”. In: *Cell* 92.3, pp. 401–13.
- Stoica, G. E. et al. (2001). “Identification of anaplastic lymphoma kinase as a receptor for the growth factor pleiotrophin”. In: *J Biol Chem* 276.20, pp. 16772–9.
- Stoica, G. E. et al. (2002). “Midkine binds to anaplastic lymphoma kinase (ALK) and acts as a growth factor for different cell types”. In: *J Biol Chem* 277.39, pp. 35990–8.
- Strother, D. R. et al. (2012). “Outcome after surgery alone or with restricted use of chemotherapy for patients with low-risk neuroblastoma: results of Children’s Oncology Group study P9641”. In: *J Clin Oncol* 30.15, pp. 1842–8.
- Sugimoto, T. et al. (1984). “Determination of cell surface membrane antigens common to both human neuroblastoma and leukemia-lymphoma cell lines by a panel of 38 monoclonal antibodies”. In: *J Natl Cancer Inst* 73.1, pp. 51–7.
- Sugimoto, T. et al. (1991). “Alpha-smooth-muscle actin and desmin expressions in human neuroblastoma cell lines”. In: *Int J Cancer* 48.2, pp. 277–83.
- Tonini, G. P. et al. (2003). “Familial neuroblastoma: a complex heritable disease”. In: *Cancer Lett* 197.1-2, pp. 41–5.
- Toyokawa, G. et al. (2015). “Identification of a Novel ALK G1123S Mutation in a Patient with ALK-rearranged Non-small-cell Lung Cancer Exhibiting Resistance to Ceritinib”. In: *J Thorac Oncol* 10.7, e55–7.
- Trochet, D. et al. (2004). “Germline mutations of the paired-like homeobox 2B (PHOX2B) gene in neuroblastoma”. In: *Am J Hum Genet* 74.4, pp. 761–4.
- Tucker, E. R. et al. (2017). “Immunoassays for the quantification of ALK and phosphorylated ALK support the evaluation of on-target ALK inhibitors in neuroblastoma”. In: *Mol Oncol* 11.8, pp. 996–1006.

- Tumilowicz, J. J. et al. (1970). "Definition of a continuous human cell line derived from neuroblastoma". In: *Cancer Res* 30.8, pp. 2110–8.
- Umopathy, G. et al. (2014). "The kinase ALK stimulates the kinase ERK5 to promote the expression of the oncogene MYCN in neuroblastoma". In: *Sci Signal* 7.349, ra102.
- Umopathy, G. et al. (2017). "MEK inhibitor trametinib does not prevent the growth of anaplastic lymphoma kinase (ALK)-addicted neuroblastomas". In: *Sci Signal* 10.507.
- Umopathy, G. et al. (2019). "Targeting anaplastic lymphoma kinase in neuroblastoma". In: *APMIS* 127.5, pp. 288–302.
- Valentijn, L. J. et al. (2015). "TERT rearrangements are frequent in neuroblastoma and identify aggressive tumors". In: *Nat Genet* 47.12, pp. 1411–4.
- Van Roy, N. et al. (2006). "Translocation-excision-deletion-amplification mechanism leading to nonsyntenic coamplification of MYC and ATBF1". In: *Genes Chromosomes Cancer* 45.2, pp. 107–17.
- Vandesompele, J. et al. (2001). "Multicentre analysis of patterns of DNA gains and losses in 204 neuroblastoma tumors: how many genetic subgroups are there?" In: *Med Pediatr Oncol* 36.1, pp. 5–10.
- Vernersson, E. et al. (2006). "Characterization of the expression of the ALK receptor tyrosine kinase in mice". In: *Gene Expr Patterns* 6.5, pp. 448–61.
- Wada, R. K. et al. (1993). "Human neuroblastoma cell lines that express N-myc without gene amplification". In: *Cancer* 72.11, pp. 3346–54.
- Wan, W. et al. (2006). "Anaplastic lymphoma kinase activity is essential for the proliferation and survival of anaplastic large-cell lymphoma cells". In: *Blood* 107.4, pp. 1617–23.
- Wang, H. Q. et al. (2017). "Combined ALK and MDM2 inhibition increases antitumor activity and overcomes resistance in human ALK mutant neuroblastoma cell lines and xenograft models". In: *Elife* 6.
- Weichselbaum, R. R. et al. (1984). "Repair of fractionated radiation in plateau phase cultures of human tumor cells and human multicellular tumor spheroids". In: *Radiother Oncol* 2.1, pp. 41–7.
- Weiss, J. B. et al. (2012). "Anaplastic lymphoma kinase and leukocyte tyrosine kinase: functions and genetic interactions in learning, memory and adult neurogenesis". In: *Pharmacol Biochem Behav* 100.3, pp. 566–74.
- Wibe, E. (1980). "Resistance to vincristine of human cells grown as multicellular spheroids". In: *Br J Cancer* 42.6, pp. 937–41.
- Wiesner, T. et al. (2015). "Alternative transcription initiation leads to expression of a novel ALK isoform in cancer". In: *Nature* 526.7573, pp. 453–7.

-
- Wood, A. C. et al. (2017). “Dual ALK and CDK4/6 Inhibition Demonstrates Synergy against Neuroblastoma”. In: *Clin Cancer Res* 23.11, pp. 2856–2868.
- Yao, S. et al. (2013). “Anaplastic lymphoma kinase is required for neurogenesis in the developing central nervous system of zebrafish”. In: *PLoS One* 8.5, e63757.
- Yasuda, H. et al. (2012). “Preclinical rationale for use of the clinically available multitargeted tyrosine kinase inhibitor crizotinib in ROS1-translocated lung cancer”. In: *J Thorac Oncol* 7.7, pp. 1086–90.
- Zhu, S. et al. (2012). “Activated ALK collaborates with MYCN in neuroblastoma pathogenesis”. In: *Cancer Cell* 21.3, pp. 362–73.

Appendix

A



B

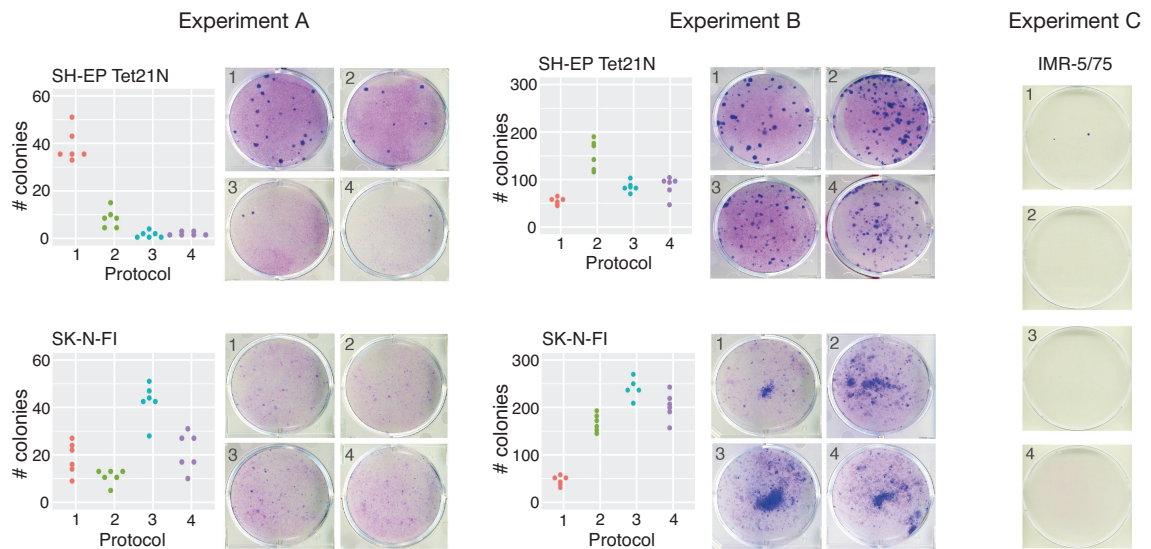


Figure 59: NB cell lines respond differently to varying treatment schedules of doxorubicine. Tet21N, SK-N-FI and IMR-5/75 cells were treated with different treatment regimens and concentrations of DOX. After additional two weeks of cultivation in normal growth media, colony formation capacity was determined using the Giemsa assay. **A** Treatment regimens. **B** Number of regrowing colonies two weeks post treatment. DOX - doxorubicine. n=3.

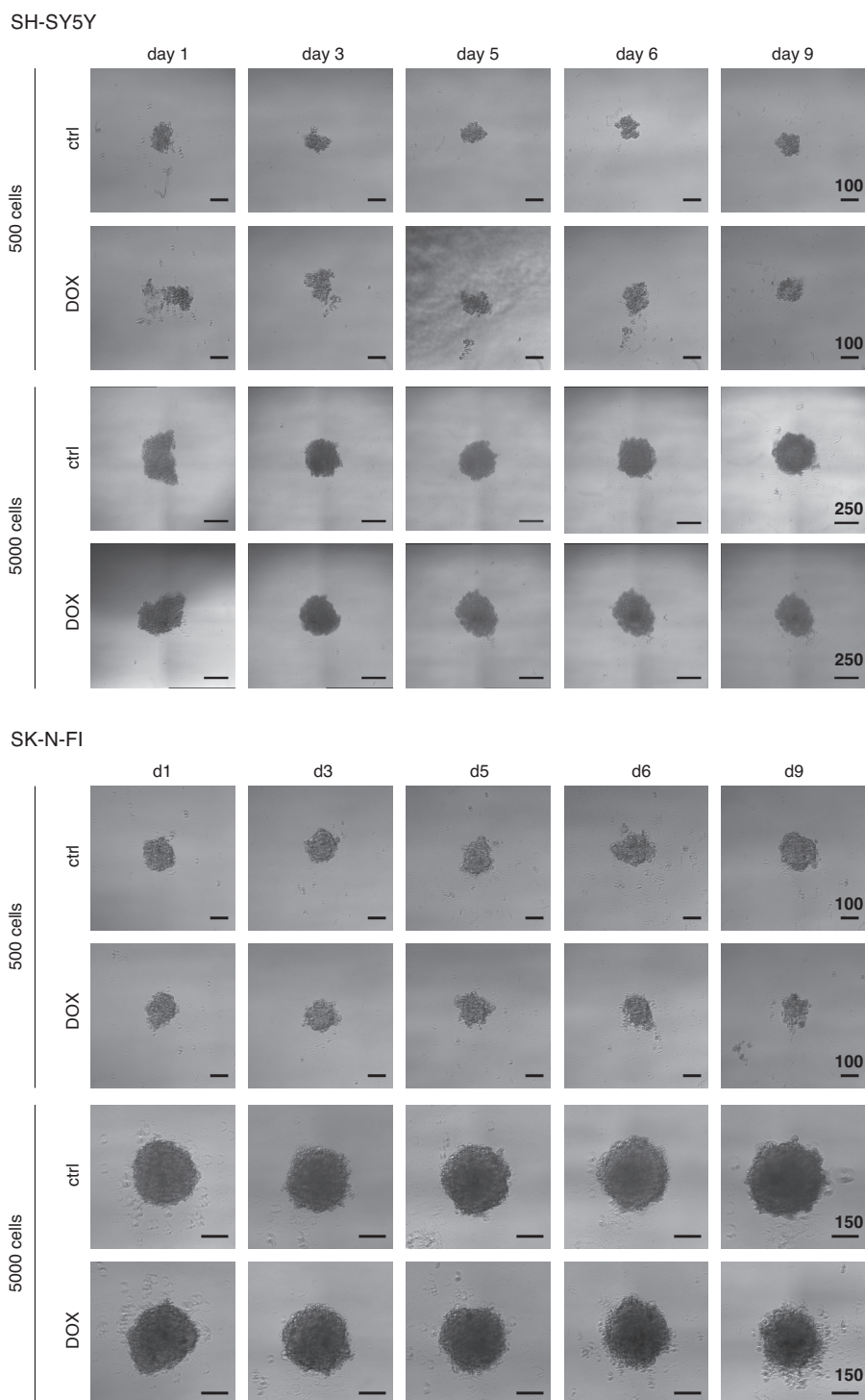


Figure 60: Normal growth of 5000-cell NB spheroids and the effect of chemotherapy on the 3D structure. 500 or 5000 cells of the respective cell lines were seeded into 1%-agarose coated 96-well plates and treated with $0.1 \mu\text{g}/\mu\text{l}$ DOX after 48h. Images were acquired on days 1, 3 (24h DOX), 5 (72h DOX), 6 (96h DOX) and 9 (168h DOX) after seeding. Scale bar is displayed in μm . $n=3$.

Replication initiation

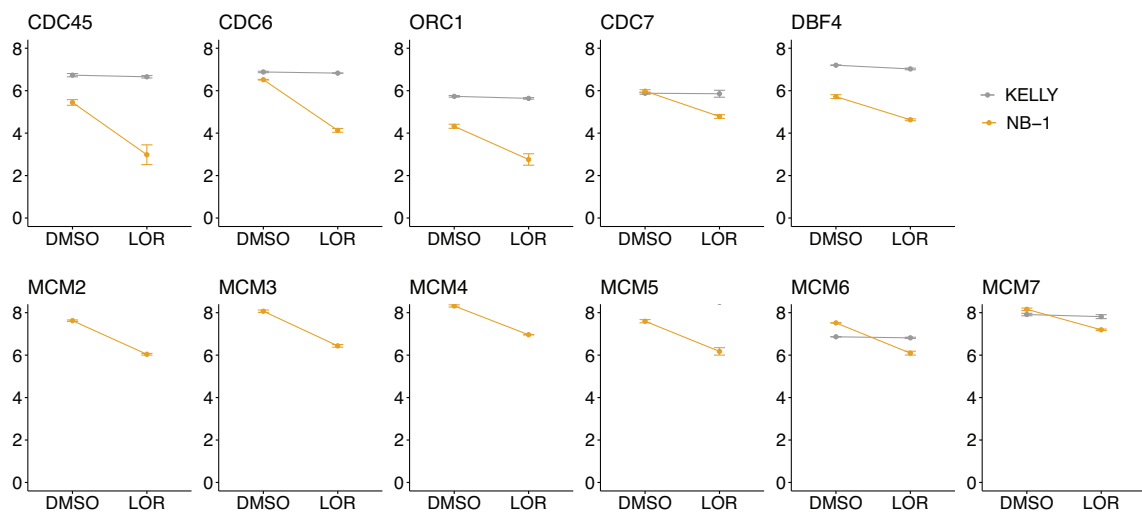


Figure 61: Genes involved in replication initiation are downregulated in LOR treated NB-1 cells. RNaseq expression of selected genes involved in replication initiation at 24h treatment with LOR. Mean \pm SD. n=2.

Acknowledgements

First of all, I would like to thank my supervisor Thomas Höfer for giving me the opportunity to do my PhD in his group. I am thankful for your excellent scientific support and guidance throughout the time of my PhD and at the same time for giving me enough freedom to develop and follow my own ideas.

Special thanks go to Frank Westermann for allowing me to work in his lab and to become part of the Neuroblastoma Genomics department with an excellent working atmosphere. I am grateful for many fruitful discussions which helped me a lot to shape my project.

I would like to express my gratitude to my two other PhD examiners Jan Lohmann and Odilia Popanda for reviewing my work and to Olaf Witt for giving me important scientific input during my TAC meetings.

My particular thank goes to Nina Claudino for being an incredible help with all the experiments throughout my PhD. Without you, I would still be sitting in the cell culture pipetting all those drug dilutions. Thank you Alessandro Greco and Dr. Xi Wang for helping me with the analysis of my sequencing data and for the patience with which you answered all my programming questions. I would like to thank Dr. Erika Kuchen, Dr. Verena Körber and Dr. Congxin Li for creative discussions and ideas for my project. Thank you Diana Best and Dr. Nick Kepper for being a tremendous support with all my organizational and computational issues during my time in the group. I want to express my gratitude to all members of the B086 department for a nice working atmosphere and the great time during our annual group retreats.

Special thanks go to Karolina Garbowicz for making long working hours really enjoyable but also for becoming an amazing friend outside the lab. I would like to thank Dr. Sina Kreth for many creative ideas concerning my project, all the support with experimental design and especially for proofreading my thesis. Thank you Jochen Kreth, Elisa Wecht, YG Park and Diana Vobis for introducing me to the lab and all the experimental help throughout the years. I thank Dr. Kai Henrich, Dr. Larissa Savelyeva and Dr. Umut Toprak for great scientific advice and of course all the girls

(Lea, Selina, Sabine, Mona, Alica) for fun times during our lab outings and after work beers. I want to express my deepest gratitude to the whole B087 department for letting me become a part of your fantastic group.

I would like to thank the Bräustadel gang for the best after work beer sessions and game nights one can imagine. My girls Jessie, Laura, Ronja and Lena I thank for fantastic wine and cheese evenings, fun trips to France and Stangenroth, exhausting sports sessions, for standing by my side on every step of the way and making my PhD time so much fun. My dear friends Markus and Micha I thank for always being there for me, listening to my problems, cheering me up and helping me find my way through this PhD. I want to thank Jorge for fun game nights, Sergej and Victor for fantastic lunch breaks and Marius for the best Sushi I have ever eaten. A big thanks goes to Alexandra for being the best office mate one can ask for, a perfect tea supplier and great listener. I want to express my deepest gratitude to all my amazing friends, who made my PhD time at DKFZ an unforgettable experience.

My long-time friends Franzi, Johannes, Sven, Hanna, Juliane, Bunny and Daniel I thank for always being there for me and for reminding me that there is still a life outside the scientific world.

Finally but most importantly I want to thank my family, especially my parents Ute and Friedrich and my brother Christian for their unlimited support and love and for always believing in me.